Supported zeolite A membranes. Feasibility of the static transverse synthesis – a new approach.

by

Sarel Petrus Jacobus Smith
M.Sc. Polymer Science

Dissertation presented for the Degree of
Doctor of Philosophy in Polymer Science

at the
University of Stellenbosch

Promotors:

Prof. Dr. R.D. Sanderson
Director, UNESCO *Associated Centre for Macromolecules and Materials*
Univeristy of Stellenbosch

Prof. J.C. Jansen
Lab. of Applied Organic Chemistry and Catalysis
Delft University of Technology

Stellenbosch December 2002

DECLARATION

I, the undersigned hereby declare that the work contained in this dissertation is my own orignal work and has not previously in its entirety or in part been submitted at any other university for a degree

ABSTRACT

As there is inadequate control of the hydrothermal synthesis technique used to date in the synthesis of zeolite A membranes, the feasibility of a new synthesis approach was investigated, namely the static transverse synthesis method. The former technique involved (i) thorough mixing of the chemical components, (ii) gel-formation and ageing and (iii) heat treatment. The proposed new method for zeolite A synthesis concerns the use of two individual nutrient pools (Al and Si) on opposite sides of a porous medium (α-alumina tube). Diffusion of these two nutrients towards each other, due to concentration differences, results in their contact in the porous medium (crystallisation front), leading to gel formation and eventual zeolite crystal growth. By means of the new static transverse synthesis technique the application of very high nutrient concentrations (0.72g NaOH, 80.0g H_2O, 8.26g $NaAlO_2$ and 15.48g Na_2SiO_3), contrary to what is used in conventional hydrothermal synthesis techniques (11.23g NaOH, 54.82g H_2O, 0.61g $NaAlO_2$ and 3.63g Na_2SiO_3), is now possible. The advantage of using high nutrient concentrations lies in the fact that supersaturation exists immediately after gel formation occurs. Supersaturation is a prerequisite for grain growth, which, in turn, is the only way in which a very thin (4-6 μm), continuous (pinhole-free) zeolite crystal layers can be prepared.

A variety of support materials have been used to provide the mechanical stability for zeolite membranes, because the chemical/physical interaction between a zeolite synthesis solution and the support also plays a role in the formation of a zeolite membrane. Hence, zeolite A crystal growth on four different types of supports was evaluated and the α-alumina tube proved to be the best support for zeolite A crystal growth.

An exploratory study into the upgrading of the static transverse synthesis to a continuous-flow synthesis was also undertaken. The nutrients were continuously passed over the opposite surfaces (internal and external) of the porous α-alumina tube. In this way the nutrients could be replenished throughout the synthesis. It was possible to make zeolite A membranes using this technique, although these membranes were not an improvement on the membranes produced with the STS method.

The zeolite A crystal population in and on the surface of the porous supports was determined by scanning electron microscopy (SEM). The zeolite A crystallinity, symmetry and morphology were characterised using x-ray diffraction (XRD). The zeolite lattice vibrations, structure sensitive and structure insensitive vibrations were determined by infra red spectroscopy (IR). The wettability of the alumina support was determined by dynamic contact angle measurements.

The zeolite A membranes prepared by the static transverse synthesis were tested for their helium permeance. They were also subjected to pervaporation experiments at 45°C, using a water/ethanol mixture (5 wt% water) and it was found that the fluxes varied between 0.2 -0.4 kg/m^2h and the separation factors varied between 5000 and 16000. These results compare very favourably with results reported in the literature.

In conclusion, the possibilities created by using a combination of membranes and catalysis, both on bench scale and in industry, are reviewed.

OPSOMMING

Weens onvoldoende beheer oor die hittebehandelingsintesetegniek wat tans vir die sintese van zeoliet-A-membrane gebruik word, is die haalbaarheid van 'n nuwe sintesetegniek, nl. die statiese sydelingse sintese-metode, ondersoek. Eersgenoemde tegniek behels (i) deeglike vermenging van die chemiese komponente, (ii) jelvorming en -veroudering en (iii) hittebehandeling. Die voorgestelde nuwe sintesetegniek vir die bereiding van ondersteunde zeoliet-A-membrane behels die plasing van twee aparte voedingsbronne (Al en Si onderskeidelik), aan teenoorgestelde kante van `n poreuse medium (α-aluminabuis). Diffusie van hierdie twee komponente na mekaar, agv konsentrasieverskille, veroorsaak dat die twee oplossings in die poreuse medium met mekaar in aanraking kom (kristallisasie front). Dit lei dan tot jelvorming en uiteindelik zeolietkristalgroei. Met die nuwe sydelingse sintesetegniek is die aanwending van baie hoë konsentrasies van die voedingsbronne (0.72g NaOH, 80.0g H_2O, 8.26g $NaAlO_2$ en 15.48g Na_2SiO_3) nou moontlik. Dit is in teenstelling met die konvensionele hittebehandelingstegnieke (11.23g NaOH, 54.82g H_2O, 0.61g $NaAlO_2$ en 3.63g Na_2SiO_3). Die voordeel van hoë voedingsbronkonsentrasies is dat oorversadiging onmiddelik na jelvorming bereik word. Absolute oorversadiging is `n voorvereiste vir partikelgroei, wat op sy beurt die enigste manier is om baie dun (4–6 μm), aaneenlopende zeolietkristallae te verkry.

`n Verskeidenheid van draermateriale is al gebruik om meganiese stabiliteit aan zeolietmembrane te verleen, aangesien die chemiese/fisiese interaksie tussen die zeolietsintese-oplossing en die draermateriaal `n rol speel in die vorming van die zeolietmembraan. Om hierdie rede is die groei van zeoliet-A-kristalle op vier verskillende tipes draermateriale ondersoek en die α-aluminabuis is as die beste draermateriaal vir zeoliet-A-kristalgroei bewys.

`n Aanvanklike studie na die moontlike opgradering van die statiese sydelingse sintese na aaneenlopende vloeisintese is ook onderneem. In hierdie studie is die voedingsbronne deurlopend oor die teenoorgestelde oppervlaktes (intern en ekstern) van die poreuse α-aluminabuis gepomp. Sodoende kon die voedingstowwe voortdurend tydens die sintese aangevul word. Dit was moontlik om zeoliet-A-membrane met behulp van hierdie tegniek te maak, alhoewel hierdie membrane nie 'n verbetering was op dié wat deur middel van dei statiese sydelingse sintesetegniek gemaak is nie.

Die teenwoordigheid van die zeoliet-A-kristalle op die verskillende oppervlaktes van die poreuse buis is met behulp van `n skandeerelektronmikroskoop (SEM) bepaal. Die zeoliet-A-kristalliniteit, -simmetrie en -morfologie is met behulp van x-straaldiffraksie (XRD) gekarakteriseer. Die zeolietlatwerk-, struktuursensitiewe- en struktuuronsensitiewe vibrasies, is met behulp van infrarooispektroskopie (IR) en die benatbaarheid van die aluminabuis met dinamiese kontakhoekbepalings bepaal.

Die zeoliet-A-membrane berei met die statiese sydelingse sintese-metode is vir helium-deurlaatbaarheid getoets en ook aan pervaporasie eksperimente by 45°C, deur gebruik te maak van `n water/etanol mengsel (5 wt% water), onderwerp. Daar is gevind dat vloei tussen 0.2 – 0.4 kg/m^2h en dat skeidingsfaktore tussen 5000 en 16000 gevarieer het. Hierdie resultate vergelyk baie goed met die resultate in die literatuur.

Samevattend word 'n oorsig gegee van die moontlikhede wat geskep word deur membraanskeidingstegnologie te kombineer met katalise op laboratorium- en industriële skaal.

To my loving parents:

Pieter and Lenie Smith

ACKNOWLEDGEMENTS

I wish to express my very sincere thanks to:

Prof. Dr. R.D. Sanderson, Director of the Institute for Polymer Science, University of Stellenbosch, for his enthusiasm, encouragement and help throughout this study.

Prof J.C. Jansen, TU Delft, for giving me the opportunity to work with the best in the world. For always believing in me and being there to support this project. For always accepting me into your laboratory and providing me with the best advice possible. I will hold dear to me our numerous discussions on the subject of zeolites, catalysis, membranes and above all LIFE.

Sasol Technology for financial support for this project.

Dr. A.J. van Reenen, Dr. A.H. Roediger and Dr. E.P. Jacobs, for their friendship and numerous fruitful discussions held during this project.

All personnel at the Institute for Polymer Science, for making the years at IPS the best ever.

Dr. B. Nkosi, my mentor at Sasol Technology, for his encouragement and assistance throughout this project.

Dr. M.J. Hurndall, proof-reading this thesis and continued assistance and support.

Department Geology, University of Stellenbosch, for use of their XRD.

Department of Physics, University of Stellenbosch, for the use of the SEM.

Department of Chemical Engineering, Unversity of Cape Town, for occational use of their laboratories.

A word of thanks to all my friends at the Institute for Polymer Science, without whom all those years would not have been the same, **Willie Opperman, Charl Morkel, Jaco Theron, Erinda Cooper, Ewan Sprong, Deon Koen, Willem Truter, Elna M^{c}Leary, Dimitri and Natasha Bessarabov**.

Monja Smith, my wife, for your love and support and encouragement during these years. I will always love you for that. "My sun rises and sets with you".

LIST OF CONTENTS

LIST OF TABLES

CHAPTER 6

LIST OF FIGURES

CHAPTER 2

CHAPTER 3

CHAPTER 4

CHAPTER 5

function of the feed concentration of the reactant. For the metathesis of propene: (a) ethene/propene; (b) trans-2-butene/propene and for the metathesis of cis-2-butene: (c) trans-2-butene/cis-2-butene.

CHAPTER 1

Introduction

1.1 Introduction

The past 25 years has seen the dawning of the zeolite age. Since 1975 we have witnessed the birth of zeolite membranes in a variety of forms and shapes. Synthetic zeolites have been used in numerous catalytic reactors. What might the 21st century bring? Researchers are already aiming at combining these two disciplines (membrane separation and catalytic reactors) into one very useful tool, namely the catalytic membrane reactor (CMR)[1-10]. The result of the integration of these two techniques, separation and catalysis, will be of great value to industry, because the installations will be smaller, cheaper and more simplified. Less operating parameters will be needed.

The author is of the opinion that in order to achieve successes in the field of zeolites, in the 21st century, past shortcomings associated with zeolite membranes need to be addressed. These shortcomings are related to the performances of the available zeolite membranes and catalytic zeolite reactors.

As far as membranes are concerned, the flux of gas/liquid through a membrane needs to be high enough, without compromising the selectivity of the membranes[10]. This can only be achieved if one can prepare a thin (one crystal layer), continuous (pinhole-free) coating of zeolite on a porous support[11]. Past efforts to do so have been unsuccessful; thin zeolite crystal layers have been made, but these lack continuity. Repeated syntheses result in pinhole-free membranes but, using conventional synthesis techniques, the crystal layers become too numerous and too thick[12]. This is the case for both hydrophilic and hydrophobic zeolites. Catalytic zeolite reactors show pressure-drop problems in the packed bed configuration[10].

Various synthesis techniques to prepare zeolite membranes have been used by numerous researchers. These include (i) embedding zeolite crystals in a polymer

matrix[13-17], (ii) hydrothermal synthesis (self-supporting[18-22] and supported[23-28] membranes), (iii) solid gel conversion techniques[29-32], (iv) zeolite-in-metal membranes[33,34], (v) single crystal membranes[35-37], (vi) zeolite nanocrystals-colloidal suspension[38] and (vii) the seed film method[39]. These techniques will be discussed in full detail in Chapter 2.

To date, the membrane layers have proved to be too thick to allow high fluxes of permeating gases. The latter is of utmost importance if these membranes are to be implemented in industrial processes. The specific issue of membrane thickness is addressed in this thesis.

A new synthesis technique for the preparation of a thin zeolite A membrane is suggested here; it is referred to as the static transverse synthesis (STS) method. It involves the diffusion of the two single components, namely silica and alumina (building blocks for zeolite A crystals), from opposite sides of a porous medium (α-alumina tube), towards each other. This is achieved due to concentration gradients across porous support. On contact, aluminosilicate gel formation occurs, followed by zeolite crystal formation. The uniqueness of this technique lies in the fact that no further contact between the two components is possible, because the pores of the tube are blocked with the gel. This prevents unwanted crystal formation, which can lead to thick crystal layers. This technique should allow us to grow thin crystal layers, a feature which is very important in the application of these zeolite membranes.

1.2 Objectives

This study focused on devising a new synthesis approach towards the preparation of supported zeolite A membranes. The main objective was to prepare a very thin (single crystal layer) supported zeolite A membrane. In order achieve this it was necessary to,

(1) Identify a suitable membrane support.

(2) Determine exactly what happens during the static transverse synthesis process by studying the following:

- the sequence of the occurring events,
- the influence of experimental parameters (i.e. time, temperature and concentration) on the crystallisation in/on the tube,

- the influence of the position of the respective nutrients (Si and Al),
- the effect of the concentration of the nutrients on the position of the crystallisation front in the pores of the alumina tube,
- the effect of pure Si added to an alumina support,
- the hydrodynamics of the nutrient flow in the continuous flow synthesis (CFS) system,
- the wettability of the α-alumina tubes.

(3) Prepare zeolite A membranes successfully and reproducibly.

(4) Characterise the above membranes with the aid of scanning electron microscopy (SEM), infra red (IR) spectroscopy and x-ray diffraction (XRD) to determine the thickness of the crystal layer, its integrety and to determine whether the correct zeolite crystal phase had been prepared.

(5) Assess the solidity of the crystal layer and determine whether the crystal layer was void of pinholes, by doing vapour-pressure tests.

(6) Test the membranes for possible use in a separation process.

1.3 Technical overview

Zeolites are microporous crystalline tectosilicates. Their microporosity ranges from 0.25 nm to 1.4 nm and their pore geometry can be 1-, 2- or 3-dimensional, in the form of (non) intersecting channels or connecting cavities. As the pores are hosts for small organic guest molecules of slightly smaller sizes than the pore dimensions of the zeolites, configurational diffusivity occurs. To reduce diffusion limitation, crystallites of zeolite are made as small as possible, typically between 50 nm and 300 nm.

Thanks to the crystallinity of the zeolite materials, the tectosilicate framework as well as the pore geometry can be determined by single crystal structure analysis. For membranes, in particular, it is important to understand the orientation of the pores in the crystal form. Thus preferred orientation, for example in MFI (family of zeolites) to use uniquely the straight channels, as well as small crystals in a continuous layer, should provide the smallest tortuosity and diffusion path, respectively, which is preferred for a membrane configuration.

A drawback of the crystalline properties of the zeolitic material is, however, the formation of well-shaped crystals. To obtain a continuous layer from crystals with well-defined crystal facets is probably impossible. To close a pinhole between the crystals needs the provision of a nutrient flow that is, however, taken out by the crystal facets. The strategy here is to grow so-called grains. This is crystalline material of which the crystal form has a very rough surface, caused by growth from highly supersaturated solutions. The ultimate goal is to obtain oriented grains that are thin.

By controlling the aluminosilicate composition one can control the catalyst site concentration of these zeolitic materials. In the case where the catalytic site cannot be accommodated in the zeolitic membrane, a separate, probably macroporous phase of catalyst, can be coated on the zeolite membrane layer. Alternatively the zeolite layer can be grown by *in situ* crystallisation on a porous catalytic phase. Both approaches might be interesting, depending upon the reactant or product selectivity that is required.

1.4 Presentation of the dissertation

In this study the author tried to address the problems as far as the preparation of the zeolite membrane are concerned. Chapter 2 is a literature review of the history of zeolites and molecular sieves, covering different subjects, including zeolite membranes, synthesis techniques and synthesis parameters. Also included in this chapter are aspects of crystal growth in membrane formation, permeation characteristics of zeolite membranes and possible uses of zeolite membranes and coatings.

Prior to achieving the set goals, an appropriate support material and support configuration must be selected. Considerations pertaining to this are discussed in Chapter 3.

The problems related to the preparation of zeolite membranes will be addressed. This will be done by introducing a new synthesis approach, static transverse synthesis (STS), as described in Chapter 4. Experimental parameters, followed by theoretical elucidations or/and interpretations of the tendencies observed are included.

In Chapter 5 the feasibility of expanding the STS method, for zeolite membrane preparation, to a continuous flow synthesis (CFS) process is discussed. This is of interest if the need to upscale the synthesis reactor should arise.

Pervaporation experiments, dealing with the separation of water/ethanol mixtures, were were carried out, and these results are presented in Chapter 6. These are important features of the zeolite membranes.

Chapter 7 reviews the application of catalytic membrane reactors in a variety of reactions that are interesting for industry. These include catalytic zeolite membrane reactors. These reactors might prove to be the bridge between the 20th and the 21st century in as far as the field of application of zeolites is concerned.

In the final chapter, Chapter 8, final conclusions regarding the research conducted during this study will be drawn.

1.5 References

1. J.N. Armor, *Chemtech*, 1992, 557.
2. G. Saracco and V. Specchia, *Catal. Rev.-Sci. Eng.*, **36**, 1994, 305.
3. J. Shu, B.P.A. Grandjean, A. van Neste and S. Kaliaguine, *Can. J. Chem. Eng.*, **69**, 1991, 1036.
4. M.P. Harold, C. Lee, A.J. Burggraaf, K. Keizer, V.T. Zaspalis and R.S.A. de Lange, *MRS Bulletin*, 1994, 34.
5. N. Itoh, *Sekiyu Gakkaishi*, **33**, 1990, 136.
6. H.P. Hsieh, *Catal. Rev.-Sci Eng.*, **33**, 1991, 1.
7. J.-A. Dalmon, in: G. Ertl, H. Knozinger and J. Weitkamp (Eds.), *Handbook of Heterogeneous Catalysis*, VCH, Weinheim, Germany, 1997, 1387.
8. J. Zaman and A. Chakma, *J. Membr. Sci.*, **92**, 1994, 1.
9. G. Saracco, G. Versteeg and W. van Swaaij, *J. Membr. Sci.*, **95**, 1994, 105.
10. J.N. Amor, *J. Membr. Sci.*, **147**, 1998, 217.
11. J.C. Jansen and T. Maschmeyer, *Topics in Catalysis*, **00**, 1999, 1-10.
12. L. Gora, J.C. Jansen and T. Maschmeyer, *Stud. Surf. Sci. Catal.*, **125**, 1999, 173.
13. M. Demertzis and N.P. Evmiridis, *J. Chem. Soc., Faraday Trans.* 1, **82**, 1986, 3647.
14. H.J.C. te Hennepe, W.B.H. Boswerger, M.H.V. Mulder and C.A. Smolders, *J. Membr. Sci.*, **89**, 1987, 39.

15. M.-D. Jia, K.-V. Peinemann and R.-D. Behling, *J. Membr. Sci.*, **57**, 1991, 289.
16. I.R. Bellobono, F. Muffato, C. Ermondi, E. Selli, L. Righetto and M. Zeni, *J. Membr. Sci.*, **55**, 1991, 263.
17. S.P.J. Smith, E.P. Jacobs and R.D. Sanderson, *Proc. IMSTEC`96*, Australia, November`96.
18. T. Sano, Y. Kiyozumi, M. Kawamura, F. Mizukami, H. Takaya, T. Mouri, W. Inaoka, Y. Toida, M. Watanabe and K. Toyoda, *Zeolites*, **11**, 1991, 842.
19. J.G. Tsikoyiannis and W.O. Haag, *Zeolites*, **12**, 1992, 126.
20. T. Sano, Y. Kiyozumi, F. Mizukami, H. Takaya, T. Mouri and M. Watanabe, *Zeolites*, **12**, 1992, 131.
21. T. Sano, F. Mizukami, H. Takaya, T. Mouri and M. Watanabe, *Bull. Chem. Soc. Jpn.*, **65**, 1992, 146.
22. G.J. Myatt, M. Budd, C. Price and S.W. Carr, *J. Mater. Chem.*, **2**, 1992, 1103.
23. E.R. Geus, M.J. den Exter and H. van Bekkum, *J Chem. Soc., Faraday Trans.*, **88**, 1992, 3101.
24. M.-D. Jia, K.-V. Peinemann and R.-D. Behling, *J. Membr. Sci.*, **82**, 1993, 15.
25. T. Masuda, A. Sato, H. Hara, M. Kouno and K. Hashimoto, *Applied Catalysis A: General* **111**, 1994, 143.
26. T. Sano, H. Yanagishita, Y. Kiyozumi, F. Mizukami and K. Haraya, *J. Membr. Sci.*, **95**, 1994, 221.
27. Z.A.E.P. Vroon, K. Keizer, M.J. Gilde, H. Verweij and A.J. Burggraaf, *J. Membr. Sci.*, **113**, 1996, 293.
28. H. Kita, K. Horii, Y. Ohtoshi, K. Tanaka and K. Okamoto, *J. Mater. Sci. Lett.*, **14**, 1995, 206.
29. D.M. Bibby and M.P. Dale, *Nature*, **317**, 1985, 157.
30. Q. Huo, S. Feng and R. Xu, *J. Chem. Soc., Chem. Commun.*, 1988, 1486.
31. W. Xu, J. Li, W. Li, H. Zhang and B. Liang, *Zeolites*, **9**, 1989, 468.
32. W. Xu, J. Dong, J. Li, J. Li, and F. Wu, *J. Chem. Soc., Chem. Commun.*, 1990, 755.
33. P. Kolsch, D. Venzke, M. Noack, P. Toussaint and J. Caro, *J. Chem. Soc., Chem. Commun.*, 1994, 2491.
34. J. Girnus, M.M. Pohl, J. Richter-Mendau, M. Schneider, M. Noack, D. Venzke and J. Caro, *Adv. Mater.*, **7**, 1995, 711.

35. D.B. Shah, S. Chokchal-acha and D.T. Hayhurst, *J. Chem. Soc., Faraday Trans.*, **89**, 1993, 3161.

36. D.B. Shah and H.Y. Liou, *Zeolites*, **14**, 1994, 541.

37. D.B. Shah and H.Y. Liou, *Stud. Surf. Sci. Catal.*, **84**, 1994, 1347.

38. M. Tsapatsis, T. Okubo, M. Lovallo and M.E. Davis, *Mat. Res. Soc. Symp.Proc.*, **371**, 1995, 21.

39. J. Hedlund, B.J. Schoeman, A. Erdem-Senatalar and J. Sterte, *Zeolites*, **19** (1), 1997, 21-28.

CHAPTER 2

Zeolite membranes: An historic overview

2.1 Molecular sieves and zeolites

Molecular sieves are porous solids with pores of molecular diameter 0.3-2.0nm. Examples include zeolites, carbons, glasses and oxides. Some are crystalline, with a uniform pore size delineated by the crystal structure, for example, zeolites. Others are amorphous, for example, carbon molecular sieves. Most current commercial molecular sieves are zeolites[1].

Zeolites are crystalline aluminosilicates containing cations of group 1 and group 2 elements, such as sodium, potassium, magnesium and calcium[2]. Chemically, they are represented by the empirical formula:

$$M_{2/n}O \cdot Al_2O_3 \cdot ySiO_2 \cdot wH_2O,$$

where y is 2-10, n is the cation valence and w represents the amount of water contained in the voids of the zeolite. Structurally, zeolites are complex, crystalline, inorganic polymers, based on an infinitely extending three-dimensional, four-cornered framework of AlO_4 and SiO_4 tetrahedra linked to each other by the sharing of oxygen ions. Each AlO_4 tetrahedron in the framework carries a net negative charge, which is balanced by the cation. The framework structure contains channels or interconnected voids that are occupied by the cations and the water molecules.

2.1.1 Early history

In the 1980`s, van Bekkum *et al.*[1] reviewed the history of zeolites and molecular sieves, from the discovery of the first zeolite mineral to the explosion in the field of new compositions in molecular-sieve structures. The first zeolite mineral, stilbite, was discovered in 1756 by the Swedish mineralogist, Cronstedt; it marked the beginning of zeolite history[3]. The name of the mineral is derived from two Greek words, "zeo" and "lithos", meaning "to boil" and "a stone", because Cronstedt noticed that a

powder bed on a spoon heated by a flame showed small eruptions because of boiling water leaving the material. A few years later Fontana described the phenomenon of adsorption on charcoal[4]. In 1840 Damour observed that zeolite crystals could be reversibly dehydrated, with no apparent change in their morphology[5].

The hydrothermal synthesis of quartz was reported in 1845 by Schafhautle[6], who heated a gel of silica with water in an autoclave. The nature of ion exchange in soils was explained by Way and Thompson in 1850[7], while in 1858 Eichhorn demonstrated the reversibility of ion exchange on zeolite minerals[8]. St. Claire Deville reported on the first hydrothermal synthesis of a zeolite, lecynite, in 1862[9]. The idea that zeolites consisted of open, spongy frameworks was formulated in 1896 by Friedel[10], when he observed that various liquids (alcohol, benzene and chloroform) were occluded by dehydrated zeolites. A few years later, in 1925, Weigel and Steinhoff[11] reported the first molecular-sieve effect[11], based on size and polarity of molecules when they found that chabazite crystals excluded acetone, ether and/or benzene, while water, methyl alcohol, ethyl alcohol and formic acid were rapidly adsorbed.

In 1927 Leonard found that x-ray diffraction could be used for the identification and determination of structure in mineral synthesis[12]. Soon after this, in 1930, the first zeolite structures were determined by Taylor and Pauling[13,14]. Two years later McBain established the term "molecular sieve" to define porous solid materials that act as sieves on a molecular scale[15]. Therefore, by the mid-1930s the literature contained descriptions of ion exchange, adsorption, molecular sieves and the structural properties of zeolite minerals, as well as of a number of syntheses of zeolites. Barrer[16] (1945) presented the first classification of the then-known zeolites on the basis of molecular-size considerations and in 1948 reported the first definitive synthesis of zeolites, including the analogue of the zeolite mineral mordenite[17].

2.1.2 Synthetic zeolites

The successes achieved by Barrer in the mid-1940s inspired Milton of the Linde Division of Union Carbide Corporation to initiate research into zeolite synthesis, in search of new approaches to the separation and purification of air. Between 1949 and 1954 Milton and his co-worker Breck discovered a variety of commercially significant zeolites, types A, Y and X. In 1954 synthetic zeolites were commercialised

by Union Carbide as a new class of industrial materials for separation and purification. In the following year, synthetic zeolite A`s structure was reported by Reed and Breck[2]. The first bulk-separation process using true molecular sieving selectivity (normal-isoparaffin separation) was marketed in 1959 by Union Carbide[18]. In the same year they also marketed zeolite Y, as an isomerisation catalyst[18].

In 1962 Mobil Oil introduced the use of synthetic zeolite X as a cracking catalyst and a few years later Mobil reported on the synthesis of the high-silica zeolites beta and ZSM-5 (1967-1969). Henkel introduced zeolite A into detergents (1974) instead of the environmentally-suspect phosphates. In 1977 zeolites were first used for ion-exchange separations (Union Carbide). In the 1980`s extensive work was done on the synthesis and applications of ZSM-5 and on a number of other members of the high-silica zeolite family. Syntheses of aluminophosphate and metallosilicate molecular sieves were disclosed in the mid-1980`s[19]. During the 1980`s there were major developments in the secondary synthesis and modification chemistry of zeolites, as well as in the introduction of silicon-rich frameworks and framework metal substitutions. The 1980`s was a time of an explosion in new compositions and structures of molecular sieves.

2.1.3 Zeolite structures

There are two types of zeolite structures: one provides an internal pore system comprising interconnected cage-like voids, the second provides a system of uniform channels which, in some instances, are one-dimensional channel systems. The preferred zeolite structure type has two- or three-dimensional channels to provide rapid intracrystalline diffusion in adsorption and catalytic applications.

In most zeolite structures the primary structural units, the AlO_4 or SiO_4 tetrahedra, are assembled into secondary building units, which may be simple polyhedra such as cubes, hexagonal prisms, or octahedra. The final structure framework consists of assemblies of the secondary building units. More than 50 novel, distinct, framework structures of zeolites are known. They have pore sizes ranging from 0.3 to 0.8 nm, and pore volumes from about 0.10 to 0.35 cm^3/g.

Typical zeolite pore sizes, using oxygen-packing models, are shown in Figure 2.1.

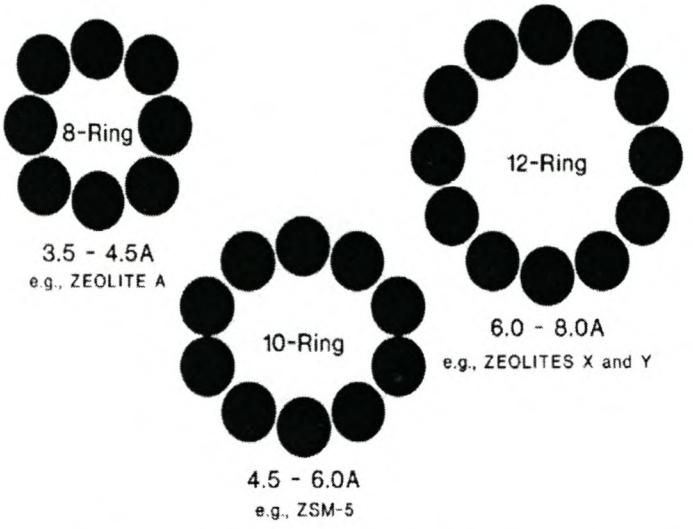

Figure 2.1: Typical zeolite pore-sizes, given in Å, illustrated with an oxygen (radius 0.136 nm) packing model[1].

They include: small-pore zeolites with eight-ring pores, with free diameters of 0.30 – 0.45 nm, e.g., zeolite A; medium-pore zeolites formed by a ten ring, 0.45 – 0.60 nm in free diameter, which could change slightly upon deformation to range between 0.4 – 0.7 nm, e.g., ZSM-5; and large-pore zeolites with 12-ring pores, ~0.8 nm, e.g., zeolites X and Y. The molecular sieve effect of a calcium A zeolite with an eight-ring pore of oxygens, is shown in Figure 2.2. n-Octane (top) readily accesses the internal void of the zeolite through the pore whereas iso-octane (bottom) is larger than the pore and is totally excluded.

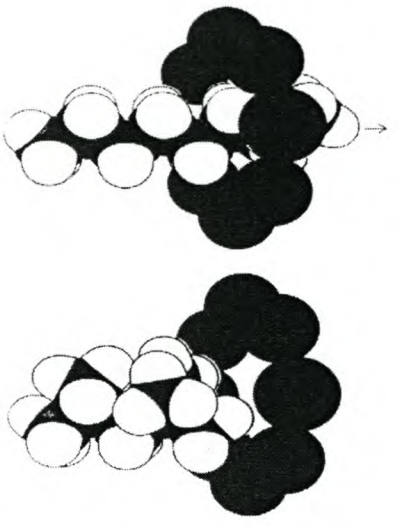

Figure 2.2: Schematic representation of the molecular sieving effect[1].

A straight chain molecule of n-octane, with a kinetic diameter of 0.42 nm (top), passes through the eight-ring aperture of 0.45 nm (NaCaA) zeolite, while a mono- and di-branched molecule of iso-octane, with kinetic diameters of 0.5 and 0.6 nm (bottom), respectively, cannot.

The zeolite framework should be viewed as slightly flexible, with the size and shape of the framework and the pores responding to changes in temperature and guest species. For example, ZSM-5 has a 0.56 nm near-circular pore, but with substituted aromatics as guest species the pore adopts an elliptical shape, 0.45 to 0.70 nm in diameter.

Some of the more important zeolite types, most of which have been used in commercial applications, include the zeolite minerals: mordenite, chabazite, erionite and clinoptilolite, and the synthetic zeolites types A, X, Y, L, omega, "Zeolon" mordenite, ZSM-5 and zeolites F and W.

Structural characteristics of some of the important zeolites are shown in Figures 2.3 - 2.5 below. The figures on top show a schematic representation of the channel system, as it is orientated within a crystal of typical morphology. The framework structures are shown at the bottom of these three figures. These structures were taken from W.M. Meier and D.H. Olson, Atlas of Zeolite Structure Types, IZA Structure

Commission, 1987. Figure 2.3 shows zeolite A, Figure 2.4 shows ZSM-5 and Figure 2.5 shows Mordenite.

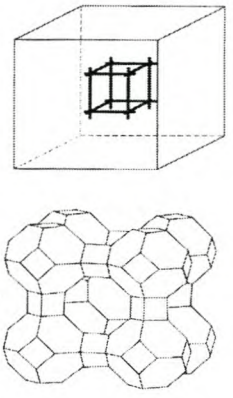

Figure 2.3: Zeolite A. Orientation of the 3-D pore system in the crystal (top). Framework topology of the unit cell (bottom).

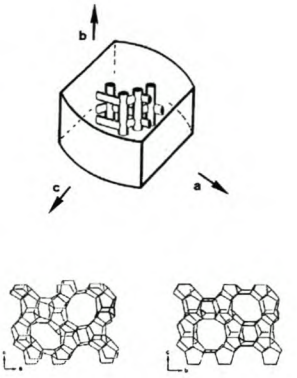

Figure 2.4: ZSM-5. Orientation of the 2-D pore system in the crystal (top). Framework topology of the a, b and c direction is also shown (bottom).

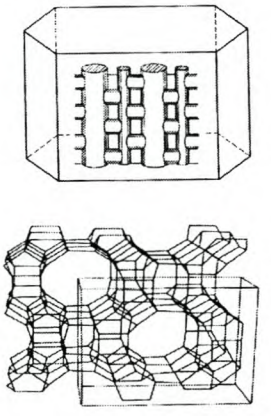

Figure 2.5: Mordenite. Orientation of the 1-D pore system in the crystal. The framework topology is shown at the bottom.

For reasons of clarity the centers of T-atoms are connected and the oxygen positions are not shown.

2.2 Zeolites and zeolite based membranes

2.2.1 Background

Separation processes are used in numerous industries. Separation methods include distillation, crystallisation, centrifugation, extraction, adsorption and membrane techniques. Chemical conversions often run incompletely, as dictated by the

thermodynamic equilibrium or by the wish to obtain high selectivity, which may require relatively low conversion or the use of one of the reactants in excess. There has been a growing interest in combining reactions and separations and this has resulted in the industrial application of catalytic membranes and membrane reactors[20].

2.2.2 Membranes

Membranes can be classified according to the driving force (concentration or pressure difference) that causes the flow of permeate through the membrane, or the material(s) they consist of (organic polymers or inorganic materials)[21]. Membranes can be either dense or porous. Examples of dense membranes are palladium foils and films of organic polymers, such as polyvinyl alcohol (PVOH). Oxygen permeation through dense ceramic membranes (e.g. perovskites) has been studied extensively, because these membranes can be used at temperatures higher than 600°C. Porous membranes include porous polymer films (cellulose, polyamides, polysulphones, etc.), as well as amorphous inorganic materials (alumina and silica).

Different permeation principles apply to dense and porous membranes; these are dissolution/diffusion and adsorption/diffusion, respectively. A schematic representation of the gas flow through macro-, meso- and microporous membranes and through dense membranes is shown in Figure 2.6, from top to bottom, respectively. Convective flow, dominated by molecule-molecule interactions, occurs in relatively large pores or at high pressures, while Knudsen diffusion, dominated by molecule-wall collisions, occurs in smaller pores at low pressures or high temperatures. Surface diffusion is an activated transport due to adsorption of molecules on the pore walls. It is the latter permeation principle that applies to zeolite-based membranes[22].

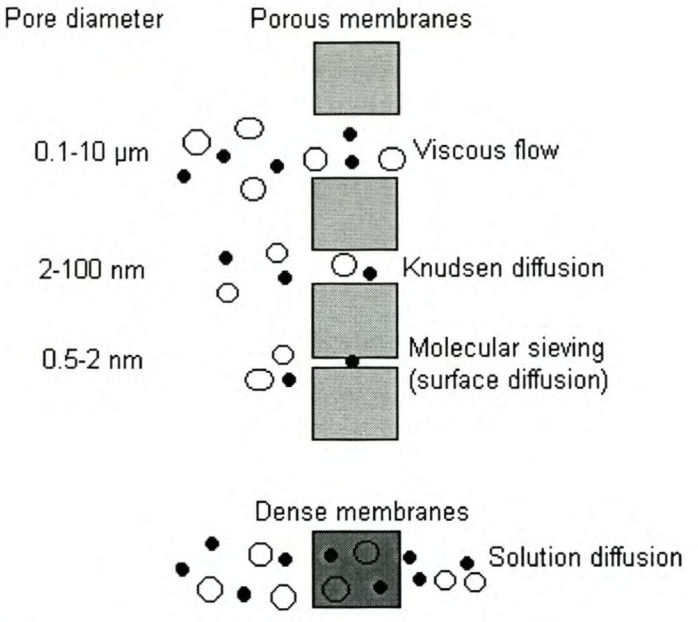

Figure 2.6: Mechanisms for the permeation of gases through porous and dense gas-separation membranes[22].

Porous, especially microporous, membranes are able to separate the components in a mixture based on the sizes of the molecules. When molecules are too large to enter the largest pores of a membrane, absolute separation can be achieved. In the case where both components of a binary mixture can access the micro-pore, adsorption strength or diffusion rate is the dominating step at lower and higher temperatures, respectively.

2.2.3 Zeolites as membrane materials

In the field of ceramic membranes the focus has, to date, been on amorphous porous aluminas and silicas[23,24]. Other inorganic materials studied include: titania, zirconia, non-oxide ceramics (carbides), and microporous carbons.

Zeolites, as crystalline materials, are useful membrane materials for the following reasons:

(1) they have strictly defined pore structure and size,

(2) given a particular zeolite structure, it is possible to tune the pore wall character by altering the Si/Al ratio and by ion exchange,

(3) there are known methods of introducing catalytic entities on the way to catalytic membranes,

(4) outer-surface modification can be carried out in several ways.

The pore architecture of zeolites is unique for each type of zeolite and can be: one-dimensional (parallel tubes), two-dimensional or three-dimensional. In the case of one-dimensional zeolites the orientation of the zeolite crystals should be such that the channel direction is perpendicular to the membrane layer configuration.

2.2.4 Zeolite membrane configurations

A schematic diagram of several zeolite membrane-based configurations in which zeolites govern, or contribute to, membrane permeation, is given in Figure 2.7.

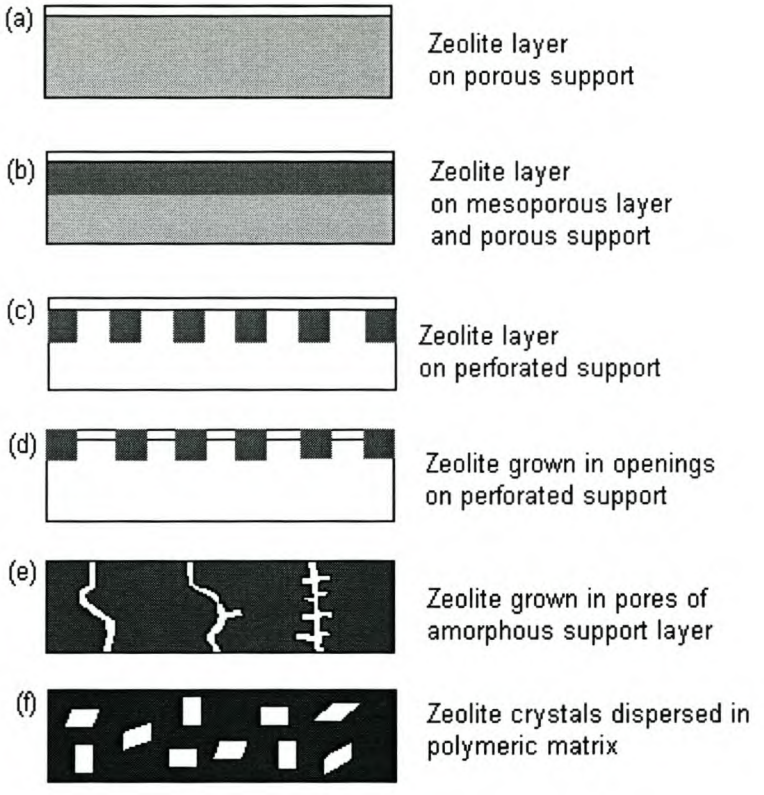

Figure 2.7: Zeolite-based membrane configurations[22].

Zeolite crystal layers can be grown by hydrothermal synthesis onto porous supports, for example: clay, alumina, sintered metals and carbon, as shown in Figure 2.7 (a,b).

MFI-type zeolites have been studied extensively[25-28]. These MFI layers are able to withstand the template removal and subsequent thermal cycles up to 350°C. This is taken as a strong indication of the strength of the chemical bonding of the crystal

layer to the support interface[29]. In order to understand chemical attachment to metals one has to consider that metals, on exposure to air, will be covered with a thin (1-2 nm) oxide film. Sometimes an intermediate mesoporous layer has been applied, e.g. a metakaolin film on clay or on zirconia[25], or metal wool on sintered metal[26]. As far as could be determined, no adherence exists between a zeolite layer and a Teflon[30] or carbon support. In this case the binding possibilities between the zeolite layer and the support are lacking.

An additional approach to bind a zeolite layer to a support, is to use a dense support (e.g. stainless steel) with regular perforation, Figure 2.7 (c,d). The *in situ* growth of zeolite is then aimed at either the creation of a zeolite layer which covers the entire support or at zeolite growth in the pores of the support.

The next configuration, Figure 2.7 (e), is (in a way) similar to the configuration in (d); Figure 2.7 (e) shows that the pores of the mesoporous support are filled with zeolite by "inside" crystallisation. Generally, several crystallisations will be necessary to achieve an essentially complete, leak-free filling of the pores in the amorphous support.

A fundamentally different zeolite membrane configuration is achieved by loading a polymer film, e.g. poly(dimethylsiloxane) (PDMS) or polyimide (PI)[31] with zeolite crystals, as shown in Figure 2.7 (f). In this case the zeolites only contribute to the permeation by acting as selective reservoirs of components. Hydrophobic (silicalite-1) as well as hydrophilic (zeolite A) zeolites have been studied in such a configuration.

2.2.5 Characteristics and performance of zeolite membranes

Zeolitic membranes can be designed to separate chemical mixtures, and the performance targets are usually set according to economic considerations. The performance is determined in terms of membrane permeability and selectivity, which are generally inversely related. For MFI type zeolites (in analogy with polymer membranes[32]) an upper bound, which is probably in the neighbourhood of satisfactory performance, can be drawn when the permeability of one component is plotted against the permselectivity (i.e., the ratio of permeability to selectivity) of the membrane for that component, see Figure 2.8. The curve indicates the "upper band" performance of

the zeolite membrane[40]. The data were taken from literature, with numbers indicating references.

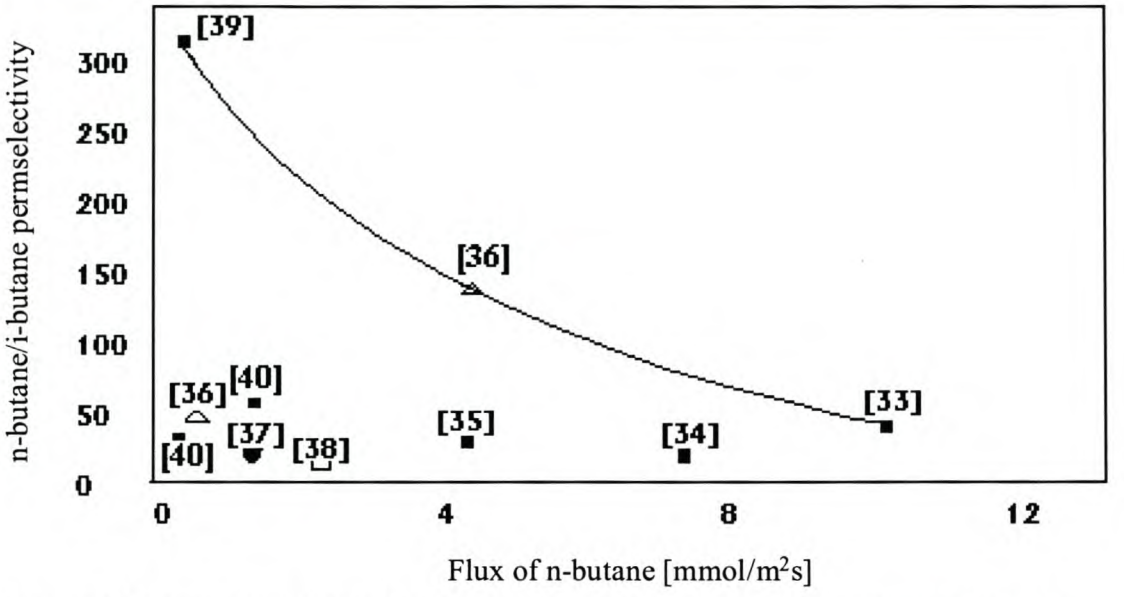

Figure 2.8: Permeation of zeolite membranes as a function of the permselectivity for n-/i-butane.

From the data given, the separation factor can be determined at a certain n-butane permeation level[33]. Jansen *et al*[41] suggested that is unlikely that membrane performance can be fully described by the intrinsic zeolite properties. The behavior of the membrane is probably also determined by the continuity of the zeolite phase, as well as the membrane thickness, as determined by the number and size of the crystals in the membrane. In addition to this, the following also play a major role: obstructions or bypasses caused by boundary layers between the crystals, the orientation and connectivity of the pores as well as the success of the calcination step, (during the preparation of the membrane), to avoid cracks in the zeolite phase. During the formation of zeolite crystal(lite)s from an aqueous mixture, there is an intrinsic difference in density between the SiO_2-nutrient in the aqueous phase (d = 0.3 g/cm^3, for MFI) and the SiO_2-crystal phase (d = 1.9 g/cm^3, for MFI). Thus, an extremely high concentration of SiO_2-nutrient and at the same time a relatively low viscosity are needed to supply enough mass to obtain a solid continuous zeolite phase[41]. When thin layers are formed (typically < 5 μm), a closed layer is achieved by grain growth on the support, see Figure 2.9(a)[40,41]. This effect results from a high crystal nucleation rate, which can be influenced by the support material, and from a low crystallisation

rate (for example, at low synthesis temperatures, when small crystals are formed). Preparation of a thin layer from well-shaped crystals via a low nucleation rate and high crystal growth rate (for example, high synthesis temperatures, when large crystals are formed) results in a layer with systematic pinholes between the crystals, see Figure 2.9(b). In the case that the crystal layer are formed by large, well-shaped crystals, the formation of pinholes is dramatically reduced. This is because the crystals have sufficient opportunity to grow in lateral directions, see Figure 2.9(c).

Figure 2.9: MFI-type layers on a porous support, viewed perpendicularly and

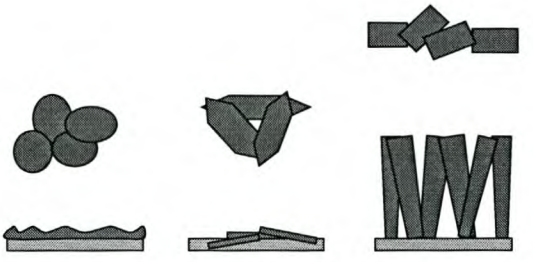

along the support with (a) grain growth which forms a closed thin layer, (b) small well-defined crystals in a thin layer with endless pinholes and (c) large crystals forming a thick closed layer with ended cavities[40].

The presence of pinholes in a zeolite membrane is often inferred from a relatively high permeation and a low separation performance – a continuous zeolite membrane shows an inverse pattern of performance. The thickness of the membrane should be small (less than 200 nm for MFI) to achieve a high permeation rate.

The type of grain boundary obstructing or bypassing micropore channels and the overall number of grain boundaries (low between large crystals, or high between very small crystals) located in the membrane, will influence the permeation characteristics[41]. Thus, thick membranes might show the same permeation characteristics as thin membranes, but that is usually due to bypasses via grain boundaries or pinholes. However, these are secondary effects, which can be

synthetically adjusted. The pore orientation and connectivity, intrinsic to a given zeolite, are of fundamental importance for gas separation purposes[41].

2.3 Synthesis of zeolite membranes

2.3.1 Synthesis techniques

Various methods of synthesis have been used to make zeolites membranes. These include:

2.3.1.1 Embedding zeolite crystals in a polymer matrix

The first attempts to make zeolites in membrane form were done by embedding granular zeolites in polymer matrixes, such as FAU-epoxide resin[42], LTA-epoxide resin[43], silicalite-1-silicone rubber[43-45], LTA-cellulose membranes[46] and NaA-polysulphone membranes[47]. Hennepe *et al.*[43,44] made MFI (Al-free) filled silicone rubber (PDMS) membranes and used them then for the separation of ethanol/water mixtures. Jia *et al.*[45] used MFI (Al-free) silicone composite membranes for gas separation and found that the composite membranes had better separating characteristics than the parent silicone membrane.

The disadvantages of these composite membranes are that in the separation process, full use of the molecular sieving effect of the zeolites cannot be used because of the inevitable, undesired transport of molecules outside the pores of the zeolite. In addition, the good properties of zeolites, such as high thermal resistance, high mechanical strength and chemical inertness, cannot be taken advantage of.

2.3.1.2 Hydrothermal synthesis

Zeolite membranes prepared by hydrothermal synthesis have two types of configurations; one is a self-supporting membrane and the other is a membrane supported by a porous material.

Self-supporting membranes

These zeolitic membranes are typically prepared from a hydrogel or sol composed of SiO_2, Al_2O_3, Na_2O and an organic templating agent. Typical silica sources for MFI synthesis are colloidal silica and silica powder (Aerosil). The tetrapropylammonium (TPA) cation was mostly used as the templating agent. Sano *et al.*[48] and Tsikoyiannis *et al.*[49] first reported on the synthesis of self-supporting MFI membranes.

Sano and coworkers[48,50,51] synthesised MFI membranes on a Teflon sleeve from a clear aqueous solution with a composition of 0.1 TPABr: 0.05 Na_2O: 0.01Al_2O_3: SiO_2: 40-100 H_2O. The synthesis mixtures with H_2O/SiO_2 ratios greater than 70 crystallised to form MFI membranes, without stirring. They also reported the synthesis of highly siliceous MFI (SiO_2/Al_2O_3 = 100 to infinity) membranes on filter paper (cellulose) as well as on a Teflon slab[52]. Calcination of a cellulose-supported zeolite layer resulted in a mechanically more stable zeolite membrane than that formed on a Teflon slab.

Tsikoyiannis and Haag[49] hydrothermally synthesised MFI layers on various non-porous supports, including Teflon slabs, silver and stainless steel, and on the external surface of a porous vycor disk. The resulting zeolite layers were easily removed from the Teflon slab. Although the surface on the Teflon side consisted of submicron-sized crystals, the solution-side surface consisted of a continuous array of densely intergrown crystals.

Besides the MFI membranes, self-supporting Na-type LTA (family of zeolites)[53], gmelinite (GME)[54] and Mordenite (MOR)[55] membranes were also hydrothermally prepared. Self-supporting, oriented MFI membranes were synthesised by Kiyozumi *et al.*[56] who employed liquid mercury as a substrate. The b axis of the MFI crystals was perpendicular to the mercury plane.

Supported membranes

It is well known that the mechanical strength of self-supporting zeolite membranes is insufficient for their application in separation processes. Hence, most of the studies on the synthesis of zeolite membranes have been performed on porous supports. It is mainly the results of studies on high silica MFI membranes that have been reported to date. These results are summarised in Table 2.1.

Table 2.1: Summary of studies reported on high silica MFI membranes

Authors	**Composition:** $Na_2O:SiO_2:Al_2O_3:TPA:H_2O$	**Support (pore diameter)**	**Synthesis conditions**	**Thickness (μm)**
Geus *et al.*[25]	1.6:1:0:1.5:166.66	Clay, zirconia	453K, 1-5 d	100
Geus *et al.*[26]	0:100:0:6:6330	Sintered metal, stainless steel	453K, 1-7 d	60-400
Jia et al.[57]	0.75:9:0:1.0:70	Ceramic disk	453K, 3-72 h	5
Jia et al.[58]		γ-alumina (5 nm)	453K, 3-72 h	10
Masuda *et al.*[59]	34:71:1:0	α-alumina (2 μm)	473K, 2 d	10-25
Sano *et al.*[60,61]	0.05:1:0:0.1:80	Stainless steel (0.5-2 μm)	443K, 2 d	400-500
Yan *et al.*[27]	0-4:6:0-0.6:1:96-700	α-alumina (0.5 μm)	448K, 4-24 h	10
Yan *et al.*[62]	2:6:0.005:1:571:1	α-alumina (0.5 μm)	448K, 16 h	10
Meriaudeau *et al.*[63]	0:1:0:0.051:22.5	Porous glass (10-20 μm)	448K, 72 h	150
Bai *et al.*[64]	0.071:1:0:0.071:42	γ-alumina (5 nm)	453K, 12 h	10
Chiou *et al.*[65]	5:100:0:10:10000	Anodic alumina (0.2 μm)	473K, 1-4 d	130
Vroon *et al.*[66]	5.3:100:0:30:1420	α-alumina	393K, 3 h	5

Supported MFI membranes have typically been prepared from a hydrogel or sol composed of SiO_2, Al_2O_3, Na_2O and tetra-propyl-ammonium (TPA) cation, similar to the preparation of self-supporting membranes. A reaction mixture, in which a porous support is immersed, is placed in an autoclave. Crystallisation is carried out under autogeneous pressure at temperatures of between 443 and 473K.

Most zeolite membrane research has been done on macroporous supports with pore sizes ranging from 0.1 to 10 μm, such as α-alumina and sintered stainless steel. A γ-alumina with an average pore size of 5 nm was also used by Jia *et al.*[58]. Table 2.2 summarises studies done on other types of zeolite membranes. LTA zeolite membranes were prepared under atmospheric pressure[67-69] and, since the syntheses are conducted at temperatures below 373K, it was not necessary to seal the vessel or reactor.

Table 2.2: Summary of studies reported on zeolite membranes other than MFI membranes

Author	Product	Composition $Na_2O:SiO_2:Al_2O_3:TPA:H_2O$	Synthesis conditions	Support	Thickness (μm)
Suzuki *et al.*[70]	MOR	0.38:1:0.025:0:40	433K, 40 h	Silica-alumina, quartz glass	23
Geus *et al.*[25]	ANA	1.6:1:0:1.5:166.66	453K, 1-5 d	α-alumina	
Masuda *et al.*[59]	LTA		343-373K, 6-18 h	α-alumina	5-25
Mimura *et al.*[71]	ANA	67.5:67.3:1.0:1.0:3375	423-453K, 0.1-3 d	α-alumina	60
Kita *et al.*[67]	LTA	2:2:1:0:120	373K, 3.5 h	α-alumina (1 μm)	30
Yamazaki *et al.*[69]	LTA	4.25:2.5:1.0:0:111	433K, 40 h	Silica	
Yamazaki *et al.*[55]	MOR	3:20:1:0:200	453K, 1-5 d	Stainless steel	

MOR – Mordenite
ANA - Analcime
LTA – Zeolite A (Linde Type A)

Kita *et al.*[67] coated a porous α-alumina support with seed crystals of Na-type LTA before placing the support in a gel with composition 2.0 Na_2O: 2.0 SiO_2: Al_2O_3: 120 H_2O. After hydrothermal treatment at 373K for 3.5 h, a LTA membrane of approximately 30 μm thickness was obtained. Prolonged crystallisation resulted in the formation of P-type zeolite crystals in the membrane. Yamazaki *et al.*[69] also used seed crystals of LTA zeolite to synthesise LTA membranes on three different supports, silicon plate, quartz glass and a filter of quartz glass fiber. Masuda *et al.*[59] prepared LTA membranes on the outer surface of a cylindrical alumina support by repetitive hydrothermal treatment. MOR membranes on porous silica-alumina[70]and sintered stainless steel[55] as well as ANA-type membranes on an alumina support were also prepared[71].

2.3.1.3 Solid gel conversion technique

Bibby and Dale[72] first synthesised zeolite from a non-aqueous system, suggesting that water, as solvent, is not essential for the crystallisation of zeolites. Pure silica zeolites with a sodalite (SOD) structure were obtained using ethylene glycol as solvent. Since then, several types of zeolites have been synthesised using organic solvents. Huo and coworkers[73] synthesised Al-free MFI, ZSM-39 (MTN) and ZSM-48 using glycerol, ethylene glycol or butyl alcohol as solvent. Xu *et al.*[74] synthesised MFI and ZSM-35 (FER) from an aluminosilicate gel in a solution of ethylenediamine

(EDA) and triethylamine (Et_3N), showing that not only alcohol but also amines are effective as solvents in non-aqueous systems.

Zeolites have been synthesised from solid gel in gas phase. Xu *et al.*[75] were the first to report on the conversion of a dry aluminosilicate gel to MFI by contacting it with water vapor, EDA and Et_3N at 453K. Kim *et al.*[76] showed that this solid gel conversion technique could be used for synthesising various types of zeolites, and referred to this method as the vapor phase transport (VPT) method. It was shown that different organic templates give different crystallisation fields of MFI in the Na_2O-SiO_2-Al_2O_3 system[75-77].

Dong *et al.*[78] first used the VPT method to synthesise self-supporting MFI and FER membranes. Another solid gel conversion technique was studied by Crea *et al.*[79], who used the tetrapropyl ammonium (TPA) cation as a templating agent. Self-bonded MFI crystals in pellet form were produced, under steam, from a dense hydrogel which contained the TPA cation. Althoff *et al.*[80] described a new reaction for the synthesis of MFI zeolites from a fluoride-containing dry gel, with the composition 80 SiO_2: Al_2O_3: 145 NH4F: 6 TPABr: 0-300 H_2O.

2.3.1.4 Zeolite-in-metal membranes

Kolsch *et al.*[81,82] developed a particular method for preparing a defect-free membrane. High quality MFI (Al-free) crystals were embedded in silver or nickel foils by galvanic metal deposition. The MFI crystals were vertically orientated in the resulting MFI-in-metal membrane, as shown in Figure 2.10.

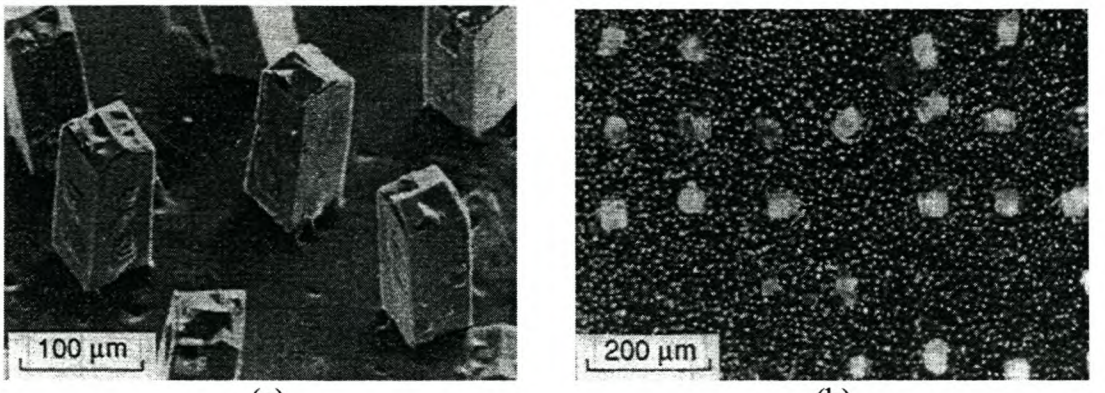

(a) (b)

Figure 2.10: (a) SEM micrograph of the vertically orientated MFI crystals attached to an Ag lacquer, which conducts electricity. (b) A transmission light microscope picture of the membrane after electrolysis, where every light spot corresponds to a MFI crystal vertically embedded in the Ni foil.

$AlPO_4$-5 crystals were synthesised using microwave heating and the resulting crystals were aligned in the mesh of a Ni grid, after which electrochemical deposition of Ni was done[83,84]. The resulting membranes were one-dimensional because of the one-dimensional pore system of the $AlPO_4$-5 crystals.

2.3.1.5 Single crystal membranes

Shah and coworkers[85-87] prepared MFI (Al-free) membranes by embedding a single large (300 × 100 × 100 µm) MFI crystal in an epoxy resin, in order to measure the rates of hydrocarbon transport in a MFI crystal. The diffusivities of C_4 hydrocarbons and aromatic hydrocarbons were determined and are listed in Table 2.3. This type of membrane is useful for the measurement of intracrystalline diffusivity in zeolites rather than for use in gas separation purposes.

Table 2.3: Diffusion coefficients of butane and aromatics in MFI at 298K[86]

Hydrocarbon	**Inlet pressure [Torr]**	**Diffusivity[a] [$cm^2 s^{-1}$]**	**Diffusivity[b] [$cm^2 s^{-1}$]**
n-butane	11.70	1.01×10^{-8}	
i-butane	12.00	1.12×10^{-8}	
benzene	9.93	8.387×10^{-14}	7.489×10^{-14}
toluene	9.56	8.835×10^{-14}	1.909×10^{-13}
m-xylene	9.38	6.173×10^{-14}	1.192×10^{-13}
o-xylene	10.13	5.989×10^{-14}	1.637×10^{-13}
p-xylene	8.91	8.903×10^{-14}	1.036×10^{-13}

(a) Diffusivity calculated from the time lag

(b) Diffusivity calculated from the slope

2.3.1.6 Zeolite nanocrystals colloidal suspension

Tsapatsis and coworkers[88] demonstrated that stable colloidal suspensions of ultra-fine zeolite L (LTL) particles can be formed and used for thin film preparation. The preparation scheme is shown in Figure 2.11.

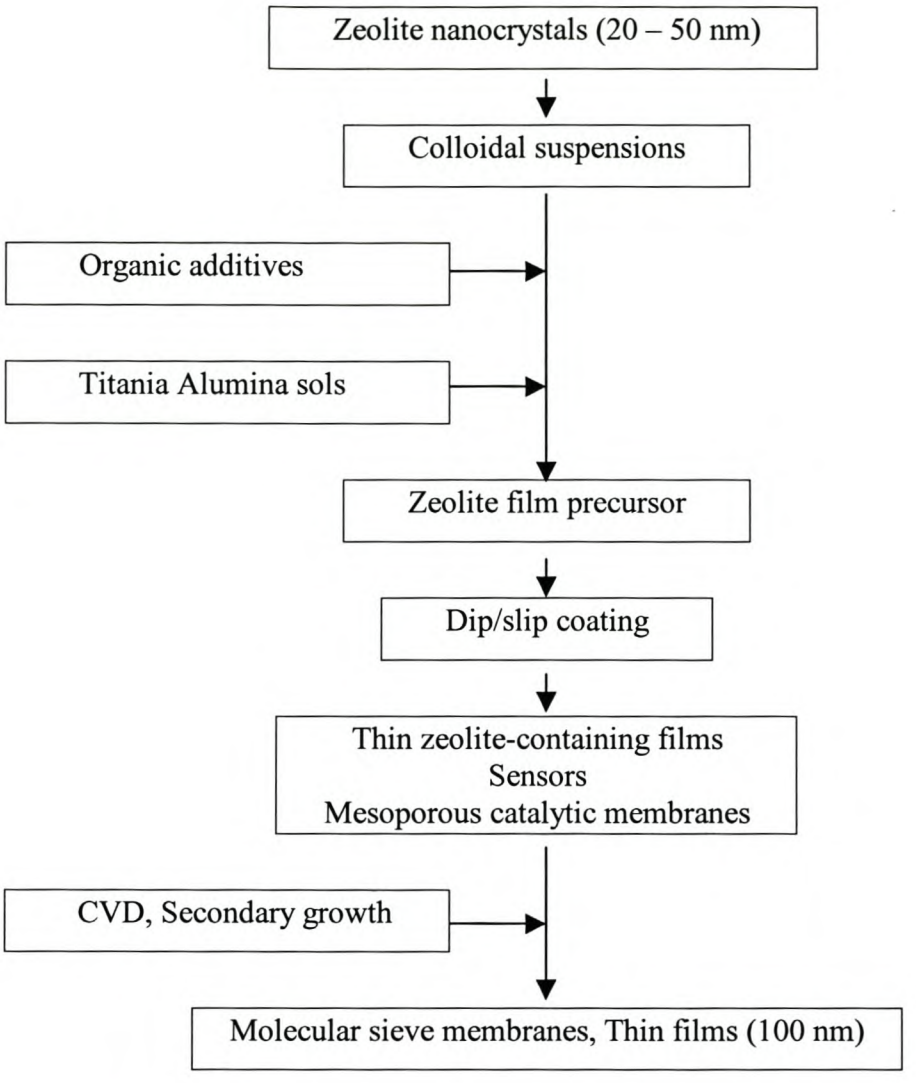

Figure 2.11: Schematic representation of the suspension of colloidal zeolite into a membrane.

The average zeolite particle size in the suspension, as determined by dynamic light scattering (DLS), was as low as 20 nm. Films, free of micro cracks, were prepared from these suspensions by evaporating the water.

2.3.1.7 Seed film method

Continuous, thin MFI (Al-free) films (<100 nm) were prepared on a single crystal silicon wafer. This involved a two-step mechanism[89]. First, a monolayer of discrete colloidal zeolite seed crystals was adsorbed on the substrate. Second, the crystals were allowed to grow to form a continuous film, under hydrothermal treatment in a synthesis mixture with a composition of 3 TPAOH: 25 SiO_2: 1500 H_2O: 100 EtOH.

This technique is very useful for the preparation of an ultra-thin zeolite film, which can be used as sensor devices.

2.3.2 Aspects of zeolite synthesis

2.3.2.1 Synthesis parameters

Temperature

An increase in the synthesis temperature will accelerate all the processes which take place during the synthesis, such as dissolution and mixing of nutrients, liquid phase diffusion, crystal nucleation and growth. Also, due to increased silica solubility, the relative silica supersaturation is decreased somewhat and hence (depending on kinetics) one of these above-mentioned processes will be enhanced. The effect of temperature on the zeolite growth curve is schematically shown in Figure 2.12.

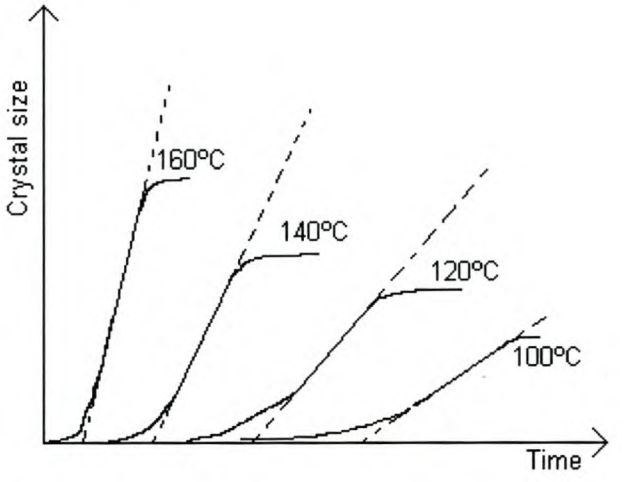

Figure 2.12: Effect of temperature on zeolite crystallisation, showing the change in linear crystal growth rate and induction time.

Increasing the temperature will promote crystallisation by enhancing the rate of crystal growth and decreasing the induction time. The induction time is the period before crystal growth, during which the conditions in the synthesis mixture are optimised for zeolite growth. This occurs through rearrangement of aluminosilicate species and the formation of crystal nuclei, both of which are a strong function of temperature. From the linear growth rates, as a function of temperature, the apparent activation energy for zeolite growth can be obtained. This generally ranges from 40 to 100 kJ/mol, indicating that the rate-determining step for crystal growth is a chemical

step. It is probably the hydrolysis/condensation reaction of a building block at the crystal surface, rather than a diffusion step, which would have a value of ca. 16 kJ/mol, depending on the viscosity of the solution[90]. In the syntheses of zeolite NaA[91] and NaY[92] and in MFI-type syntheses[93,94], less crystals are nucleated at higher temperatures, indicating the relative enhancement of crystal growth over crystal nucleation. Lowering the temperature to ambient is expected to yield a very large number of extremely small and hardly growing nuclei. This phenomenon was observed when the effect of the ageing of NaA was studied. The nuclei formed at low temperatures get the chance to grow at higher temperatures.

Effect of relative supersaturation

Relative supersaturation (σ) is the driving force for crystallisation, from solution, of zeolite building units. An excess of these building blocks is a prerequisite for nucleation and crystal growth. As the relative supersaturation increases, the crystal morphology is altered due to changes in the growth mechanism. At low supersaturation ($\sigma < 1.5$) the zeolite crystal can grow smoothly in a layer-by-layer mode, by two-dimensional nucleation or, preferably, when screw dislocations are present, in a spiral-growth mechanism and according to the BCF-theory[95]. The latter has been observed for zeolite A[96], and recently for zeolites Y[97] and heulandite[98], using atomic force microscopy (AFM). Higher supersaturation will change the growth mechanism, resulting in roughened growth as the smooth crystal faces disappear. The transition between smooth and roughened growth for different crystal faces of the same type of zeolite may appear at different supersaturations. This is illustrated in Figures 2.13 and 2.14. Figure 2.13 shows the smooth octahedral [111] faces of relatively large (4 μm) zeolite Beta crystals[99] and Figure 2.14 shows the roughened growth of which the crystalline surface cannot be identified with indices.

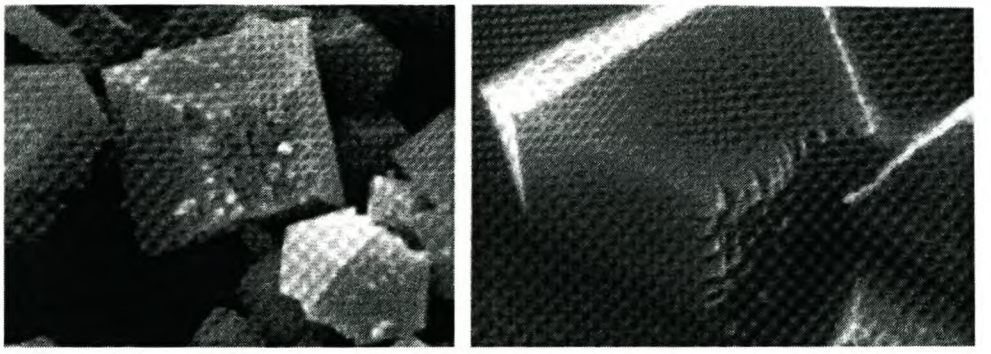

Figure 2.13: Electron micrographs of zeolite Beta crystals showing smooth octahedral [111] faces[99].

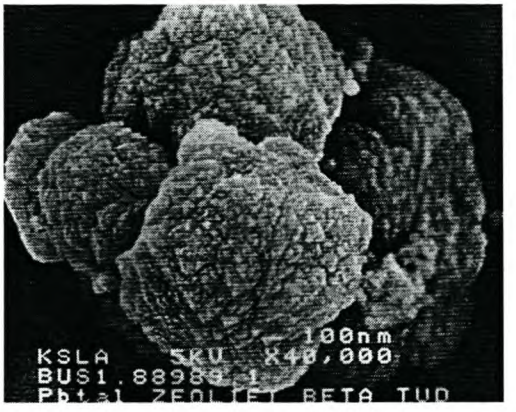

Figure 2.14: HRSEM micrograph of zeolite Beta, with an apparent primary particle size of 30 – 50 nm, forming aggregates of about 1 μm[100].

The same occurs with the so-called cubic MFI-type crystals, where smooth [010] and [100] faces coexist with rounded [h01] faces. Growth above the roughening transition will often be faster at the edges of a crystal face than in the middle, as the heat of crystallisation can be transferred to the solution most easily at these places. With cubic crystals this may lead to "hopper" crystal faces[91], and at even higher supersaturations to dendritic growth. All the zeolite building blocks must be in supersaturation for crystal growth to occur. Furthermore, zeolite synthesis systems are generally highly buffered with respect to soluble silicate building blocks, and thus independent of nominal silica concentrations, *i.e.* the total amount of silica added to the system.

Concentrations of nutrients

A model study on the crystallisation of silicalite-1 on the [100] surface of a silicon wafer showed that a concentrated synthesis mixture resulted in the formation of a gel layer on the support and subsequently growth of crystals with a lateral orientation. A diluted synthesis mixture gave axially-orientated crystals[101], as shown in Figure 2.15.

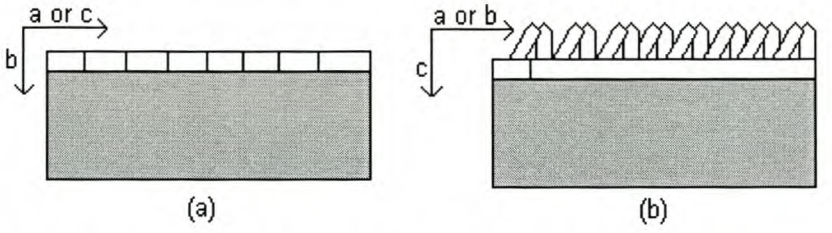

Figure 2.15: (a) Lateral and (b) axial orientation of MFI-type crystals on a silicon wafer support.

When the silicalite-1 crystals are laterally orientated, the b-direction of the crystals is perpendicular to the support and the a-direction is parallel to the support. This configuration is most suitable for membrane applications. In the axial orientation the c-direction of the crystals is perpendicular to the support surface, and thus this configuration is most suitable for catalysis at the internal MFI crystal surface[102].

Nucleation

The nucleation rate must be high, for formation of a large number of small crystallites. For this purpose the template concentration should be high and the nutrients well mixed. It was shown in the crystallisation of silicalite-1 that the gel spheres do not contain templates and that nucleation starts at the interface between the bulk liquid phase and the gel[101]. The same type of crystal growth is postulated for the laterally-orientated crystals on silicon. In dilute synthesis mixtures nucleation starts at the support surface[103]. Pretreatment of the support surface by impregnation or spincoating with an appropriate template solution can direct the formation of crystallites on the support. This concept was successfully used in the synthesis of ordered films of crystalline mesoporous silica, which were formed after pretreatment of a mica support with template solution[104].

Another example of crystal orientation is the significant improvement in the *in situ* zeolite beta crystallisation by pre-adsorption of the template onto the alumina supports[105]. Improved nucleation can also be obtained by the use of seed crystals, as applied in the crystallisation of silicalite-1 on carbon fibres[106]. The surface of the fibers was modified by adsorption of a cationic polymer, followed by adsorption of colloidal seed crystals of silicalite-1. These seeds induced the growth of a continuous silicalite-1 film.

Mixing of nutrients

In order to achieve fast nucleation and crystal growth, the mixing of the nutrients is of great importance. The gel-ageing period that normally precedes a synthesis therefore serves to optimise the distribution of nutrients. Slow release of silicon species from the precursor into the mixture is one of the main reasons for the slow crystallisation of zeolite beta in conventional synthesis procedures. In aluminium containing syntheses, the formation of a separate, insoluble aluminium hydroxide phase during ageing can occur. To prevent this, the aluminium salt is dissolved separately and slowly added to the aqueous mixture of silica and template.

2.3.2.2 Support material

Type of support

The type of support used for zeolite synthesis is, in the first instance, dependent on the application of the zeolite coating. In most cases the support is needed to provide mechanical strength to the zeolite layer or, at least, to facilitate the handling thereof. When zeolite coatings are used in membrane applications, the support should be porous for gasses or liquids. For catalysis purposes the support should have a high surface area in order to attain a high activity per volume of catalyst and have a reasonably good thermal conductivity to transport the heat flow. For electrochemical purposes the support is often required to be electrically conductive. In the case of a piezoelectric sensor system the support should be quartz or another piezoelectric material, if the use of an intermediate layer is to be avoided.

Hydrophobicity/hydrophilicity of the support surface

If zeolite crystals are synthesised from a clear solution and nucleation takes place at the surface, then the support surface must contain hydroxy groups, in order for

chemical bonds to form between the support surface, the nuclei and eventually the growing crystals. If the zeolite crystals are synthesised from a gel phase, good wetting of the support surface by the gel should take place for effective crystal growth. The support surface must be cleaned before synthesis, so that both bonding and wetting can be maximised. The hydrophilic character of the support can also be enhanced by oxidation or pretreatment with the template.

Stability of the support

In all cases the support must be stable under the conditions of synthesis, which are usually high temperature and high pH. In other words, the kinetics of dissolution of the support must be slower than the kinetics of crystal growth. It could however be advantageous to keep these two kinetic factors comparable, as will be discussed later in Section 4.4.6[107]. The formation of a gel layer during the synthesis can protect the support surface and create a local environment with a lower pH, preventing dissolution of the support. During synthesis some interaction between the gel and the support surface might take place, leading to the formation of a connecting layer between the support and the zeolite layer. This layer could be used as a catalytic domain between the support surface and the zeolitic coating[102].

Support-zeolite interactions

The bonding of zeolite crystals to the support surface is determined by the hydrophilicity of the support (number of OH-groups per nm^2), the support texture and the zeolite growth mechanism. The possible connecting interactions between support and zeolite, for MFI crystals, for example, are shown in Figure 2.16 (a-c).

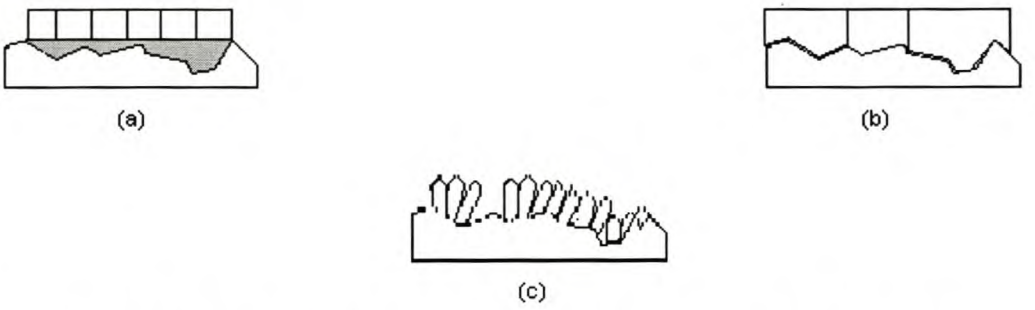

Figure 2.16: Possible connecting interactions between support and zeolite crystals, (a) amorphous interconnecting layer, (b) adherence to corrugation of the support and (c) chemical bonding at support surface.

In Figure 2.16(a) the crystals are obtained by crystallisation from a gel layer on the support. Nucleation commences at the interface between the gel and the bulk liquid, after which crystal growth progresses towards the support surface. If the crystallisation is incomplete or if the support dissolves, an amorphous or intermediate phase is formed which connects the crystallites. In Figure 2.16(b) the crystals are also formed from a gel layer on the support, but here the gel phase is consumed completely during crystallisation. In this example, chemical bonds can be present between the support and the crystal layer, or the adherence could be via van der Waals interactions or hydrogen bonding to the corrugated support surface. Figure 2.16(c) shows a crystal layer that is formed by nucleation at the support surface and subsequent crystal growth from the surface. Under these circumstances the crystals are mainly chemically bonded to the support surface.

During the calcination process, condensation of crystal Si-OH and surface -OH groups could increase the amount of chemical bonds. In this context the thermomechanical properties of zeolites and the supports (expansion coefficients) should be considered[108].

Setting of the support

Researchers have proposed various ways in which to place the support in the synthesis solution[40,58]. Figure 2.17 (a-d) shows four typical ways of placing the support in an autoclave.

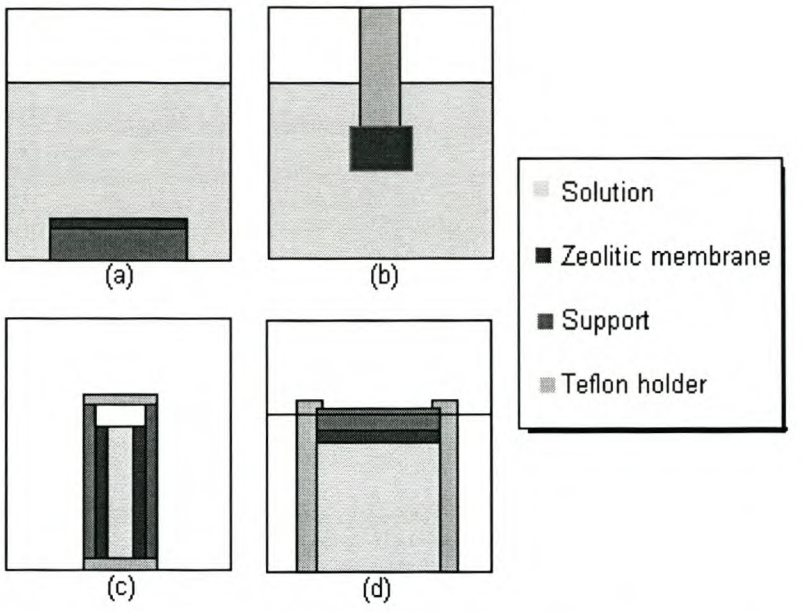

Figure 2.17: Four typical placement positions of a support in an autoclave.

The most typical placing of the support in the autoclave is shown in Figure 2.17(a). Porous supports were placed horizontally at the bottom of a Teflon vessel. This method was later improved by Jansen *et al.*[40], as shown in Figure 2.17(b). Here the support was placed in the upper part of the synthesis mixture, with the aid of a simple Teflon holder mounted on the inner side of the cover of the autoclave. This configuration was preferable as convection, which influences nucleation, is avoided.

Jia *et al.*[58] transferred a gel into an alumina tube and plugged both ends with Teflon caps, in order to grow crystals on the inner surface of the alumina tube only, as shown in Figure 2.17(c). In Figure 2.17(d), the porous plate was supported horizontally by a Teflon holder. The upper level of the synthesis solution was kept at a constant height in order to be able to dip only the bottom part of the support into the synthesis mixture, therefore growing crystals on the bottom part of the support only.

In hydrothermal synthesis, the placement of the support does seem to play an important role in the formation of the zeolite membrane. This could be partly attributed to the deposition of the homogeneously formed nuclei and crystals on the support, either by convection or segregation.

2.3.3 Aspects of crystal growth in membrane formation

2.3.3.1 Crystal type and size

Selection of a certain zeolite depends on the eventual application of the zeolite coating. The type of zeolite determines the size and, to a lesser extent, the hydrophobicity/hydrophilicity of the species that can be contained in the zeolite crystal. For catalysis and membrane applications, diffusion limitation is a factor to be taken into consideration. In the case of optical or electrical applications, often no mobility of species other than electrons, protons or photons within the zeolite is required. Larger immobile clusters can now be formed, or smaller pore zeolites can be used, as shown in Table 2.4.

Table 2.4: Approximate diameters of molecules or clusters in zeolites and zeolitic materials[103]

	Diffusion range (Å)	Max. adsorption size (Å)
Clathrasil	< 2.5	3-4
Medium-pore zeolite	< 5.5	5.5-8
Large-pore zeolite	< 8	9-15
Mesoporous material (MCM-41-type)	< 20-80	20-80

Only small molecules, such as helium and hydrogen and up to carbon dioxide, will diffuse through Clathrasils, such as, in the case of DD3R, whereas large-pore zeolites will easily permit branched hydrocarbons to permeate.

The hydrophobicity of a zeolite is determined by the intrinsic charge of the framework. An all-silica framework without defects has zero charge and is quite hydrophobic. On the other hand, a zeolite with a silicon to aluminum ratio of 1 has a highly negative framework charge, which has to be compensated for by cations residing in the channels. This makes the total system quite polar, and therefore hydrophilic. Certain zeolites can be made with different silicon to aluminum ratios, and thus different hydrophobicities. Clathrasils can only be made with high to very high Si/Al ratio, zeolite A has a Si/Al ratio of about 1, while a MFI-type zeolite can be made with a Si/Al ratio ranging from 1 to infinity.

Having chosen the zeolite type, depending on the application, the size of the zeolite crystals is of importance. In the case of monolayer coverage on a support, the zeolite crystal size will directly determine the layer thickness. When diffusion of a species within the zeolite phase is relevant, the crystal size should be minimised. With catalysis, external surface activity might result in loss of selectivity. Reducing the crystal size will proportionally increase the ratio of the external to internal surface area. Thus, the ratio of energies of adsorption/desorption versus diffusion will change and contribute in the overall flux of the membrane.

The crystal size will also have an effect on the pinhole size, which is of importance in the case of membrane separation. This is schematically illustrated in Figure 2.18. Not only will a reduction in crystal size reduce the pinhole size, but the morphology of crystals will change. This is very advantageous for separation purposes.

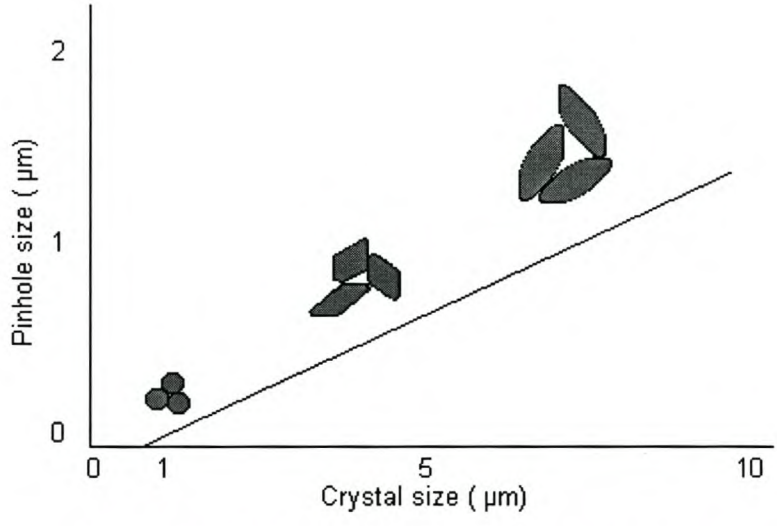

Figure 2.18: Pinhole size versus crystal size in a zeolite layer.

2.3.3.2 Crystal orientation

For certain applications and zeolite types it may be advantageous to have a coating consisting of oriented crystals. Many zeolites and $AlPO_4$'s possess a one-dimensional channel system. Generally, the longest crystal axis runs parallel with the channel direction, which is unfavorable for diffusion. In order to maximise

accessibility, in this case, the crystals forming the coating should be orientated with their long axes perpendicular to the support surface. On the other hand, cubic or spherical crystals with a three-dimensional channel system have the least benefit from a preferential orientation of the individual crystals, as the reduction in diffusion pathway through the zeolite is minimal. An example of this is zeolite A, which has actually been prepared in an oriented coating of about 500 nm thickness by secondary growth of a deposited crystallite suspension[109].

Epitaxy

Three stages of crystal orientation are illustrated in Figure 2.19 (a-c). Of these, it is epitaxial growth which is the ultimate form of orientated growth.

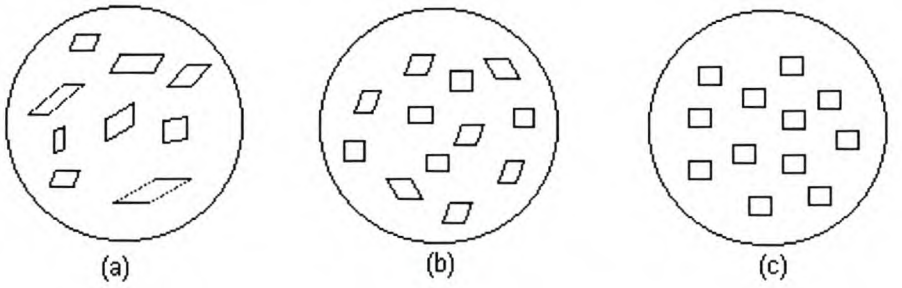

Figure 2.19: Progressive ordering of crystals on a disk support surface: (a) non-oriented, (b) texture orientation; a crystal plane is parallel to the support surface, (c) epitaxy; also in plane orientation[103].

In the case of epitaxy, a nucleation and growth relationship exists between two crystalline phases, where the guest crystal phase grows in a structure-dependent manner onto the host crystal[110]. Epitaxial growth can occur by formation from solution, melt, or from gas-vapor phase. Both nucleation and growth stages can be important in obtaining epitaxy. After nucleation, growth of the nuclei will lead to agglomerates and island formation. At a later stage, these islands join up until only canals are left. Eventually these will also disappear and a continuous film will be obtained. In certain systems it has been observed that the islands drift on the support during growth, that they even rotate and that they rapidly merge after contact via a surface-diffusion process. In growing films recrystallisation by grain boundary

migration occurs also. These grain boundaries are formed in the necks between islands of different orientation and remain there until the neck is eliminated. This recrystallisation, or grain growth, occurs rapidly when the islands are small, but after a certain critical growth stage, no further recrystallisation can occur by this process. Further grain growth can be achieved by annealing the final film.

Important conditions for epitaxial growth are: low supersaturation and high adsorption energies. These conditions are difficult to attain during zeolite synthesis. Often the supersaturation is quite high in order to form the metastable zeolite phases. Adsorption energies of zeolite building blocks on supports will have to be high. The best opportunity for epitaxial growth must be the use of a zeolite template/support combination that forms a strong interaction, where the templating function towards the zeolite is also substantial. The latter is necessary in order to use relatively low supersaturations. It is generally found that the zeolite-building block interaction is much larger than the zeolite-support and building block-support interactions. Under these conditions epitaxial growth will not occur.

2.3.3.3 Crystal growth modes in the context of membrane formation

Growth modes

Thin films are formed on a substrate by a process of nucleation and growth. The initial stage is the formation of small clusters of the film material from individual atoms or molecules. A (continuous) film is formed as time progresses and more clusters are nucleated that grow and coalesce[111]. A general theory on the formation of coatings, including the thermodynamic and kinetic aspects of film formation, have been reviewed by Jansen *et al.*[40]. A classification of different growth modes is made according to the type of film formed. The growth mode determines the morphology, structure and properties of the film surface. Types and characteristics of the most observed film growth modes are given in Table 2.5. Generally, the most desired growth mode is a uniform monolayer or multilayer coverage with a single crystal structure, formed according to the layer mode.

Table 2.5: Film growth modes and their resulting coverage[40]

Growth mode	**Coverage**
Layer mode (*Frank van der Merwe mode*)	Substrate coverage by one or a few mono-atomic layers.
Island mode (*Volmer-Weber mode*)	Substrate coverage by nucleation and growth of separate island-like crystallites of multi-atomic height. Grain boundaries may be developed between the separate crystallites and the film may become polycrystalline.
Layer-plus-island mode (*Stranski-Krastanov mode*)	Combination of layer and island growth. Formation of one or more monolayers is followed by growth of island-like crystallites on top of the monolayer/s.
Continuous mode (*normal or liquid-like mode*)	Substrate coverage by simultaneous filling of several monolayers. Filling is a random process and not nucleation mediated. Film is of low crystallinity or even amorphous.

The reason or reasons for the formation of different growth modes is still not fully understood, but Bauer[112] gave a thermodynamic explanation of this phenomenon. Before the formation of the film, a single substrate/solution (or gel) interface with specific free energy σ_s (J/m^2) exists. After formation of a continuous, uniformly thick film, the specific energies of the film/solution (or gel) (σ_f) and the substrate/film (σ_{sf}) result in the following energy change: $\Delta\sigma = \sigma_f + \sigma_{sf} - \sigma_s$, where $\Delta\sigma$ represents the specific energy change of film formation. Obviously, if $\Delta\sigma \leq 0$, then the formation of the film as a continuous layer is energetically favorable; this is the thermodynamic criterion for layer growth. Conversely, when $\Delta\sigma > 0$, the system is in a lower energy state if the film is broken into separate parts (islands) and this, thermodynamically, is the criterion for island growth. The $\Delta\sigma \leq 0$ condition implies that binding between a molecule of the film and a molecule of the substrate is stronger than, or equal to, the binding between two molecules of the film, and corresponds to the condition for complete wetting of substrates by liquid films. The opposite is true when $\Delta\sigma > 0$, which is also the condition for incomplete wetting; a film/substrate molecular pair is then more weakly bound than two molecules of the film. The

conclusion from the above considerations is that for a given film/substrate system (i.e. $\Delta\sigma$), thermodynamics favor either the layer or island mode of growth.

Membrane formation

Researchers have proposed various formation processes for zeolite membranes. Sano *et al.*[51] proposed the formation process for a MFI membrane as shown in Figure 2.20. The MFI zeolite membrane was formed by successive accumulation of large zeolite crystals (5 – 10 μm) on the support, followed by filling of the voids, among the large crystals, with microcrystals.

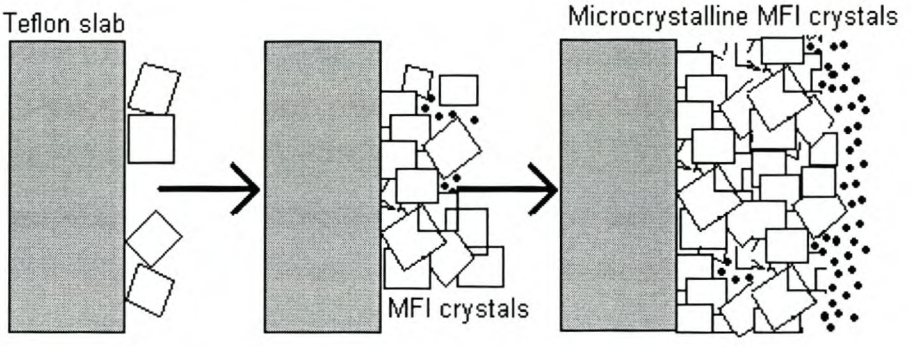

Figure 2.20: Formation process of a MFI membrane as proposed by Sano *et al.*[51].

Myatt and coworkers[53] proposed four mechanisms for zeolite membrane formation, as shown in Figure 2.21 (a-d), comprising the following steps.

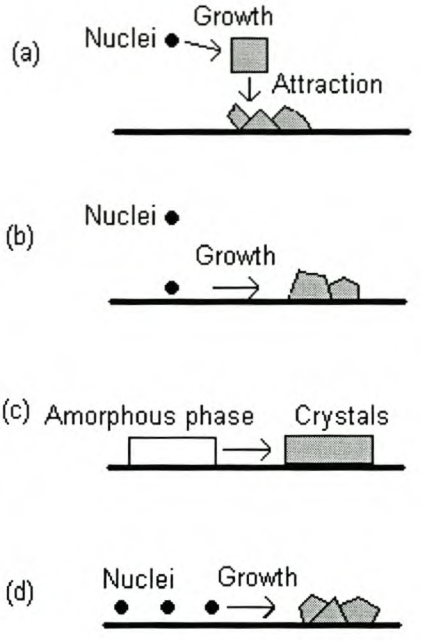

Figure 2.21: Formation mechanisms of zeolite membranes as proposed by Myatt *et al.*[53].

(a) Production of nuclei and growth of crystals in the bulk solution followed by their attraction to, or collision and association with, the substrate.

(b) Production of nuclei in the bulk solution, but diffusion to and accumulation at the support before significant growth has occurred.

(c) Diffusion of colloidal amorphous aluminosilicate to, and concentration thereof at, the substrate, providing more favorable conditions for nucleation and growth in the vicinity of the substrate.

(d) Production of nuclei on the substrate surface, followed by growth.

Self-supporting LTA membranes were hydrothermally synthesised on a polyethylene substrate from a clear solution which contained no precipitate. After crystallisation for 18 h the clear solution became slightly cloudy and after 24 h a deposit was observed on the polyethylene substrate. Due to the fact that clouding is always observed prior to LTA deposition, it was concluded the LTA membrane was formed by the mechanism described in (a). Valtchev and co-workers[113] reported on the growth of MFI and FAU (Y type) zeolites on a copper substrate. Three stages of

film growth were reported: (i) initial nucleation on the substrate, (ii) linear increase in crystal size and (iii) saturation of film growth. These are similar to the steps in the formation mechanism described in (d). In the formation process proposed by Kita *et al.*[67] a gel layer is first formed on the surface of the support, after which it is crystallised. This mechanism correlates with (c) above.

Jansen *et al.*[40] prepared orientated MFI crystals (a straight-channel pore system perpendicular to the support surface) on a support. They studied the crystallisation process of MFI particles and membranes in detail and proposed a novel mechanism for the formation of these orientated MFI membranes. According to an *in situ* observation of a synthesis, without supports, large gel spheres were formed during crystallisation. IR spectroscopic and elemental analyses indicated that no TPA ions were present in the gel phase, indicating that the crystallisation started at the interface of the gel spheres and liquid phase, as shown in Figure 2.22. Crystals with smooth, rounded top faces, caused by kinetic roughening under the high supersaturation prevailing, were formed.

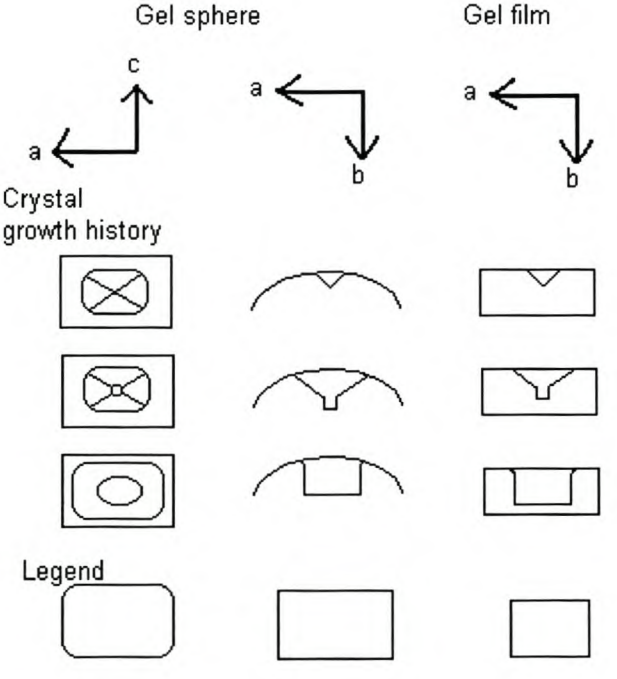

Figure 2.22: Schematic representation of the steps in the crystallisation process of MFI in free gel spheres and a supported gel film[40].

As the MFI crystals on the support showed smooth, rounded top faces and a gel layer was observed on the support prior to the crystallisation, it was concluded that a similar growth process occurred. Thus, the MFI crystals nucleated at the interface of the gel phase formed on the support and the liquid by a mechanism similar to (c), page 41. As soon as the crystal touched the support surface, the ac-plane (the largest plane of the crystal) was attracted to the support and the crystals were laterally orientated with the support.

2.4 Permeation characteristics of zeolite membranes

2.4.1 Theory

In 1990 Barrer[114] proposed a model for the transport of gases through a zeolite layer. A schematic illustration of the five steps involved is given below, in Figure 2.23.

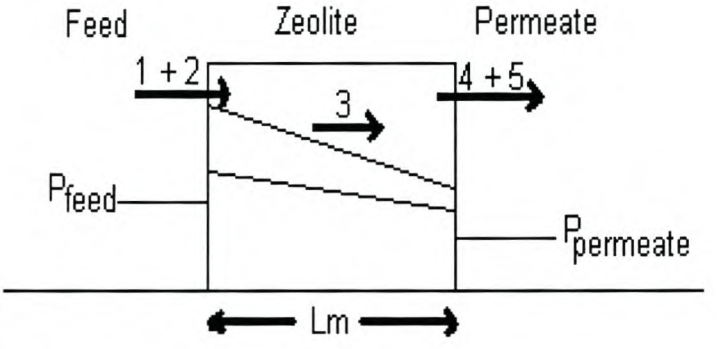

Figure 2.23: Transport model through a zeolite layer, as proposed by Barrer[114].

The following are the proposed 5 steps in which gas molecules are transported across a zeolite crystal.

The two lines in the zeolite layer refer to species with different adsorption strengths within the zeolite pores[114].

(1) Adsorption of gas molecules, from the gas phase, onto the external surface the zeolite.

(2) Transport of gas molecules to the micropores from the external surface of the zeolite crystals.

(3) Intracrystalline diffusion.

(4) Transport of gas molecules from the micropores to the external surface of the zeolite crystals on the support side.

(5) Desorption of gas molecules from the external surface to the gas phase.

Each step or combination of steps can be rate limiting. The conditions on either side of the membrane will determine the rates of steps 1 and 5. The properties of the gases can also determine the rates of steps 1 and 5. High temperatures and weakly adsorbing species will give hardly any adsorption on the external surface. The steps 1 and 2 and also 4 and 5 can be regarded as combined processes, respectively. In pores with sizes matching the kinetic diameter of the gas molecule, step 3 (diffusion in pores) is assumed to be rate determining. The thicker the membrane, the greater is the validity of this assumption.

Two types of gas permeation measurements have generally been performed. These are illustrated in Figure 2.24.

(a) Pressure gradient method (PG), where the flux is measured under a known pressure gradient.

(b) Concentration gradient method (CG), where the measurement is performed under constant pressure, while the driving force is a concentration difference between faces.

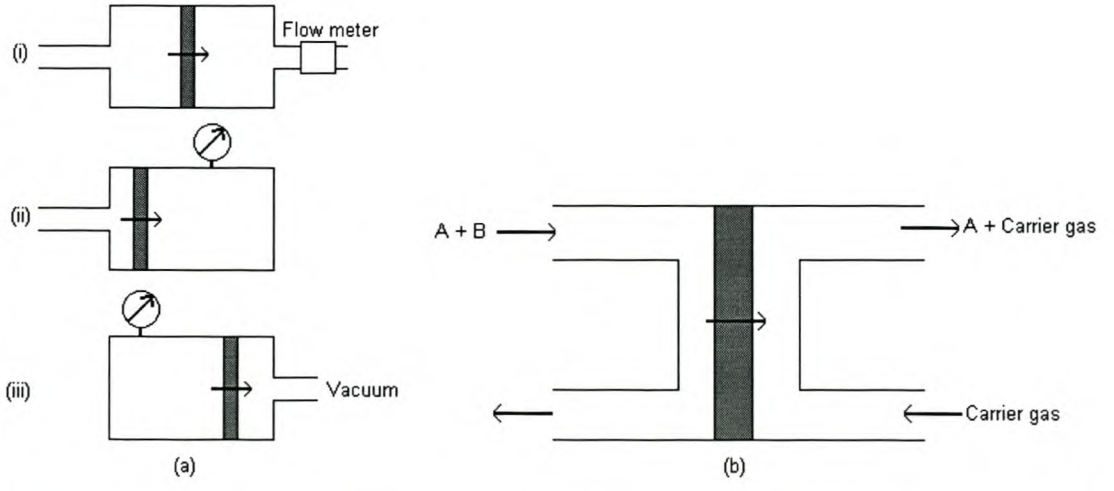

Figure 2.24: Gas permeation measurements: (a) pressure gradient (PG) method and (b) concentration gradient (CG) method.

Either of these methods can be applied under steady state or transient conditions. In the steady-state PG method, the flux is measured under quasi-state conditions such that a constant pressure is maintained on one side of the membrane while the pressure on the other side of the membrane is also kept constant (i). In the other PG method, the downstream pressure is monitored in a closed system of a limited volume while the upstream pressure is maintained (ii), or the upstream pressure is monitored while the downstream pressure is maintained (iii).

Although these methods of measurements provide simple and convenient ways to measure flux, these are restricted to one-component systems, where the required sample amounts for the analysis affect the pressure at the permeate side. In methods (ii) and (iii), a time dependent model should be used because conditions are continuously changing at one side.

The second measurement method (CG) is performed by the Wicke-Kallenbach cell, first introduced by Wicke and Kallenbach[115]. In this method a stream of carrier gas containing a small concentration of the test gas passes over one face of the membrane while pure carrier gas (sweep gas) passes over the other face of the membrane, see Figure 2.24(b). The permeate is analysed by mass spectrometry or gas chromatography. Although this method is available for multi-component permeation measurements, it must be kept in mind that back diffusion of sweep gas occurs and affects the permeation behavior of the objective component.

2.4.2 Permeation studies

2.4.2.1 Single-gas permeation

A summary of the permeation measurements of single-component gases, which include inorganic gases and light hydrocarbons, through MFI membranes, is given in Table 2.6.

Table 2.6: Single-gas permeation measurements through MFI membranes

Authors	**Method of measure-ment***	**Sweep gas**	**T [K]**	**Single-component gases**
Geus *et al.*[25]	PG		294 – 418	H_2, N_2, CH_4, CO_2, O_2, CF_2Cl_2,
Geus *et al.*[26]	CG	He	298	CH_4, Ne, n-C_4, i-C_4
Bakker *et al.*[116]	CG	He	300 – 623	Kr, C_2H_6, Ar, n-C_4, i-C_4, Ne, CF_2Cl_2
Jia *et al.*[57]	PG		293	N_2, He, n-C_4, i-C_4, c-C6, CO_2, CH_4, C_2H_6, C_3H_8
Jia *et al.*[58]	PG		298 – 373	H_2, N_2, He, n-C_4, i-C_4
Kapteijn *et al.*[117]	CG	He	300 – 630	i-C_4
Bai *et al.*[64] and Noble *et al.*[118]	CG, PG	Ar, SF_6	300 – 737	H_2, n-C_4, i-C_4, Ar, SF_6
Meriaudeau *et al.*[63]	PG		298 – 419	H_2, N_2, He, i-C_4
Yan *et al.*[62]	PG		303 – 458	H_2, N_2, He, i-C_4, CH_4, O_2, n-C_4
Yan *et al.*[27]	PG		303 – 453	H_2, N_2, i-C_4, CO_2, O_2, n-C_4, neo-C_5H_{12}
Exter *et al.*[119]	CG	He	200 – 623	CH_4, C_2H_6, C_2H_4, n-C_4, i-C_4
Kusakabe *et al.*[37]	CG	Ar	303 – 423	CH_4, C_2H_6, n-C_4, i-C_4, CO_2, N_2
Kusakabe *et al.*[37]	CG	He	303 – 373	CH_4, He, n-C_4, i-C_4, CO_2, N_2
Bakker *et al.*[35]	CG	He	193 – 673	CH_4, C_2H_6, C_2H_4, C_3H_8, C_3H_6, n-C_4, i-C_4, CO_2, H_2, i-C_8
Vroon *et al.*[66]	C	He	273 – 473	CH_4, C_2H_6, C_3H_8, n-C_4, i-C_4

* See 2.4.1 for explanation of methods

Only a few such measurements have been carried out above 450K[45,46,63,115] since it is difficult to seal an apparatus at a high temperature, as polymeric sealing materials cannot be used.

The permeability, defined in Equation 2.1, is a term generally used to describe the performance of polymeric membranes, while membrane performance in inorganic

membranes is described by the term, permeance (Equation 2.2). This is due to the fact that the effective thickness of inorganic membranes cannot easily be determined.

$$P'(Permeability) = \frac{Flux[mol.s^{-1}.m^{-2}].d[m]}{\Delta p} \qquad 2.1$$

$$P(Permeance) = \frac{Flux[mol.s^{-1}.m^{-2}]}{\Delta p} \qquad 2.2$$

Permeation of hydrocarbons (alkanes and alkenes) through a MFI membrane was thoroughly studied by Bakker *et al.*[35]. It was shown that the order of permeation flux at 100 kPa feed pressure at steady state was: methane > ethane > propane > n-butane >> i-butane. This showed that the permeation fluxes decreased with increase in molecular size. It was shown that the alkenes permeated faster than their alkane counterparts.

Geus *et al.*[26] performed some transient gas permeation measurements on CH_4, n-butane, neon and i-butane at room temperature. The permeation values were in the following order: CH_4 > n-butane > neon > i-butane. They reported a high permeance ratio of 64 for n-butane to i-butane at 298 K. This was attributed to the larger kinetic diameter of i-butane than that of n-butane.

2.4.2.2 Mixed-gas permeation

Tests for the permeation of mixed gas systems through zeolite membranes were carried out on a Wicke-Kallenbach cell. In most cases either Ar or He was used as sweep gas. A summary of results of studies conducted on the permeance of two-component mixtures is given in Table 2.7.

Table 2.7: Two-component gas permeation measurements

Authors	**Sweep gas**	**T [K]**	**Two-component gases**
Tsikoyiannis and Haag[49]	He	296, 322	N_2/O_2, H_2/CO, n-C_6/2,2DMB*
Geus *et al.*[26]	He	298 – 623	CH_4/n-C_4, CH_4/n-C_4/i-C_4
Bai *et al.*[64] Noble *et al.*[118]	Ar, SF_6	300 – 737	H_2/SF_6, Ar/SF_6, H_2/i-C_4
Kapteijn *et al.*[120]	He	300 – 673	H_2/n-C_4, CO_2/H_2
Kapteijn *et al.*[121]	He	292	C_2H_6/C_2H_4, C_3H_8/C_3H_6
Exter *et al.*[119]	He	300, 200 – 650	CH_4/C_2H_6, C_2H_6/C_2H_4
Kusakabe *et al.*[122]	Ar	373	n-C_4/i-C_4
Vroon *et al.*[66]	He	298 – 473	CH_4/n-C_4, n-C_4/i-C_4, n-C_6/2,2DMB
Bakker *et al.*[35]	He	295 – 623	n-C_4/H_2, H_2/CO_2, n-C_4/i-C_4, CH_4/i-C_8
Bakker *et al.*[116]	He	293 – 623	CH_4/n-C_4, CH_4/i-C_4, CH_4/Ne, i-C_8/CH_4

*DMB: dimethylbutane

Tsikoyiannis and Haag[49] showed that the selectivity for a n-hexane/2,2-dimethylbutane mixture, through a self-supported MFI membrane, was as high as 17.2. This is much higher than that in the Knudsen region, which is 1. Bai and coworkers[64] also reported separation selectivities higher than expected in the case of Knudsen diffusion (H_2/SF_6 = 12.8 and H_2/i-C_4 = 11.9).

Geus *et al.*[26] reported on the transient permeation behavior of a 50/50 methane/n-butane mixture through a MFI membrane. The permeance of n-butane was similar to that in the pure gas permeation experiment for n-butane, indicating that the presence of methane hardly affected the permeation behavior of n-butane. Here, the separation was apparently governed by the reduced mobility of methane within the zeolite micropores, in the presence of strongly adsorbing molecules. Due to the strong adsorption of n-butane, hardly any methane could enter the zeolite pores, resulting in a reduced driving force for methane permeation.

The permeation behavior of a 50/50 methane/n-butane mixture as a function of temperature was also studied. A monotonous increase in the n-butane flux was observed up to 430 K, while the methane permeation rate remained low up to 410 K. At higher temperatures, the methane flow became substantial and even exceeded the

n-butane flow, up to 500 K. At even higher temperatures the methane permeation leveled off. This meant that at low temperatures the methane permeation rate was governed by the n-butane adsorbate concentration, while at higher temperatures the n-butane desorbed, allowing the methane flux to increase (increased mobility of methane). These observed features could be attributed to the fact that both diffusion and adsorption are temperature dependent. Similar trends were observed by Kapteijn *et al.*[120], for the study of the permeation of a H_2/n-butane mixture through a silicalite-1 membrane.

Bakker *et al.*[35] compared the permeation fluxes of alkane/alkene mixtures with those of their single component permeations. Alkenes permeate faster than alkanes in a single component system. In mixtures, however, the position was reversed; the alkanes had a higher permeation rate than the alkenes. They also measured adsorption isotherms of ethane, ethene, propane and propene at 295 K, and determined parameter values of the Langmuir adsorption isotherm fit. The adsorption strength decreased in the following order: propane > propene > ethane > ethene. It was therefore concluded that the strongly adsorbing component suppresses the permeation of the other component in binary systems.

In conclusion, the permeation results of binary mixtures reported in the literature to date, show that:

(i) in many cases the separation factor does not reflect the permeance ratio in a unary system,

(ii) the difference in adsorption strengths plays a major role in the separation factor – strongly adsorbed gases suppress the permeation of weakly adsorbed species and

(iii) an inversion in permeation ratios can be encountered with an increase in temperature, when the separation mechanism shifts from adsorption to diffusion.

2.4.2.3 Vapor permeation

A summary of results of some of the vapor permeation experiments conducted to date is given in Table 2.8.

Table 2.8: Results of vapor permeation experiments reported in the literature

Authors	Sweep gas	T [K]	Vapor phase
Jia *et al.*[58]	He	298, 373	MeOH/H_2
Mariaudeau *et al.*[63]	He	333 – 413	n-C_6, 2,2DMB
Baertsch *et al.*[123]	He	380 – 480	PX, MX, EB, TL, BZ, PX/OX, PX/EB
Funke *et al.*[124]	He	350 – 480	n-C_6, n-C_7, i-C_8, n-C_7/i-C_8, n-C_6/n-C_7/i -C_8

PX: p-xylene, MX: m-xylene, OX: o-xylene, EB: ethylbenzene, TL: toluene, BZ: benzene, 2,2DMB: 2,2-dimethylbutane and MeOH: methanol.

Separation factors larger than 1000 were obtained for MeOH/H_2 mixtures at 373 K, probably due to MeOH adsorption in the MFI pores and therefore blocking the pores for H_2 permeation. Vapor permeation of aromatic hydrocarbons through a MFI membrane was reported by Baertsch *et al.*[123]. Single component permeations of p- and m-xylene were significantly higher than permeances of ethylbenzene, toluene and benzene at 380 – 480 K. However, no separation was achieved with binary mixtures of p-xylene/o-xylene, p-xylene/ethylbenzene, p-xylene/toluene and m-xylene/ethylbenzene at 380 – 480 K. The permeation curves for the mixtures are identical to the pure component permeance curve of the slowest component. It was therefore concluded that the pores of MFI are too small for aromatic hydrocarbon molecules to pass each other. This means that the molecule with the slowest permeation rate limits diffusion and slows the other species down to its "own rate".

Funke *et al.*[124] found that the same MFI membranes, as above, could separate n-octane from i-octane. n-Octane molecules prevent i-octane molecules from entering the zeolite pores in a mixture, resulting in a selectivity for n-octane/ i-octane and no selectivity for p-xylene/ethylbenzene. This shows that subtle differences in molecule size and shape can result in opposite trends in permeation behavior.

2.5 Possible uses of zeolite membranes and coatings

2.5.1 Gas separation

There are many applications of zeolite coatings. The one most frequently reported on is the preparation of zeolite membranes for gas separation purposes. The preparation and testing of zeolite MFI-type membranes for gas separation has been explored extensively[22,25-27,39,48,49,63,64,66,125,126]. Other zeolites applied in membranes are NaA[53,68,69], ferrierite[77,127] and mordenite[77,55,128]. Recently two excellent review papers were published on the subject of zeolite membrane preparation and performance[41,129]. The permeation characteristics of a large variety of molecules through various types of zeolite membranes have been reported[35,60,62,117,120,123,144].

2.5.2 Electroanalysis and sensor devices

In electroanalysis, the measurement of charge, current, or equilibrium potential is related to the concentration of the unquantified electrolyte. In electroanalysis, zeolite coatings are applied in the form of zeolite-modified electrodes[130]. The electroanalytical suitability of zeolite-modified electrodes is demonstrated by:

(i) the use of the zeolite present in the electrode composite or coating to sequester the electrolyte (often via cation exchange with mobile extra-framework cations),

(ii) their ability to follow the pre-concentration step, by sweeping the potential of the electrode to react with the harvested analyte while measuring the amount of Faradaic current that flows, and

(iii) their use in calibration curves, devised using known concentrations of the analyte (preferably in the same solution environment (matrix) as the known, to determine the concentration of the analyte).

Bein and co-workers[131] grew thin zeolite composite films on piezoelectric devices, such as surface acoustic wave devices, and achieved molecular sieving of gas-phase organic electrolytes. They also prepared quartz crystal microbalances, where the mass, due to sorbed gases, is monitored as a change in the frequency of the piezoelectric device[131]. In the latter, microporous thin films composed of a molecular coupling layer, zeolite A crystals, and a porous silica overlayer were formed on the gold electrodes of quartz crystal microbalances (QCMs).

2.5.3 Catalytic membrane reactors

The use of membrane reactors has been advocated for numerous reacting systems. In dehydrogenation reactions, the yield can be increased beyond thermodynamic equilibrium by selectively removing hydrogen from the reaction mixture. Moreover, a catalytic reactor offers the advantage of combining catalysis and separation in the same reactor. An example is the dehydrogenation of ethane[133], using a porous alumina membrane tube covered with Pt crystallites. The catalyst promotes reaction and the reaction products are continuously removed by diffusion through the membrane, causing the reaction to proceed far beyond its equilibrium.

Isomerisation reactions are an example of possible application, where the required isomer yield and purity can be obtained in a single-step continuous process. In all cases, the zeolite-support composite leads to a performance that is beyond the limitations of unsupported zeolites, by adding mechanical strength and, depending on the particular use, improved heat transfer or catalytic activity. For feasible applications of this type of structured catalysts, *e.g.* using MFI- or BEA-type zeolites, advantages in terms of pressure drop, catalyst efficiency or selectivity, or improved mass and heat transfer, should pay back the extra costs of the structured catalyst packing compared to random packing of particles in a fixed bed reactor. Further examples of possible applications are in flue gas treatment, *e.g.* deNOx, selective oxidation and (de)-hydrogenation, *e.g.* ethylbenzene dehydrogenation, trickle flow processes, *e.g.* hydrodesulphurisation and catalytic distillation, *e.g.* methyl-tert-butylether (MTBE), ethyl-tert-butylether (ETBE) and ethylbenzene synthesis.

2.5.4 Pervaporation

Pervaporation is a combination of permeation and evaporation. In pervaporation, part of a liquid feed is separated by a membrane that is selectively permeable for that substance[133], while there is a vacuum on the other side which causes the liquid there to evaporate - no equilibrium. An example is the dehydration of alcohol, i.e. the separation of a water/ethanol mixture. Water is preferentially sorbed in the hydrophilic (zeolite A) membrane material and then diffuses through the membrane and evaporates in the vacuum at the permeate side of the membrane.

Results reported by Kita *et al.*[134-137] showed enormous potential for the application of zeolite A membranes in pervaporation. It was shown that the zeolite A (LTA) membranes synthesised on alumina supports exhibited fluxes and separation factors of water/ethanol mixtures that were superior to results obtained with polymeric membranes. The separation factors (water/ethanol) and the total flux were greater than 10000 and 2.15kg/m^{2}h, respectively, showing that the performance of LTA membranes were the most favorable for pervaporation applications. A summary of some of the results obtained are given in Table 2.9.

Table 2.9: Flux and separation factors of LTA (NaA) membranes in the pervaporation of water/organic mixtures[134]

Liquid	Feed Comp. (H_2O wt %)	Temp. (°C)	Separation Factor	Flux (kg/m^{2}h)
Ethanol	10	75	10000	2.15
	5	75	16000	1.10
Methanol	10	50	2100	0.57
	5	50	2500	0.23
Acetone	10	50	5600	0.91
	5	50	6800	0.83
Dioxane	10	60	9300	1.87
DMF	10	60	8700	0.95

Zeolite membranes produced by microwave treatment of the precursor gels (SiO_2/Al_2O_3 = 2, Na_2O/SiO_2 = 1, H_2O/Na_2O = 120), showed good selectivity and flux through these zeolitic membranes[138]. A summary of the results are shown in Table 2.10, below.

Table 2.10: Pervaporation flux (Q) and separation factor through NaA zeolite membranes synthesised by microwave heating[138].

Mode of Heating		System	Temp	Sep. Factor	Flux (Q)
Temp (°C)	Time (min)	10wt%H_2O	(°C)	(α)	(kg/m^2h)
95	10	H_2O/EtOH	75	2600	1.3
100	15	H_2O/EtOH	75	5300	2.2
		H_2O/i-PrOH	75	5600	1.5
		H_2O/MeOH	50	640	0.4
100	20	H_2O/EtOH	75	2500	1.3
105	20	H_2O/EtOH	75	2600	1.1

In addition to zeolite A membranes, much attention has been given to high silica zeolites as attractive materials (instead of silicone rubber membranes) for organic-selective separation due to their strong hydrophobic nature. MFI (Al-free) membranes have been prepared on α-alumina and stainless steel supports[60,61]. The MFI membrane exhibited a high selectivity for ethanol with a separation factor (α) (EtOH/H_2O) of more than 60 for a 5 vol % aqueous solution. Adsorption experiments for alcohol and water suggested that the high alcohol selectivity was attributed to the sorption of alcohol into the MFI membrane. In their conclusion, the separation of ethanol/water mixture took place mainly through the 1nm pinholes with the high hydrophobic property (zeolite pore sizes between 0.3 – 0.5 nm). Furthermore, lower separation factors were observed in the case of the α-alumina supported MFI membrane, compared to the higher performances of the stainless steel supported MFI membranes. The suggested reason for this phenomenon was that the aluminium was incorporated into the MFI framework, in the vicinity of the alumina support. Liu *et al.* also reported lower separation factors for the alumina supported MFI membranes compared to the stainless steel supported membranes[139]. In their study methanol, ethanol and acetone were separated from their aqueous solutions by pervaporation through the MFI (Al-free) membranes. For methanol/water separation, a relatively constant separation factor between 11 and 14 was obtained over a wide feed range of methanol feed concentration. Separation factors as high as 255 were obtained at an acetone concentration of 0.8 wt %. Generally, the overall selectivity of a pervaporation process is determined by (i) sorption properties of the organic molecule from the

liquid phase into a membrane and (ii) mobility of the organic molecule in the membrane. The mobility of acetone might be less than the mobility of water in the MFI membrane, because acetone is a larger molecule than water and it has a stronger affinity to MFI than water. Therefore, they concluded that the overall separation is determined by the sorption step.

Methylethylketone (MEK) could be preferentially removed from aqueous solution by pervaporation through a MFI (Al-free) membrane as shown by Smetana *et al.*[140]. separation factors ranged from 70-140 for feed concentrations of 1-15 wt % at 307 K. Once again it was shown that the α-alumina supported MFI membrane had lower performance than the corresponding stainless steel supported MFI membrane. In conclusion, it was shown that the MFI membranes could be used for pervaporation applications, however, only the Al-free MFI membranes could be used, due to the fact that the hydrophobicity of these membranes play such an important role.

It was felt that the major gain to be made in this research area would be the preparation of zeolite A membranes in tubular form and thus bringing this technology closer to being brought into practise.

2.5.5 Catalytic distillation

Catalytic distillation involves a combination of distillation and catalysis in a single column[141]. In industry, it is already used in the production of MTBE and cumene. Cumene is formed from benzene and propene:

$$C_6H_6 + CH_3\text{-}CH{=}CH_2 \rightarrow C_6H_5\text{-}CH(CH_3)_2 \quad \text{(exotherm)}$$

Subsequent reactions are the formation of di- and tri-isopropylbenzenes (DIPB, TIPB). These secondary products can react back to form cumene by disproportionation:

$$\text{DIPB} + C_6H_6 \rightarrow 2 \text{ cumene} \quad \text{(exotherm)}$$

From this reaction it is clear that recycling the heavy products can enhance the yield of cumene. Coating of the reactor packing of the column inner wall with catalyst-exchanged zeolite crystals may provide a low pressure drop, dustproof operation, with a large catalytic surface. Besides, the formation of di- and tri-mers will be minimised, because of the steric hindrance in the zeolite channels.

2.5.6 Hydrocarbon conversion processes

2.5.6.1 Improvement in octane yield in catalytic cracking

The octane and total yield in catalytic cracking (both fluid (FCC) and thermofor (TCC)) can be enhanced by *in situ* crystallised ZSM-5 on a clay aggregate support[142]. The silica/alumina ratio of the support should exceed 5, to preserve the crystallinity of the zeolite crystals during the extreme cracking conditions. It was found that zeolite composites derived from clay aggregates were hydrothermally more stable than the corresponding other composites. The steam may be present in the feed, produced as a reaction product, added to remove the products and unreactive feed from the catalyst or generated during regeneration. In coke ageing, however, the catalyst can be restored to almost its original activity by conventional regeneration techniques, where the carbonaceous coke deposits are removed by burning at elevated temperatures. As in catalytic cracking, steam stability is far more important than coke ageing. The catalyst spends over 80% of the total residence time in the regenerator at elevated temperatures, in the presence of steam. Impregnation of the composite with silver may enhance the steam stability, however, the improved liquid selectivity (to gasoline) will be lost, although the resistance to hydrothermal deactivation is improved.

2.5.6.2 The Fischer-Tropsch (FT) process

The hydrogenation of carbon monoxide by the FT process permits the synthesis of hydrocarbons ranging from methane to high melting point paraffin waxes, depending on the catalyst and process conditions. Cobalt-based catalysts for FT synthesis were extensively used during the first half of the century, until the end of World War II. Nowadays, cobalt-containing catalysts are still being used in the Shell plant at Bintulu, whereas Sasol (South Africa) applies an iron-based catalyst.

A composite catalyst comprising a water-gas shift catalyst, coated by a thin zeolite film, which, in turn, has a FT catalyst deposited on its outer surface, has been

reported[143]. The zeolite has a gatekeeper function; it allows short chain hydrocarbons and steam into the water-gas shift catalyst and allows the return of carbon monoxide and hydrogen products back to the FT catalyst at its outer surface.

A stream of short chain hydrocarbons (e.g. $C_1 - C_4$ alkanes or alkenes) and steam is passed to the catalyst composite where it diffuses past the FT catalyst, through the zeolite layer to the water-gas shift catalyst. At the surface, the short chain hydrocarbon reacts with water to produce carbon monoxide and hydrogen. These products then diffuse back through the zeolite-covered surface where they react on the FT catalyst to produce hydrocarbon oligomers.

Here a zeolite FT catalyst has 3 advantages:

(i) The FT function can be highly dispersed in the fresh catalyst, reducing the metal loading needed to attain a specific activity.

(ii) The zeolite can selectively modify (by acid-catalysed, shape-selective reactions) the primary FT product.

(iii) A water-gas shift function can be introduced into a molecular sieve-based catalyst. For example, Co-APO-34 can be modified by Zn and Cu components, to introduce the water-gas shift activity.

2.5.7 Pollutant emission control by structured catalysts

Cars and stationary engines have been identified as the main sources of environmental pollution and photochemical smog. Their exhaust gases contain NOx, SO_2, hydrocarbons and carbon monoxide. Selective catalytic reduction (SCR) of nitric oxide is an end-of-pipe process that requires a dustproof, low pressure drop reactor, to remove the pollutant. This is in conflict with the need for extensive contact between the gas flow and the catalyst. For this extensive contact time between the gas and the catalyst, special structured catalyst packings were developed, such as the honeycomb reactor and the parallel-passage reactor. The currently most widely used catalyst for the SCR of NOx with ammonia consists of vanadia, often in combination with titania, on an amorphous silica or alumina carrier. The catalyst is present as a washcoat on the surface of the ceramic body of a honeycomb reactor (monolithic shape). Some NOx reduction studies using zeolites are given in Table 2.11.

Table 2.11: NO_x reduction processes using zeolites

NOx-reduction process	**Remarks**	
Selective catalytic reduction of NOx in dustproof, low pressure drop reactors[144]	Reductant: Catalyst: Temp:	NH_3 Cu-ZSM-5 deposited on stainless steel wire gause 350°C
Reduction of automotive NOx emissions in lean-burn internal combustion engine exhaust[145]	Reductant: Catalyst: Temp:	H_2:C_3H_6:CO = 1:1.2:3.1 Cu-ZSM-5-clay aggregates 500°C
Catalytic removal of NOx from total energy installation flue-gases[146]	Reductant:	Urea
Selective catalytic reduction of NOx[147]	Reductant: Catalyst: Temp:	NH_3 H-ZSM-5 deposited on alumina 350 – 550°C

2.6 References

1. H. Van Bekkum, E.M. Flanigen and J.C. Jansen, *Introduction to Zeolite Science and Practice*, Elsevier Amsterdam, **58**, 13-33, 1991.
2. D.W. Breck, *Zeolite Molecular Sieves, Structure, Chemistry and Use*, John Wiley and Sons, Inc., New York, 1974, reprinted by Krieger, Malabar, Florida, 1984.
3. A.F. Cronstedt, *Akad. Handl. Stockholm*, **18**, 1756, 120-130.
4. F. Fontana, *Mat. Fis. Soc. Ital. Sci.*, **1**, 1777, 679.
5. A. Damour, *Ann. Mines*, **17**, 1840, 191.
6. G.W. Morey and E. Ingerson, *Econ. Geol.*, **32**, 1937, 607.
7. H.S. Thompson and J. Roy, *Agr. Soc. Engl.*, **11**, 1850, 68.
8. E. Eichhorn, *Ann. Phys. Chem.*, **105**, 1858, 126.
9. H. de St. Claire-Deville, *Compt. Rend.*, **54**, 1862, 324.
10. G. Friedel, Bull. Soc. Franc. Mineral. Crystallogr., **19**, 1896, 94-118.
11. O. Weigel and E. Steinhoff, *Z. Kristallogr.*, **61**, 1925, 125-154.
12. R.J. Leonard, *Econ. Geol.*, **22**, 1927, 18-43.
13. W.H. Taylor, *Z. Kristallogr.*, **74**, 1930, 1.
14. L. Pauling, *Proc. Nat. Acad. Sci.*, **16**, 1930, 453; *Z. Kristallogr.*, **74**, 1930, 213.

15. J.W. McBain, *The Sorption of Gases and Vapors by Solids*, Ch. 5, Rutledge and Sons, London, 1932.

16. R.M. Barrer, *J. Soc. Chem. Ind.*, **64**, 1945, 130.

17. R.M. Barrer, *J. Chem. Soc.*, 1948, 2158.

18. R.M. Milton, in M.L. Occelli and H.E. Robson (Eds.), Zeolite Synthesis, *ACS Sympos. Ser. 398, American Chemical Society*, Washington, D.C., 1989, 1-10.

19. E.M. Flanigen, B.M. Lok, R.L. Patton and S.T. Wilson, in Y. Murakami, A. Ijima and J.W. Ward (Eds.), *Proc. 7th Intl. Zeolite Conf.*, Tokyo, August, 1986, 103.

20. J.A. Dalmon, A. Giroir-Fendler, C. Mirodatos and H. Mozzanega, *Catalysis Today*, **25**, 1995, 97.

21. I. Matsuura, *Synthetic Membranes and Membrane Separation Processes, CRC Press*, Boca Raton, 1994. (b) R.W. Baker, *Kirk-Othmer Encyclopedia of Chemical Technology*, **16**, 1995, 13.

22. M.J. den Exter, *PhD Thesis*, University of Delft, The Netherlands, 1996.

23. A.J. Burggraaf, K. Keizer, R.S.A. de Lange, Z.A.E.P. Vroon and V.T. Zaspalis, *Proc. 9th IZC*, Montreal, 1992, 47.

24. K. Keizer and H. Verwey, *Chem. Tech.*, 1996, 37.

25. E.R. Geus, M.J. den Exter and H. van Bekkum, *J Chem. Soc., Faraday Trans.*, **88**, 1992, 3101.

26. E.R. Geus, H. van Bekkum, W.J.W. Bakker and J.A. Moulijn, *Microporous Mat.*, **1**, 1993, 131.

27. Y. Yan, M.E. Davis and G.R. Gavalas, *Ind. Eng. Chem. Res.*, **34**, 1995, 1652.

28. S.P.J. Smith, V.M. Linkov, R.D. Sanderson, L.F. Petrik, C.T. O`Connor and K. Keizer, *Microporous Mat.*, **4**, 1995, 385.

29. J.C. Jansen, W. Nugroho and H. van Bekkum, *Proc. 9th IZC*, Montreal, 1992, 247.

30. W.O. Haag and J.G. Tsikoyiannis, *Zeolites*, **12**, 1992, 126.

31. I.F.J. Vankelecom, E. Merckx, M. Luts and J.B. Uytterhoeven, *J. Phys. Chem.*, **99**, 1995, 13187.

32. L.M. Robeson, *J. Membr. Sci.*, **62**, 1991 165.

33. L. Gora, J.C. Jansen and T. Maschmeyer, *Stud. Surf. Sci. Catal.*, **125**, 1999, 173.

34. J.M. van de Graaf, *PhD Thesis*, University of Delft, The Netherlands, 1998.

35. W.J.W. Bakker, F. Kapteijn, J. Poppe and J.A. Moulijn, *J. Membr. Sci.*, **117**, 1996, 57 and 107.

36. Z.A.E.P. Vroon, K. Keizer, A.J. Burggraaf and H. Verweij, *J. Membr. Sci.*, **144**, 1998, 65.

37. K. Kusakabe, S. Yoneshige, A. Murata and S. Morooka, *J. Membr. Sci.*, **116**, 1996, 39.

38. Y. Yan, M.E. Davis and G.R. Gavalas, *J. Membr. Sci.*, **123**, 1997, 95.

39. Y. Yan, M.E. Davis and G.R. Gavalas, *J. Membr. Sci.*, **126**, 1997, 53.

40. J.C. Jansen, D. Kashchiev and A. Erdem-Senatalar, *Stud. Surf. Sci. and Catal.*, **85**, 1994, 215.

41. J.C. Jansen and T. Maschmeyer, *Topics in Catalysis*, **00**, 1999, 1-10.

42. M. Demertzis and N.P. Evmiridis, *J. Chem. Soc., Faraday Trans.* 1, **82**, 1986, 3647.

43. H.J.C. te Hennepe, W.B.H. Boswerger, M.H.V. Mulder and C.A. Smolders, *J. Membr. Sci.*, **89**, 1987, 39.

44. H.J.C. te Hennepe, C.A. Smolders, D. Bargeman and M.H.V. Mulder, *Sep. Sci. Technol.*, **26**, 1991, 585.

45. M.-D. Jia, K.-V. Peinemann and R.-D. Behling, *J. Membr. Sci.*, **57**, 1991, 289.

46. I.R. Bellobono, F. Muffato, C. Ermondi, E. Selli, L. Righetto and M. Zeni, *J. Membr. Sci.*, **55**, 1991, 263.

47. S.P.J. Smith, E.P. Jacobs and R.D. Sanderson, *Proc. IMSTEC`96*, Australia, November 1996.

48. T. Sano, Y. Kiyozumi, M. Kawamura, F. Mizukami, H. Takaya, T. Mouri, W. Inaoka, Y. Toida, M. Watanabe and K. Toyoda, *Zeolites*, **11**, 1991, 842.

49. J.G. Tsikoyiannis and W.O. Haag, *Zeolites*, **12**, 1992, 126.

50. T. Sano, Y. Kiyozumi, F. Mizukami, H. Takaya, T. Mouri and M. Watanabe, *Zeolites*, **12**, 1992, 131.

51. T. Sano, F. Mizukami, H. Takaya, T. Mouri and M. Watanabe, *Bull. Chem. Soc. Jpn.*, **65**, 1992, 146.

52. T. Sano, Y. Kiyozumi, K. Maeda, M. Toba, S. Niwa and F. Mizukami, *J. Mater. Chem.*, **2**, 1992, 141.

53. G.J. Myatt, M. Budd, C. Price and S.W. Carr, *J. Mater. Chem.*, **2**, 1992, 1103.

54. M.W. Anderson, K.S. Pachis, J. Shi and W. Carr, *J. Mater. Chem.*, **2**, 1992, 255.

55. S. Yamazaki and K. Tsutsumi, *Microporous Mater.*, **5**, 1995, 245.

56. Y. Kiyozumi, F. Mizukami, K. Maeda, T. Kozasa, M. Toda and S. Niwa, *Stud. Surf. Sci. Catal.*, **105**, 1997, 2225.

57. M.-D. Jia, K.-V. Peinemann and R.-D. Behling, *J. Membr. Sci.*, **82**, 1993, 15.

58. M.-D. Jia, B. Chen, R. D. Noble and J.L. Falconer, *J. Membr. Sci.*, **90**, 1994, 1.

59. T. Masuda, A. Sato, H. Hara, M. Kouno and K. Hashimoto, *Applied Catalysis A: General* **111**, 1994, 143.

60. T. Sano, M. Hasegawa, Y. Kawakami Y. Kiyozumi, H. Yanagishita, D. Kitamoto and F. Mizukami, *Stud. Surf. Sci. Catal.*, **84**, 1994, 1175.

61. T. Sano, H. Yanagishita, Y. Kiyozumi, F. Mizukami and K. Haraya, *J. Membr. Sci.*, **95**, 1994, 221.

62. Y. Yan, M. Tsapatsis, G.R. Gavalas and M.E. Davis, *J. Chem Soc., Chem. Commun.*, 1995, 227.

63. P. Meriaudeau, A. Thangaraj and C. Naccache, *Microporous Mater.*, **4**, 1995, 213.

64. Bai, M.-D. Jia, J.L. Falconer and R.D. Noble, *J. Membr. Sci.*, **105**, 1995, 79.

65. Y.H. Chiou, T.G. Tsai, S.L. Sung, H.C. Shih, C.N. Wu and K.J. Chao, *J. Chem. Soc., Faraday Trans.*, **92**, 1996, 1061.

66. Z.A.E.P. Vroon, K. Keizer, M.J. Gilde, H. Verweij and A.J. Burggraaf, *J. Membr. Sci.*, **113**, 1996, 293.

67. H. Kita, K. Horii, Y. Ohtoshi, K. Tanaka and K. Okamoto, *J. Mater. Sci. Lett.*, **14**, 1995, 206.

68. T. Masuda, H. Hara, M. Kouno, H. Kinoshita and K. Hashimoto, *Microporous Mater.*, **3**, 1995, 565.

69. S. Yamazaki and K. Tsutsumi, *Microporous Mater.*, **4**, 1995, 205.

70. K. Suzuki, Y. Kiyozumi, T. Sekine, K. Obata, Y. Sindo and S. Sin, *Chem. Express*, **5**, 1990, 793.

71. H. Mimura, T. Tezuka and K. Akiba, *J. Nucl. Sci. Technol.*, **32**, 1995, 1250.

72. D.M. Bibby and M.P. Dale, *Nature*, **317**, 1985, 157.

73. Q. Huo, S. Feng and R. Xu, *J. Chem. Soc., Chem. Commun.*, 1988, 1486.

74. W. Xu, J. Li, W. Li, H. Zhang and B. Liang, *Zeolites*, **9**, 1989, 468.

75. W. Xu, J. Dong, J. Li, and F. Wu, *J. Chem. Soc., Chem. Commun.*, 1990, 755.

76. M.H. Kim, H.X. Li and M.E. Davis, *Microporous Mater.*, **1**, 1993, 191.

77. N. Nishiyama, PhD Thesis, Osaka University, Japan, 1997.

78. J. Dong, T. Dou, X. Zhao and L. Gao, *J. Chem. Soc., Chem. Commun.*, 1992, 1056.

79. F. Crea, R. Aiello, A. Nastro and J.B. Nagy, *Zeolites*, **11**, 1991, 521.

80. R. Althoff, K. Unger and F. Schuth, *Microporous Mater.*, **2**, 1994, 557.

81. P. Kolsch, D. Venzke, M. Noack, P. Toussaint and J. Caro, *J. Chem. Soc., Chem. Commun.*, 1994, 2491.

82. P. Kolsch, D. Venzke, M. Noack, E. Lieske, P. Toussaint and J. Caro, *Stud. Surf. Sci. Catal.*, 1994, 1075.

83. J. Girnus, M.M. Pohl, J. Richter-Mendau, M. Schneider, M. Noack, D. Venzke and J. Caro, *Adv. Mater.*, **7**, 1995, 711.

84. J. Caro, F. Marlow, K. Hoffmann, J. Kornatowski, I. Girnus, M. Noack and P. Kolsch, *Proc. -Pol. -Ger. Zeolite Colloq.,* 1995, 186-195.

85. D.B. Shah, S. Chokchal-acha and D.T. Hayhurst, *J. Chem. Soc., Faraday Trans.*, **89**, 1993, 3161.

86. D.B. Shah and H.Y. Liou, *Zeolites*, **14**, 1994, 541.

87. D.B. Shah and H.Y. Liou, *Stud. Surf. Sci. Catal.*, **84**, 1994, 1347.

88. M. Tsapatsis, T. Okubo, M. Lovallo and M.E. Davis, *Mat. Res. Soc. Symp. Proc.*, **371**, 1995, 21.

89. J. Hedlund, B.J. Schoeman, A. Erdem-Senatalar and J. Sterte, *Zeolites*, **19**(1), 1997, 21-28.

90. R.M. Barrer, *Hydrothermal Chemistry of Zeolites*, Academic Press, London, 1982.

91. L. Gora, K. Streletzky, R.W. Thompson and G.D.J. Phillies, *Zeolites*, **18**, 1997, 119.

92. B.J. Schoeman, J. Sterte and J.-E. Otterstedt, *Zeolites*, **14**, 1994, 110.

93. B.J. Schoeman, J. Sterte and J.-E. Otterstedt, *Zeolites*, **14**, 1994, 568.

94. J.H. Koegler, A. Arafat, H. van Bekkum and J.C. Jansen, *Stud. Surf. Sci. Catal.*, **105C**, Elsevier Amsterdam, 1997, 2163.

95. W.K. Burton, N. Cabrera and F.C. Frank, *Phil. Trans. Royal Soc.*, **243**, 1951, 299.

96. J.C. Jansen, Ph.D. Thesis, Delft University, The Netherlands, 1992.

97. M.W. Anderson, J.R. Agger, J.T. Thornton and N. Forsyth, *Angew. Chem. Int. Ed. Engl.*, **35**, 1996, 1210.

98. G. Binder, L. Scandella, A. Schumacher, N. Kruse and R. Prins, *Zeolites*, **16**, 1996, 2.

99. P.J. Kunkeler, D. Moeskops and H. van Bekkum, *Microporous Mater.*, **11**, 1997, 313.

100. E. Creyton, *PhD Thesis*, University of Delft, The Netherlands, 1997.

101. J.C. Jansen and G van Rosmalen, *J. Crystal Growth*, **128**, 1993, 1150.

102. N. van der Puil, PhD Thesis, Delft University, The Netherlands, 1997.

103. J.H. Koegler, PhD Thesis, Delft University, The Netherlands, 1999.

104. H. Yang, A. Kuperman, N. Coombs, S. Mamiche-Afara and G.A. Ozin, *Nature*, **379**, 1996, 703.

105. N. van der Puil, O.L. Oudshoorn, H.P.A. Calis, J.C. Jansen and H. van Bekkum, *Werkwijze ter vervaardiging van een composiet-katalysator*, patent application, 1996.

106. V. Valtchev, B.J. Schoeman, J. Hedlund, S. Mintova and J. Sterte, *Zeolites*, **17**, 1996, 408.

107. R.D. Sanderson and J.C. Jansen, Private Communications, 1999.

108. E.R. Geus, PhD Thesis, Delft University, The Netherlands, 1992.

109. L.C Boudreau and M. Tsapatsis, *Chem. Mater.*, **9**, 1997, 1705.

110. M. Gebhardt, *in Crystal Growth, an Introduction* (P. Hartman ed.), North-Holland Publishing Co., Amsterdam, 1973, 105.

111. J.A. Venables and G.L. Price, *Epitaxial Growth, Part B*, J.W. Matthews (Ed.), Academic Press, New York, 1975, 381.

112. E. Bauer, *Z. Kristallogr.*, **110**, 1958, 395.

113. V. Valtchev, S. Mintova and L. Konstantinov, *Zeolites*, **15**, 1995, 679.

114. R.M. Barrer, *J. Chem. Soc. Faraday Trans.*, **86**, 1990, 1123.

115. E. Wicke and R. Kallenbach, *Kolloid Z.*, **97**, 1941, 135.

116. W.J.W. Bakker, G. Zheng, F. Kapteijn, M. Makkee, J.A. Moulijn, E.R. Geus and H. van Bekkum, *Precision Process Technology*, (M.P.C. Weijenen and A.A.H. Drinkenburg, Eds.), Kluwer, Dordrecht, 1993, 425.

117. F. Kapteijn, W.J.W. Bakker, G. Zheng and J.A. Moulijn, *Microporous Mater.*, **3**, 1994, 227.

118. R.D. Noble and J.L.Falconer, *Catalysis Today*, **25**, 1995, 209.

119. M.J. den Exter, J.C. Jansen, J. van de Graaf, F. Kapteijn and H. van Bekkum, *Stud. Surf. Sci. Catal.*, **102**, 1996, 413.

120. F. Kapteijn, W.J.W. Bakker, J. van de Graaf, G. Zheng, J. Poppe and J.A. Moulijn, *Catalysis Today*, **25**, 1995, 213.

121. F. Kapteijn, W.J.W. Bakker, G. Zheng, J. Poppe and J.A. Moulijn, *J. Chem. Eng.*, **57**, 1995, 145.

122. K. Kusakabe, A. Murata, T. Kuroda and S. Morooka, *J. Chem. Eng. Japan*, in press.

123. C.D. Baertsch, H.H. Funke, J.L. Falconer and R.D. Noble, *J. Phys. Chem.*, **100**, 1996, 7676.

124. H.H. Funke, A.M. Argo, C.D. Baertsch, J.L. Falconer and R.D. Noble, *J. Chem. Soc., Faraday Trans.*, **92**, 1996, 2499.

125. J.M. van de Graaf, F. Kapteijn and J.A. Moulijn, *Euromembrane`97, Third Int. Symp.*, (Eds. A.B.J. Kemperman, G.H. Koops), Dinkeldruk, Oldenzaal, 1997, 242.

126. Y. Kiyozumi, F. Mizukami, K. Maeda, T. Kozasa, M. Toba and S. Niwa, *Adv. Mater.*, **8**, 1996, 517.

127. J.E. Lewis, G.R. Gavalas and M.E. Davis, *AICHE Journal*, **43**, 1997, 83.

128. N. Nishiyama, K. Ueyama and M. Matsukata, *Microporous Mater.*, **7**, 1996, 299.

129. J.C. Jansen and E.N. Coker, *Current Opinion Solid State & Mater. Sci.*, **1**, 1996, 65.

130. D.R. Rolison, *Advanced Zeolite Science and Applications*, Vol. **85**, J.C. Jansen, M. Stocker, H.G. Karge and J. Weitkamp (Eds.), Elsevier Science BV, Amsterdam, 1994, p543.

131. Y. Yan and T. Bein, *Microporous Mater.*, **1**, 1993, 401.

132. T. Bein, K. Brown, G.C. Frye and C.J. Brinker, *J. Am. Chem. Soc.*, **111**, 1989, 7640.

133. J.A. Moulijn and M. Makkee, *Process Technology*, Delft University of Technology, Delft, The Netherlands, 1993.

134. H. Kita, K. Horii, Y. Ohtoshi, K. Tanaka and K. Okamoto, *J. Mater. Sci. Lett.*, **14**, 1995, 206; H. Kita, K. Horii, K. Tanaka, K. Okamoto, N. Miyake and M. Kondo, *Proceedings of 7th International Conference on Pervaporation Processes in the Chemical Industry*, R. Bakish Ed., Bakish Materials, Englewood, USA, 1995, p.364.

135. H. Kita, *Maku (Membrane)*, **20**, 1995, 169.

136. H. Kita, K. Tanaka and K. Okamoto, *Proceedings ICOM`96*, 1996, 1102; H. Kita, T. Inoue, H. Asamura, K. Tanaka and K. Okamoto, *J. Chem. Soc., Chem. Commun.*, **47**, 1997.

137. H. Kita, K. Tanaka, K. Okamoto and M. Kondo, *Proceedings Am. Chem. Soc., PMSE*, **77**, 1997, 327.

138. H. Kita, T. Harada, H. Asamura, T. Tanaka and K. Okamoto, *Proceedings of the Fith International Conference on Inorganic Membranes*, Nagoya, Japan, June 1998.

139. Q. Liu, R. D. Noble, J.L. Falconer and H.H. Funke, *J. Memb. Sci.*, **117**, 1996, 163.

140. J.F. Smetana, J.L. Falconer and R.D. Noble, *J. Membr. Sci.*, **114**, 1996, 127.

141. R.M. Dessau, R.K. Grasselli, R.M. Lago and J.G. Tsikoyiannis, US Patent 5316661, 1994.

142. P.Chu and G.M. Pasguale, US Patent 4522705, 1985.

143. D.G. Loffler, P.F. Schubert, F. Guth and R.A. Dalla Betta, World Patent 9219574, 1992.

144. H.H. Funke, M.G. Kovalchick, J.L.Falconer and R.D. Noble, *Ind. Eng. Chem. Res.*, **35**, 1996, 1575.

145. H.P. Calis, O.L.Oudshoorn, A.W. Gerritsen, K.J.C. Jansen, C.M. van den Bleek and H. van Bekkum, *Chem.-Ing.-Tech.*, **67**, 1995, 777.

146. N.A. Bhore, F.G. Dwyer, D.O. Marler and J.P. McWilliams, US Patent 5254322, 1993.

147. R.G.H. Smeets, H.P. Calis, P.M. Lugt and C.M. van den Bleek, *Catal. Today*, **29**, 1996, 133.

CHAPTER 3

PART 1: Considerations in the search for a suitable membrane support for a zeolite membrane
PART 2: Attempted *in situ* hydrothermal synthesis of a zeolite A membrane on a tubular alumina tube

PART 1: Search for a suitable membrane support

3.1 Introduction

In order to create the two-dimensional surface of a zeolite layer, non porous, relatively inert support slabs have generally been used. It is sometimes required that the zeolite film must be removed from the support without breaking it. In most of these cases fluorocarbon polymers (Teflon, e.g. PTFE and FEP) were used as the support or reactor lining. This is because contamination and nucleation on such surfaces are minimal[1]. The metal supports that have proved to be most suitable for zeolite crystal growth are silver, nickel and mercury[2]. Aluminium, stainless steel and silicon wafers have also been considered as supports[3-5], although it is very difficult to remove zeolite films from these supports without destroying them[6]. This is due to the strong interaction of the zeolite crystals with these types of supports. The synthesis of zeolite films on metal-coated glass supports has also been mentioned in literature[4,5].

The type of support eventually to be selected is largely dependent on the eventual application of the composite membrane material[7]. In most cases the support acts as a carrier, which provides mechanical strength to the zeolite layer. For membrane applications, the support should be adequately porous, for gases or liquids to be able to pass through the support. For catalysis purposes the support should preferably have a high surface area to achieve a high activity per volume of catalyst. The support

should also have reasonable thermal conductivity to transport the heat flow generated during separations or catalysis.

Other factors that play a role in the selection of the support are:

(i) hydrophobicity/hydrophilicity of the support surface (taking chemical bonding of growing crystals to the support surface into consideration),

(ii) stability of the support (kinetics of dissolution of the support must be slower than the kinetics of crystal growth),

(iii) support-zeolite interactions (chemical interaction of support and zeolite layer gives rise to a more stable composite membrane) and

(iv) texture of the support (pore sizes and topography of support is important).

Four different types of supports will be considered and described in Sections 3.2 and 3.3:

(i) a carbon tube,

(ii) a quartz tube,

(iii) a SiC-coated alumina tube and

(iv) an α-alumina tube.

The carbon and quartz tube as well as the SiC coated alumina tube were supplied by the Centre for Porous Materials, University of Western Cape, Chemistry Department (contact person: Prof. Vladimir Linkov).

These respective tubes were immersed in zeolite A (NaA) synthesis solutions and hydrothermally treated in a hot-air oven. The results of crystal growth were studied with the aid of scanning electron microscopy (SEM), x-ray diffraction (XRD) and infra red spectroscopy (IR), as described in Section 3.3.

3.2 *In situ* hydrothermal synthesis of zeolite A on various supports

Synthesis solutions of NaA were used in all the experiments carried out to determine the most suitable support for a zeolite membrane. The compositions of the synthesis solutions and the reaction conditions of the syntheses are given in Table 3.1. The synthesis solutions were prepared by dissolving the silicate and aluminate, separately, in equal amounts of alkaline water. These two solutions were then mixed

and stirred for a certain period of time, depending on the specific synthesis. The syntheses were conducted in a Teflon-lined autoclave. In the cases where the tubes were evacuated (see Table 3.1), the procedure involved immersion of the tubes in the synthesis solution and then placement of them in a desiccator, which was evacuated with the aid of a vacuum pump. The reason for the evacuation was to remove air from the pores of the tubes and replace it with synthesis solution.

The washed membranes/tubes were dried by increasing the temperature of the oven from 30°C to 120°C, over different periods of time (days).

Table 3.1: Compositions of synthesis solutions and the reaction conditions for the synthesis of NaA on various supports

	Supports			
Reagents	**Carbon tube**	**Quartz tube**	**SiC tube**	**Alumina tube**
NaOH	11.33g	11.29g	11.28g	11.23g
H_2O	56.31g	54.73g	54.75g	54.82g
$NaAlO_2$	0.61g	0.80g	0.65g	0.61g
Na_2SiO_3	3.72g	3.63g	3.63g	3.63g
Synthesis conditions				
Pressure	Autogeneous	Autogeneous	Autogeneous	Autogeneous
Si/Al ratio	2.45	1.85	2.29	2.40
Synth. Time	3 h	3 h	3 h	3 h
Synth. Temp.	80°C	80°C	80°C	80°C
Homogen. Time	48 h	2 h	2 h	48 h
Evac. Time	0	1 h	2 h	2 h
Synth. Method	Hydrothermal	Hydrothermal	Hydrothermal	Hydrothermal
Post synthesis				
Drying time	5 days	5 days	5 days	3 days
Drying temp.	30°C - 120°C	30°C - 120°C	30°C - 120°C	30°C - 120°C

3.3 The results of NaA syntheses on various supports

The synthesised tubes were characterised by SEM, XRD and IR and the results of crystal growth on the respective tubes given in Sections 3.3.2 – 3.3.5.

3.3.1 Characterisation of zeolite material with the aid of XRD and IR

A brief background to the use of XRD and IR as analytical techniques for the characterisation of zeolites is given.

Peak Intensities: Powder Diffraction File (PDF) intensities are based on random orientation of crystallites in a sample. The relative intensity of a given d-spacing (degrees 2θ) is based on the atomic numbers (and absorption coefficients) of the atoms in any given plane [h,k,l]. In general, preferred orientation and symmetry also influences the relative peak intensities recorded. The higher the symmetry, the higher the relative intensity of the peaks, for example: isometric crystals will have less, but higher, intensities and *vice versa* for orthorhombic crystals. This is known as the symmetry factor.

Line Shift: Line shift of all reflections is due to bad experimental alignment. It can be correlated by using an internal standard.

Extra Lines: The presence of any extra lines in a spectrum may be due to the presence of a second crystalline phase or a modification of symmetry.

In the infrared spectrum of zeolites, in the range 300-1300cm^{-1}, lattice vibrations can be observed. These vibrations can be divided in structure-sensitive and structure-insensitive bands. Flanigen reported the following positions of these bands[8]:

Structure-insensitive vibrations	
- asymmetric stretch	950 - 1250 cm^{-1}
- symmetric stretch	650 - 720 cm^{-1}
- T-O bending	420 - 500 cm^{-1}
Structure-sensitive vibrations	
- asymmetric stretch	1050 - 1150 cm^{-1}
- symmetric stretch	750 - 820 cm^{-1}
- double-ring vibrations	500 - 650 cm^{-1}
- pore-opening vibrations	300 - 420 cm^{-1}

For some of the structure-sensitive bands a linear relation between the wave number and the number of lattice aluminum atoms is reported[8]. After calibration it is possible to use this relation to derive the number of lattice aluminum atoms from the band positions. Unfortunately, these calculations are only applicable to the Y-type zeolites. IR spectroscopy can also be used to determine the Bronstedt acidity of a zeolite, because of the dependence of the O-H stretching frequency on the acidity[9]. The weaker the O-H bond, the lower the stretching frequency and the higher the acid strength. A figure showing a typical IR-adsorption spectrum of a thin wafer of HNaY after dehydration is given in the literature[10]. Barthomeuf has measured the exact position of the IR peaks corresponding with the acidic hydrogen groups for a series of zeolites with varying Si/Al ratios, which means that the position of the OH stretch bands can give an indication of the Si/Al ratio of a specific zeolite[11].

3.3.2 NaA synthesis on a carbon tube

The dried carbon tube showed no visual (macroscopic) signs of zeolite growth on either of the surfaces (internal or external). There was, however, a lot of crystalline material at the bottom of the autoclave after the synthesis, which meant that crystal growth had taken place but not on the tube surface. This was confirmed by microscopy.

XRD analysis showed that the crystals found in the autoclave were indeed NaA crystals. Figure 3.1 shows the XRD spectrum of the residual crystals after NaA synthesis.

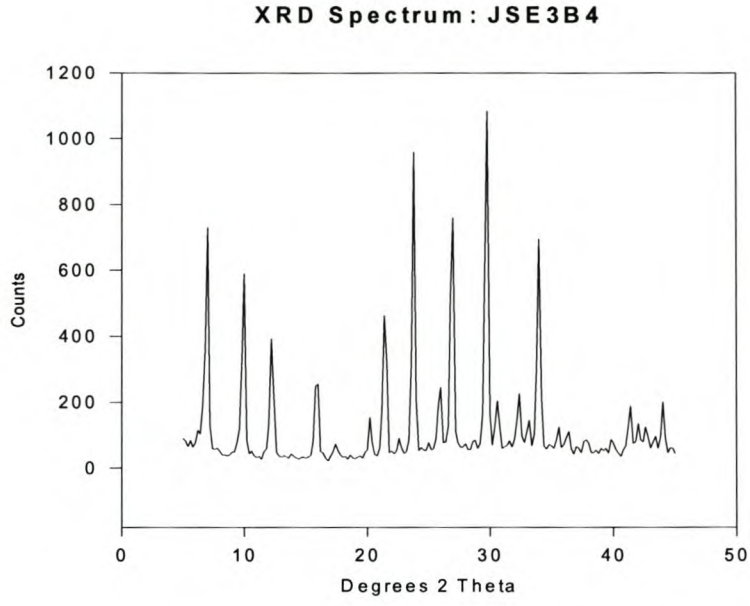

Figure 3.1: XRD spectrum of residual zeolite crystals in the autoclave after the synthesis of NaA on a carbon tube.

Use of a carbon tube as carrier or support for a zeolite A layer therefore, did not seem to be a viable option. This was probably because the carbon tube is hydrophobic, while the zeolite crystals are highly hydrophilic (factor (i) as discussed in section 3.1). This will result in a non-wetting of the surface and a repulsion force between the carbon surface and the formed nuclei, which in turn will make it very difficult for crystals to grow on the carbon surface.

3.3.3 NaA synthesis on a quartz tube

In this experiment there was complete dissolution of the support (quartz tube). There were a few crystals in the autoclave after synthesis, but not much else. The motherliquor was slightly colored (brown). This was due to the fact that the kinetics of dissolution were much higher than the kinetics of crystal growth (factor (ii) in Section 3.1). It might be possible to speed up the kinetics of crystal growth in order to be able to grow zeolite crystals on a pure silica support, but this was not the purpose of the study. Quartz was not further considered as a possible support for a zeolite membrane.

3.3.4 NaA synthesis on a SiC-coated alumina tube

During the hydrothermal synthesis on a SiC-coated alumina tube only a few crystals were formed in the autoclave. There was no visual growth of NaA crystals on either the external or on the internal surfaces of the alumina tube. SEM analysis, however, showed that there were zeolite A crystals on the internal surface of the tube, but the layer was not continuous, see Figure 3.2. Large areas, covered with crystals, were found, as well as larger uncovered areas. This was probably due to the fact that the SiC-coated surface was almost void of any reactive species (hydroxyl groups), which could be used as anchoring spots for zeolite crystals (factor (iii) in Section 3.1). That was probably why only clusters of crystals, and no continuous layer, were found on the surface.

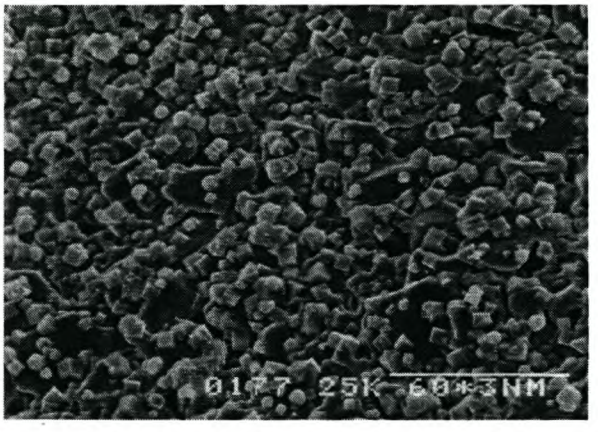

Figure 3.2: SEM micrograph of NaA crystals on a SiC-coated alumina tube.

3.3.5 NaA synthesis on a α-alumina tube

After the synthesis of NaA on an α-alumina tube, again, only a small amount of crystals were formed in the autoclave. SEM analysis showed that a very smooth surface coating was achieved. The NaA crystals were neatly intergrown with each other and it was difficult to recognise individual crystals. See Figure 3.3. Due to the geometry of the tubes it was impossible to determine whether the crystals penetrated the voids of the membranes. The crystal layer was very thick, approximately 25μm. This meant that the surface of the ceramic tube was completely covered with zeolite A crystals. The adhesion of the crystals to the internal surface was very good.

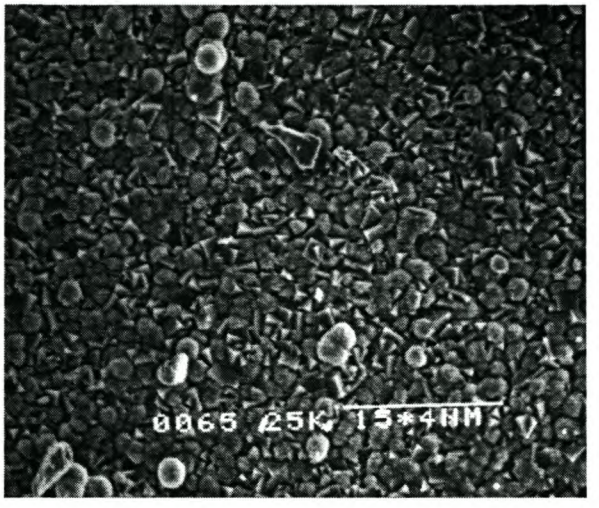

Figure 3.3: NaA crystal layer on the internal surface of α-alumina tube.

Results of XRD analysis of the residual crystals in the autoclave showed that the crystals were indeed zeolite A[12,13]. See Figure 3.4.

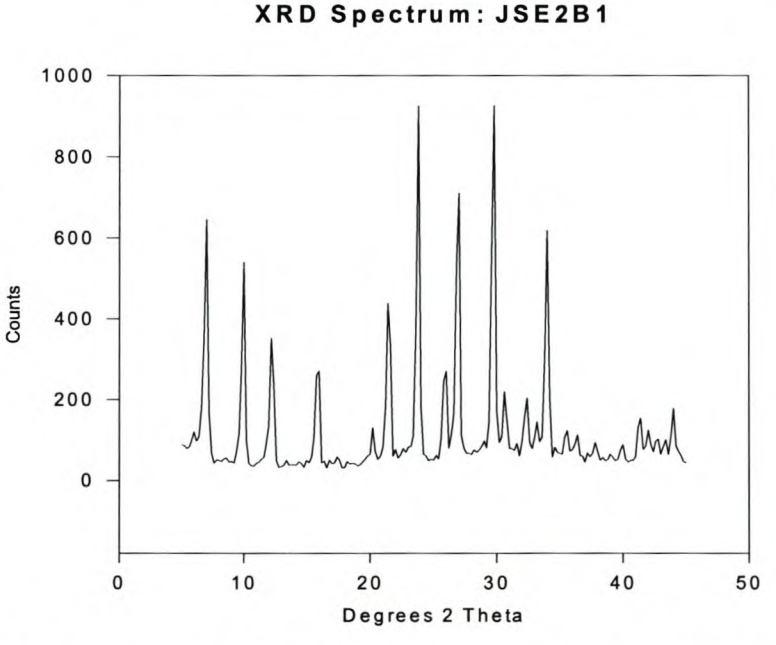

Figure 3.4: XRD pattern of residual zeolite crystals in autoclave after NaA synthesis on an α-alumina tube.

Results of IR analysis of the formed zeolite crystals showed that in the frequency range of 300 - 1300 cm^{-1} a good correlation excists between the absorption bands and those given in literature. See Figure 3.5. The bands at ± 950, 667 and 555 cm^{-1} correlate with the bands reported by Jansen *et al.* for the IR spectrum of Y-zeolites[3].

The latter have relatively sharp bands at ± 950, 667 and 555 cm^{-1}. The first two spectra lines correlate with the asymmetric and symmetric stretches of the structure-insensitive vibrations, respectively. The only structure-sensitive vibration seems to be that of the double ring vibration at 555 cm^{-1}. A broad band can be seen at a frequency of ± 3444 cm^{-1}, which correlates with the OH stretch.

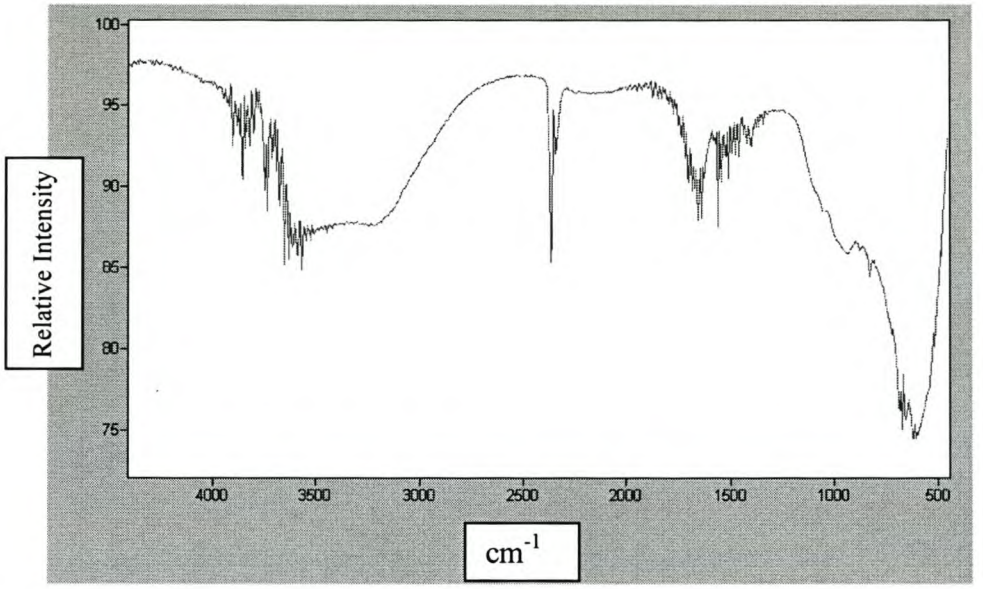

Figure 3.5: IR spectrum of a zeolite A coated α-alumina tube, prepared by normal hydrothermal synthesis.

3.4 Conclusions

The α-alumina tube appeared to be the most suitable support material for the preparation of a zeolite A membrane. It was thermally and physically stable enough to withstand the conditions used in the hydrothermal synthesis. The pore sizes (0.1μm) of the α-alumina tube were small enough to allow bridging to take place. This means that the pore sizes and the crystal sizes should be comparable, in order to achieve a continuous crystal layer. In short, the α-alumina tubes comply with the basic requirements for a good support of zeolite membranes, as described in Section 3.1.

PART 2: *In situ* hydrothermal synthesis of a zeolite A membrane on a tubular alumina tube

3.5 The α-alumina support membrane

In the second part of this chapter the synthesis and characterisation of zeolite A membranes are reported on. All syntheses were carried out *in situ*, under normal hydrothermal conditions (dilute solution synthesis).

3.5.1 Characteristics of the Atech α-alumina tubular membrane

The α-alumina tubes were purchased from Atech, Germany. The asymmetric tubes were cleaned by treatment with alkaline (NaOH) and polar (iso-propanol) solutions. These tubes were characterised by SEM prior to using them in any synthesis. Figures 3.6 and 3.7 show the nature of these α-alumina tubes.

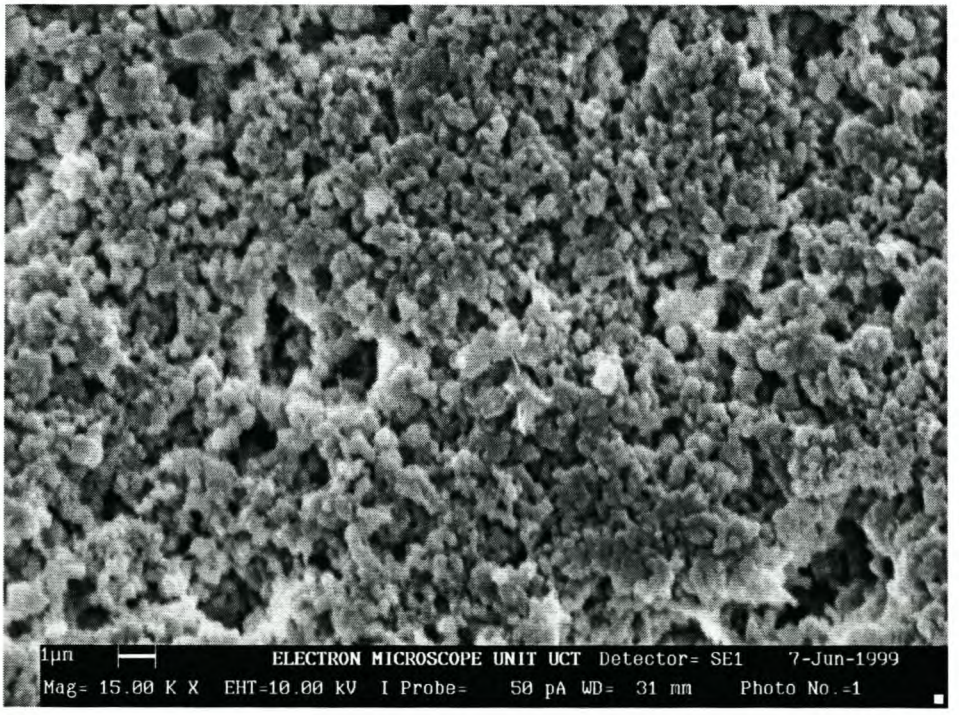

Figure 3.6: SEM micrograph of the internal surface of the Atech alumina tube.

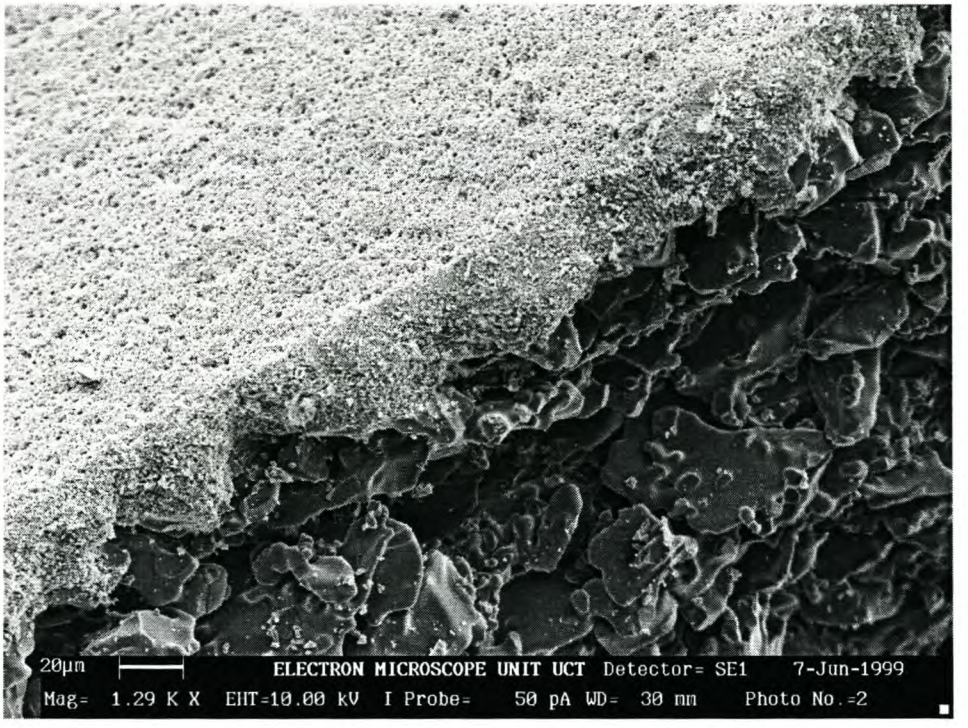

Figure 3.7: SEM micrograph of the cross section of the Atech alumina tube.

3.5.2 Specifications of the Atech membrane

The specifications of the tubes are given in Table 3.2 below. The tubes are manufactured in 600 mm lengths which are then sized down, with a diamond saw, to whatever length is required. The α-alumina layer is on the internal side of the tube, which makes these tubes easier to handle.

Table 3.2: Specifications of the asymmetric α-alumina tube

Specification	**Dimension**
External pore diameter	10-15 µm
Internal pore diameter	0.1 µm
Bore diameter	6 mm
Tube diameter	10 mm
Tube wall thickness	2 mm
α-Alumina layer thickness	20 µm
Support thickness	1980 µm

3.5.3 Placement of the support in the autoclave

The placement/setting of the supports in an autoclave, prior to hydrothermal synthesis, was discussed in Section 2.3.2.2 and the four most common placements shown in Figure 2.17. These placements were for various support configurations. In the present study, the supports were placed in a similar way to that described by Jia *et al.*[14]. Whereas they placed a gel on the internal side of the alumina tube and closed it off with Teflon caps, in the present study the alumina supports were placed vertically in a Teflon-lined autoclave. In some cases Teflon caps were used, for reasons that will be discussed later in this chapter.

The synthesis solutions were prepared by dissolving equal amounts of sodium hydroxide in equal amounts of water and then adding the silica and the alumina to the respective solutions, while stirring. The alumina solution was then added to the silica solution, whilst continuously stirring. The period for which the synthesis solution was stirred was referred to as the homogenisation time. The synthesis solutions prepared were all transparent (clear solutions), with relatively high viscosities.

Adherence of nuclei to the vertical tube surface had to be improved, because gravitational forces tended to dislodge formed gel spheres from the surface of the tube. This problem was overcome by replacing the air in the pores of the asymmetric tube with synthesis solution, by evacuating the alumina tube in the presence of the synthesis solution.

3.6 *In situ* hydrothermal synthesis

Experiments were carried out to determine the optimum composition of the synthesis solution and synthesis parameters (synthesis time, synthesis temperature, homogenisation time, evacuation time, stirred/static and plugged/unplugged) for zeolite crystal growth on the tubular alumina support. Procedures are described in sections 3.6.1 and 3.6.2.

3.6.1 Variation of synthesis solution composition

The compositions of the zeolite A synthesis solutions were varied, in a series of experiments. In the first experiment the water content of the synthesis solution was decreased by 50%. In the next five experiments the Si/Al ratio was altered, and the last experiment will show the effect of an increase in NaOH concentration.

Finding the optimal synthesis solution composition for a particular zeolite in the preparation of a composite membrane is of great importance. A summary of the experiments conducted to determine the effects of various compositions of the synthesis solutions on zeolite crystal growth is given in Table 3.3. All the syntheses described here were conducted in a hot-air oven at 80°C for 3 hours. All the tubes were evacuated for 1 hour in the presence of the synthesis solution. All the tubes used in Experiments 1 to 7 were capped with Teflon plugs, in order to prevent contact of the synthesis solution with the internal surface of the tube.

Table 3.3: Summary of experiments conducted with various compositions of the synthesis solutions for zeolite A membrane preparation

	Chemicals				Results		
Expt. number	**NaOH (g)**	**H_2O (g)**	**$NaAlO_2$ (g)**	**Na_2SiO_3 (g)**	**Crystal growth**	**Crystal layer**	**Crystal phases**
1	11.40	27.47	0.66	3.62	No	No	0
2	11.29	54.54	0.91	3.62	No	No	0
3	11.35	57.50	0.72	3.61	No	No	0
4	**11.23**	**54.82**	**0.61**	**3.63**	**Yes**	**Yes**	**1**
5	11.31	57.36	0.53	3.67	Yes	No	2
6	11.29	54.42	0.45	3.60	Yes	No	2
7	16.98	54.52	0.62	3.64	Yes	No	2

3.6.2 Variation of synthesis parameters

A range of zeolite A syntheses were conducted on the α-alumina tubes, in order to see what effects certain parameters would have on zeolite growth in or on these tubes. In addition to this, the effect of the evacuation time on zeolite crystal growth in or on the alumina tubes was also studied. The final parameter investigated was whether stirring would have an influence on the growth of zeolite A crystals on an alumina support.

Synthesis time was either 3 h or 24 h. In some cases the tubes were plugged to prevent the synthesis solution from entering the bore of the tube. The tubes were evacuated as follows: after immersing the tubes in the synthesis solution in the autoclave, the autoclave was placed in a dessicator. This was then carefully evacuated with a vacuum pump, until air bubbles were visible in the synthesis solution.

The various synthesis solution compositions and synthesis parameters are summarised in Table 3.4.

Table 3.4: Summary of the reagents used and the synthesis parameters studied in the preparation of composite zeolite A membranes

	Experiment number							
Chemicals	**8**	**9**	**10**	**11**	**12**	**13**	**14**	**15**
NaOH (g)	11.32	11.32	11.28	11.28	11.29	11.29	11.31	11.31
H_2O (g)	54.63	54.63	54.51	54.51	54.51	54.51	55.42	55.42
$NaAlO_2$ (g)	0.61	0.61	0.61	0.61	0.61	0.61	0.60	0.60
Na_2SiO_3 (g)	3.60	3.60	3.61	3.61	3.60	3.60	3.60	3.60
Synthesis parameters								
Synth. Time (h)	3	24	3	24	3	24	3	24
Synth. Temp. (°C)	80	80	80	80	80	80	80	80
Homogenisation time (h)	1.5	1.5	1	1	1	1	1	1
Evac. Time (h)	1	1	1	1	0	0	1	1
Teflon plugs used	No	No	Yes	Yes	Yes	Yes	Yes	Yes
Stirred/Static	Static	Static	Static	Static	Static	Static	Stirred	Stirred

3.7 Results and Discussion

The results of the experiments conducted with different compositions of the synthesis solutions and synthesis parameters are discussed in sections 3.7.1 and 3.7.2, respectively.

3.7.1 Composition of synthesis solution

In the first experiment (Expt. 1) it was found that a decrease in the water content lead to a alteration in the composition of the synthesis mixture. This was probably the reason why no crystal growth occurred in that experiment. During the course of the next five experiments, Expts. 2-6, the alumina content was decreased, meaning that the Si/Al ratio was increased; this increase was from 0.8 to 1.6. In the first of these experiments (Expt. 2) (Si/Al = 0.8), no crystal growth occurred and there was therefore no crystal layer formed. See Figure 3.8. This was probably due to the very low Si/Al ratio, meaning that the Al content of the zeolite synthesis mixture was too high. In the next synthesis (Expt. 3), the Si/Al ratio was 1, which is the norm for

zeolite A synthesis. No zeolite A crystal growth was detected, nor were there any crystal layers formed.

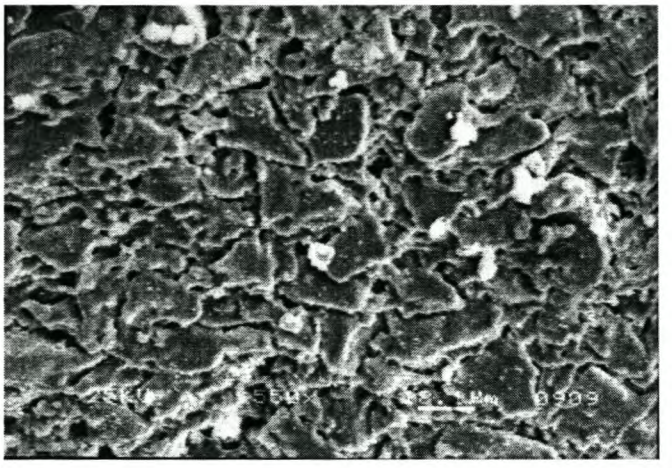

Figure 3.8: SEM micrograph of the external surface of the α-alumina tube after immersion in a NaA synthesis solution with a Si/Al ratio of 0.8.

Experiment 4 (Si/Al = 1.2) resulted in a smooth surface coating of zeolite A crystals on the tubular alumina support. The zeolite A layer was continuous and consisted of only cubic NaA crystals. See Figure 3.9. Experiment 5 (Si/Al = 1.4) showed crystal growth on the external surface, but there was no continuous crystal layer. In this case there was a second crystal phase present, one which has not been seen in any other synthesis. This will be discussed later in Section 4.4.4.

Figure 3.9: SEM micrograph of a zeolite A crystal layer on an alumina tube support.

The last synthesis in this series, of five different Si/Al ratios, (Expt. 6), gave more or less the same result as for Experiment 5. The Si/Al ratio used was 1.6, which is very high for the preparation of zeolite A, and lead to a non-continuous crystal layer on the tube surface. Again, a large amount of the second crystal phase was visible.

From these results it was clear that the best zeolite A crystal growth was achieved in Experiment 4. It was therefore decided to use the composition of synthesis solution 4 for the remainder of the syntheses.

3.7.2 Synthesis parameters

Four different experiments were conducted to determine the optimum for each of the synthesis parameters. Each experiment was carried out at two different synthesis times, resulting in eight syntheses in total.

The composition of the synthesis solution used was as in Experiment 4, section 3.6.1. As can be seen from Table 3.4, the first two experiments (Expts. 8 and 9) were conducted for 3 h and 24 h, respectively. In these cases the tubes were not capped and, further, the tubes were evacuated in the presence of the synthesis solution. This meant that the synthesis solution was in contact with both the internal and external surfaces of the alumina tube. Results of the SEM analysis showed that continuous zeolite crystal layers were formed during the three-hour hydrothermal process. See Figure 3.10. Crystal growth occurred on both the internal and external surfaces of the alumina tube. This was obviously due to the fact that both surfaces of the tube were exposed to the synthesis mixture during hydrothermal treatment. It seems as if the evacuation process, prior to synthesis, did not cause crystals to form in the cross section of the membrane. Results of XRD analysis showed that the crystals formed on the internal surface of the tube were indeed zeolite A. See Figure 3.11.

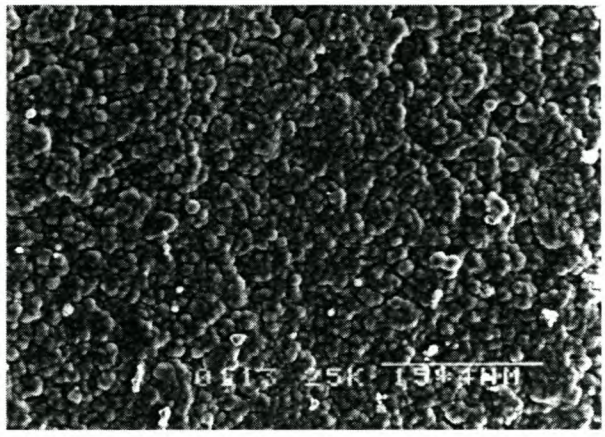

Figure 3.10: SEM micrograph of zeolite A crystals on internal surface of alumina tube, formed after 3 h.

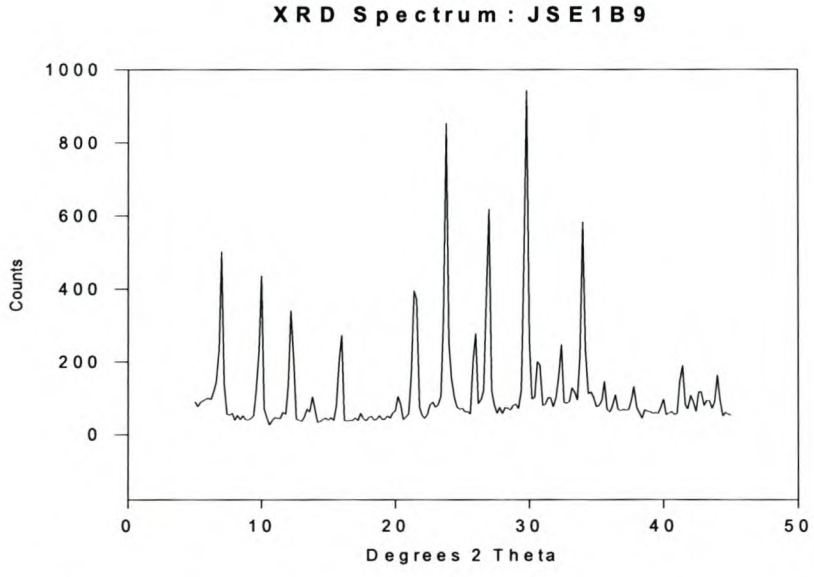

Figure 3.11: XRD spectrum of zeolite A crystals on internal surface of alumina tube.

In the 24 h experiment (Expt. 9) similar trends in zeolite crystal growth were seen. Figure 3.12 shows the internal surface of the tube and Figure 3.13 shows the external surface of the tube. Zeolite A crystals were found on both the internal and external surfaces of the tube because both these surfaces were in contact with the synthesis solution The fact that zeolite A crystals on the internal surface were intergrown to form a continuous crystal layer, while the crystals on the external surface were scattered, was due to the smaller pores on the internal side of the tube, as can be seen from SEM analysis. This once again proved that in order to obtain a

continuous zeolite layer, the crystal sizes must be comparable to the pore sizes of the support.

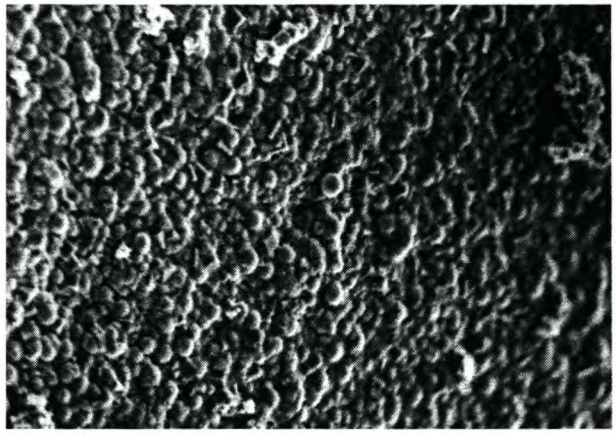

Figure 3.12: SEM micrograph of zeolite A layer on the internal surface of an alumina tube.

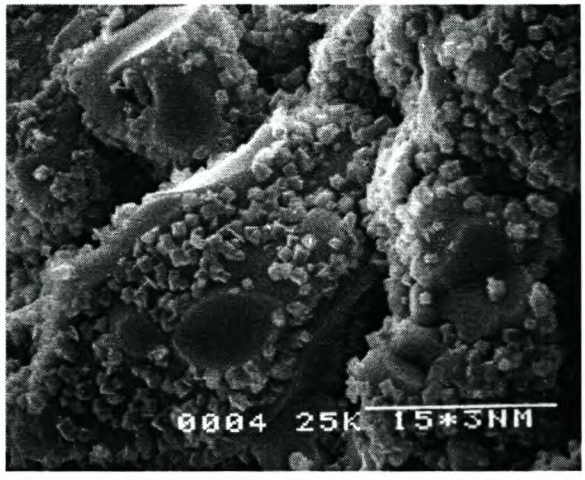

Figure 3.13: SEM micrograph of zeolite A crystals on the external surface of an alumina tube.

In the next two syntheses (Expts. 10 and 11), the tubes were capped with Teflon plugs and evacuated in the presence of the synthesis solution. SEM analysis showed that a densely-packed crystal layer was formed on the external surface of the tube and there was no crystal growth on the internal surface of the tube. The crystal layer was not very uniform and it was difficult to determine the thickness of the crystal layer. Small, isolated indents could be seen on the outer-surface crystal layer. The other "worrying factor" was that the crystals were not cubic, as would be expected for zeolite A crystals; most of the crystals seemed to be more rounded. See Figure 3.14.

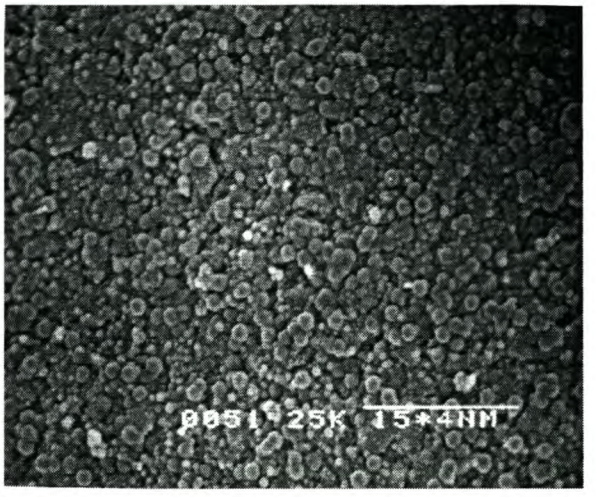

Figure 3.14: SEM micrograph of zeolite A crystals on the external surface of an alumina tube (Expt. 10).

SEM analysis further showed that the external surface of this tube was covered with zeolite A crystals and a second crystal phase (see Section 4.4.4). Figure 3.15 shows zeolite A crystals and a second crystal phase on the external surface of an alumina tube . These crystals were very well intergrown with one another and formed a continuous zeolite crystal layer.

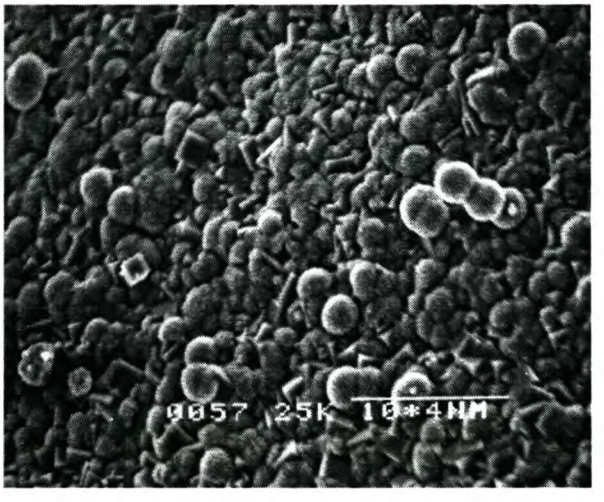

Figure 3.15: SEM micrograph of zeolite A crystals as well as a second crystal phase intergrown on the external surface of an alumina tube (Expt. 11).

The next two syntheses (Expts. 12 and 13) were carried out in a similar manner to the previous two experiments, except that they were not evacuated prior to synthesis. SEM analysis of a sample of the product of Expt. 12 showed that there were no crystals visible on the internal surface of the tube. This was expected, since the

internal side of the tube was plugged with Teflon plugs. One of the main characteristics of this coated tube was the lack of cohesion in the crystal layer. It appeared that although there were many crystals present, there was no definite crystal layer present. Some areas were well covered and could be considered to be continuous, but mostly there was no solid crystal layer. See Figure 3.16.

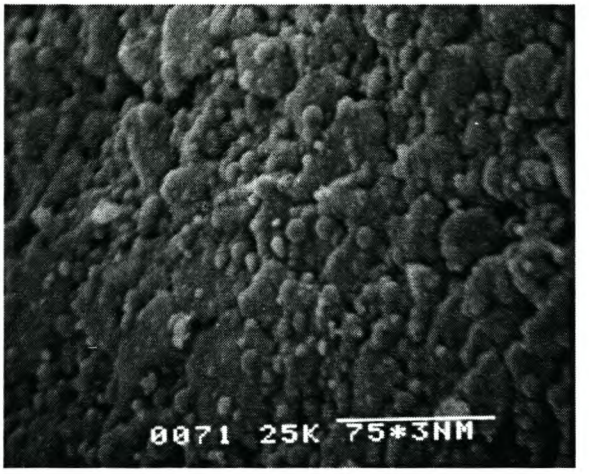

Figure 3.16: SEM micrograph of the external surface of an alumina tube, with zeolite A crystals scattered all over the external surface (Expt. 12).

At this stage there was only one possible explanation for this lack of cohesion and that was the fact that these membranes were not evacuated in the synthesis solution, prior to hydrothermal treatment. This could mean that the evacuation process was indeed necessary to promote the penetration of the synthesis solution into the pores of the alumina tube. Evacuation resulted in a stronger adhesion of the zeolite crystals to the tube surface. XRD analysis also showed that the crystals formed on the external surface of the alumina tube, in Expt. 12, were indeed zeolite A. See Figure 3.17.

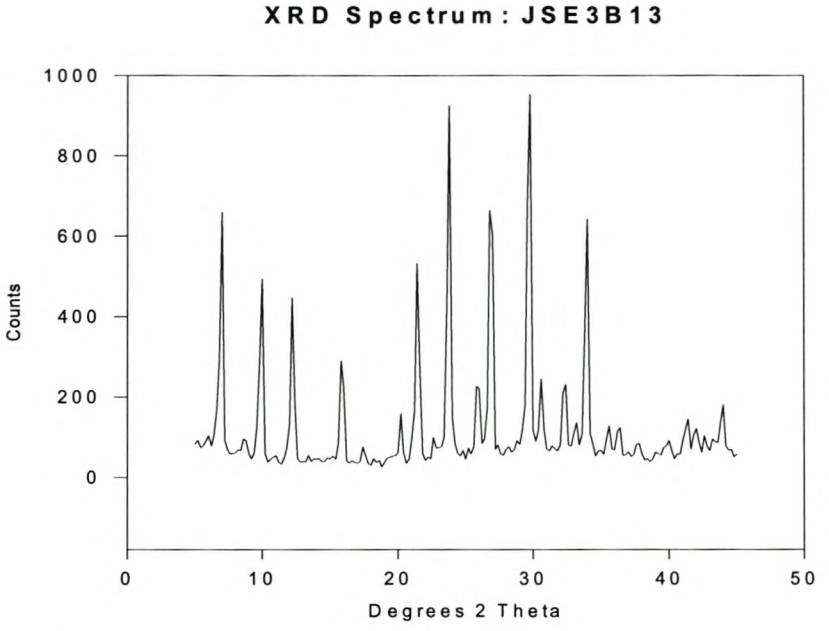

Figure 3.17: XRD spectrum of zeolite crystals on the external surface of an alumina tube (Expt. 12).

Results of the 24 hour synthesis (Expt. 13) were more or less similar to those of the previous experiment (Expt. 12). There were, however, more crystal phases present, as confirmed by XRD analysis. See Figure 3.18.

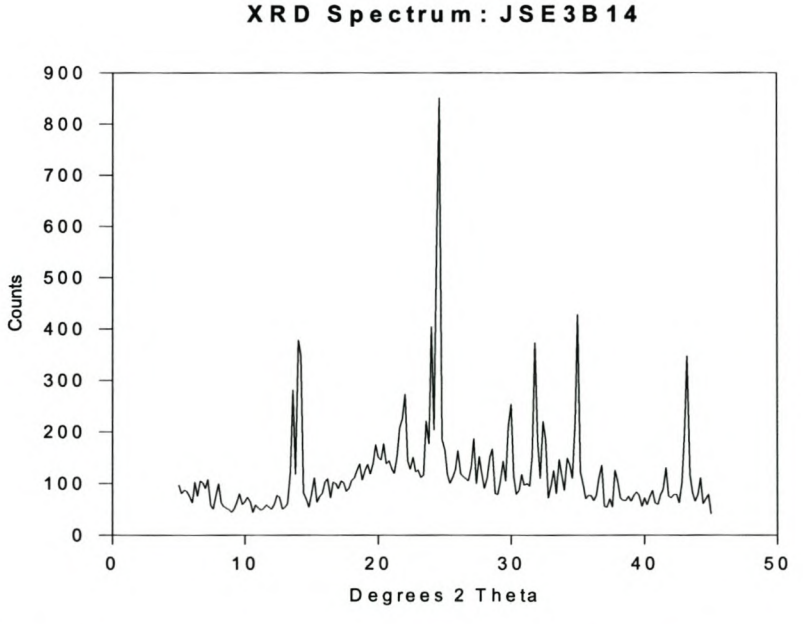

Figure 3.18: XRD spectrum of crystals present on the external surface of an alumina tube (Expt. 13).

The procedures used for the final two experiments (Expts. 14 and 15) were similar to those of Experiments 10 and 11, the only difference being that in Experiments 10 and 11 the synthesis solution was stirred for the duration of the synthesis. SEM analysis of a sample of the product of Experiment 14, prepared in a 3 h synthesis, showed flakes of the support that were covered with crystals. At higher magnification an intergrowth between the cubic crystals and the second phase could be seen. See Figure 3.19.

Figure 3.19: SEM micrograph of zeolite crystals on the external surface of an alumina tube (Expt. 14).

The resulting layer on the external surface of Experiment 15 was not very good. The external surface of the tube appeared to be covered with an amorphous phase, which included the zeolite A crystals. See Figure 3.20.

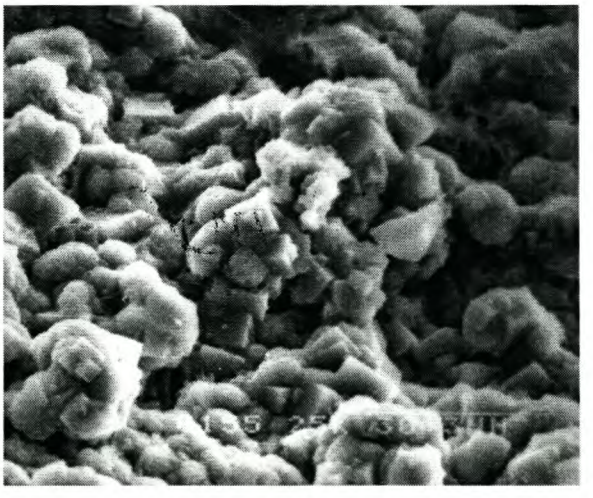

Figure 3.20: SEM micrograph of amorphous material as well as NaA crystals on the external surface of alumina tube (Expt. 15).

3.8 Conclusions

The α-alumina tube proved to be the most suitable support for the growth of zeolite A crystals. The zeolite A synthesis solution used in Experiment 4 (11.23g NaOH, 54.82g H_2O, 0.61g $NaAlO_2$ and 3.63g Na_2SiO_3), gave the best crystal growth on the internal and external surfaces of the alumina support. A synthesis time of 3 hours was sufficient for the formation of a continuous zeolite A crystal layer. Longer synthesis times, up to 24 hours, seemed to increase the occurrence of additional crystal phases; this had to be avoided.

The evacuation process seemed to have a substantial influence on the integrity of the crystals layer on the support surface. It appeared to strengthen the adhesion of the zeolite crystals to the support surface. This is of great importance for the application of these tubes.

The effect of stirring did not seem to be very significant. Results of both the stirred and static syntheses were comparable.

3.9 References

1. O.L. Oudshoorn, Ph.D. Thesis, Delft University, The Netherlands, 1998.
2. Y. Kiyozumi, K. Maeda and F. Mizukami, *Stud. Surf. Sci. Catal.*, **98**,1994, 278-280.
3. J.C. Jansen, D. Kashchiev and A. Erdem-Senatalar, *Stud. Surf. Sci and Catal.*, **85**, 1994, 215.
4. W.O. Haag and J.G. Tsikoyiannis, US Patent, 5019263, 1991.
5. W.O. Haag and J.G. Tsikoyiannis, US Patent, 5110478, 1992.
6. J.G. Tsikoyiannis and W.O. Haag, *Zeolites*, **12**, 1992, 126-130.
7. J.-H. Koegler, Ph.D. Thesis, Delft University, The Netherlands, 1999.
8. E.M. Flanigen, in "ACS Monograph 171", Ed. J.A. Rabo, 1976.
9. J.W. Ward, in "ACS Monograph 171", Ed. J.A. Rabo, 1976.
10. H. Van Bekkum, E.M. Flanigen and J.C. Jansen, *Introduction to Zeolite Science and Practice*, Elsevier Amsterdam, **58**, 1991.
11. D. Barthomeuf, in "Catalysis by Zeolites", Elsevier Amsterdam, **5**, 1980.
12. Special issue: XRD patterns of zeolites, Zeolites, **16**, 1996, 323.

13. J.J. Pluth and J.V. Smith, J. Am. Chem. Soc., **102**, 1980, 4704.

14. M.-D. Jia, B. Chen, R. D. Noble and J.L. Falconer, *J. Membr. Sci.*, **90**, 1994, 1.

CHAPTER 4

Preparation of a zeolite Na-A membrane from separate reactant sources, using a static transverse synthesis method

4.1 Introduction

Much progress has recently been made in the preparation of zeolite membranes[1-6], however, mainly in the area of an impregnation of the support by the synthesis mixture followed by an *in situ* crystallization step. Various types of zeolites have been grown on porous supports, such as MFI-[7], ferrierite-[8] and mordenite types[9] and zeolite A[10] and faujasite types[11].

Two major shortcomings have however still to be solved to promote the application of zeolite membranes. First, most of the layers are compiled of randomly oriented crystallites of a few micrometers with a broad crystal size distribution, resulting in too thick layers of 20 – 50 μm. Secondly, faults in the layers are frequently observed as a lack of control of synthesis parameters.

Since throughput is a key issue in membrane performance, conditions have to be set regarding the orientation of the zeolite crystals. As molecules, in the case of MFI-type, can migrate in three directions through the channels that differ in length and corrugation, the a-, b- and c-directions in the crystal, this can result in three different diffusion coefficients. In the case of a highly oriented layer of crystallites as a membrane for instance with the b-direction perpendicular to the support surface, the most ideal passage of molecules through the crystal layer is achieved. The second important aspect in the preparation of the zeolite layer is the continuity of the phase. As long as the layer is composed of crystals with well-defined crystal faces, systematic defects occur in the layer formation, resulting in pinholes. The fact that pinholes exist was proven by reducing the layer thickness of a MFI-type layer by an ion milling technique. SEM analysis of the new surface showed some hidden triangle-shaped holes and the fact that these holes were endless were proven with the aid of transmission electron microscopy (TEM)[12]. See Figure 4.1.

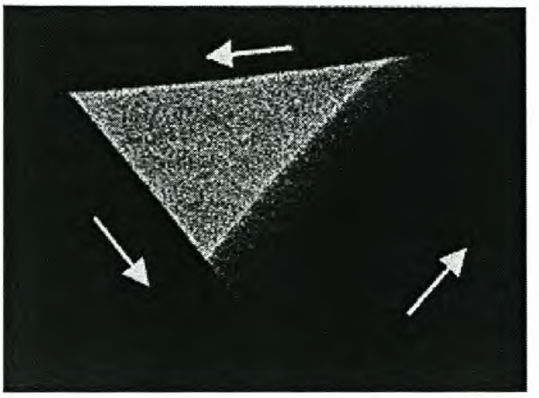

Figure 4.1: TEM image of an endless pinhole halfway through a MFI type crystal layer. Three crystals, of which the c-direction is indicated by arrows, form the pinhole.

In order to avoid systematic pinholes of this nature, the nucleation rate must be high enough to obtain crystallites with roughened crystal faces, so-called grains, which will indeed form a closed layer[1]. In this case "tripods", the interface between three grains, are observed that form a well known pattern often observed in alumina, titania and silica, see Figure 4.2. The orientation of the crystalline material is still preserved, thus with the b-direction perpendicular to the support[13].

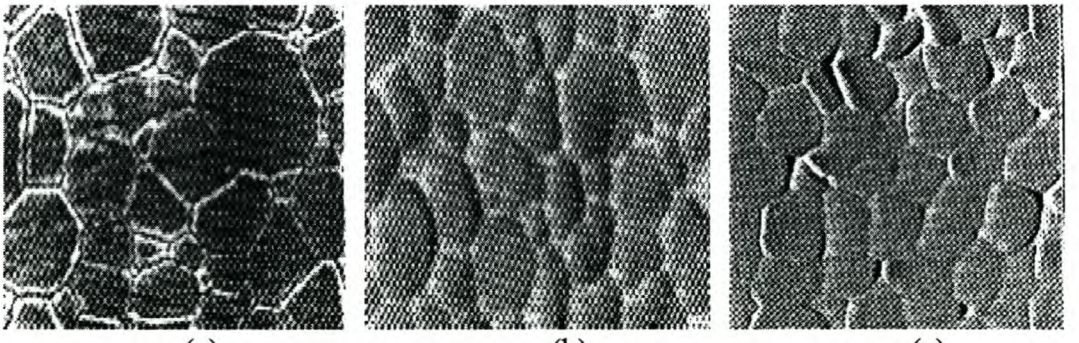

(a) (b) (c)

Figure 4.2: Thin continuous layers of oxide materials grown from grains of (a) sintered alumina, (b) sintered zirconia and (c) MFI-type zeolite, with the straight channel direction parallel to the view[10].

Pinholes, in particular triangle-shaped ones frequently observed between well shaped crystallites, are common and arise from density differences between the precursor gel (low) and the crystal phase (high). The crystal size has an effect on the

pinhole size[14]. The crystal size is important in the formation of a closed layer, as for membrane purposes. See Figure 4.3.

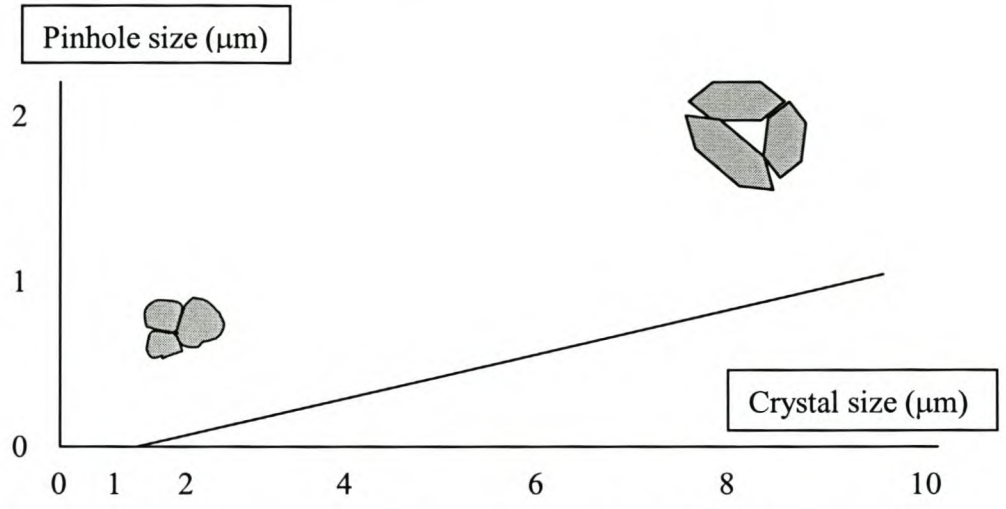

Figure 4.3: Pinhole size versus crystal size and form of crystals in a zeolite layer.

The size of the triangle-shaped pinhole formed between three relatively large zeolite crystals will decrease in size as the crystal sizes decrease. In addition, the morphology of the crystals will change as their size decrease. This evolution of the morphology of the crystals will result in a decrease in pinhole size via grain formation, as illustrated schematically in Figure 4.4.

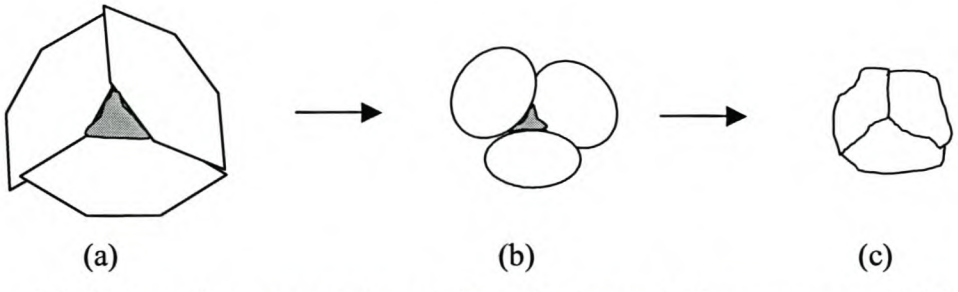

Figure 4.4: Schematic representation of the reduction and disappearance of pinholes in zeolite type MFI. (a) Triangular-shaped pinholes that are present in a zeolite layer comprising crystals with well-defined facets, (b) smaller pinholes upon smaller crystals and (c) absence of pinholes in a layer consisting of grains of crystalline material.

The growth of nearest neighboring zeolite crystals results in the formation of the triangle-shaped pinhole (a). As the morphology of the crystals changes from well-

defined crystal faces to a more rounded shape, the pinhole becomes smaller, while grain boundaries start to develop along the contact areas of these crystals (b). In the ultimate case, where the individual crystalline zeolite phases have assumed undefined shapes, the pinholes disappear, with the formation of grain boundaries ("tripods") along the contact areas of the different zeolite phases (c). This phase roughening is believed to be the only way in which a continuous pinhole-free coating on a support material can be achieved.

Activated zeolite crystal layers show cracks because of the anisotropy in expansion and tensile coefficients[15]. In zeolite A layers, particularly, the major cause of cracks upon activation is the relatively low mass- and heat transfer performance of the zeolite A, resulting in local pressure and temperature spikes[16].

In order to obtain a continuous phase of zeolite it is important, from a crystallization/precipitation point of view, to comply with the basic rules for the preparation of a continuous coating. It has been demonstrated with films of alumina, titania, silica and vanadia that high nucleation rates, preferably in an explosive nucleation mode, result in the formation of continuous phases of the above-mentioned materials[10]. A particular mosaic structure as shown in Figure 4.2 can be formed and comprises a monolayer of grains that are smaller than one micrometer and have a thickness of a few hundred nanometers.

These grains are crystalline, however the crystal growth roughening is dominating so that the crystal facets are not developed. Thus, in the case of zeolites, the crystallization/precipitation of material in grains is preferable rather than well-developed crystals with facets. MFI-type zeolite films, similar to the oxide phases, *vide supra*, have been prepared[17]. Such films are relatively thin and continuous and form relatively crack-free phases upon activation.

The preparation of zeolite A films based on the above arguments will be described and discussed in this chapter. To achieve the highest concentrations of nutrients possible, in order to increase the nucleation and decrease the crystal growth rates, to obtain pinhole free and thin layers, the reactants were separated. Static experiments were carried out with separated reactants of zeolite A, to prepare a zeolite A crystal layer in or at the end of the pores of an alumina tube. This was done by supplying to the tube one reactant solution externally and one reactant solution

internally. Thus, in the reactant pools for the crystallization, no precursor phase was formed. The precursor phase, and next the crystal growth, could therefore only occur at the surface, or preferably in, the pore system of the tube. Upon contact of the reactants, a gel was formed, in which the nucleation and crystal growth rate was high because the initial reactant concentrations were high and the process stopped as soon as the formed gel or crystal layer "separated" the solutions. In chapter 5 the dynamic experiments are described.

4.2 Experimental

4.2.1 Syntheses

Zeolite A membranes were synthesised on/in α-alumina tubes. The tubes, were purchased from Atech, Germany, were asymmetric and comprised two layers. The alumina support, which comprises the larger particles and pores, was 1980 μm thick and had a pore diameter of 15 μm. The inner α-alumina layer was 20 μm thick and had a pore diameter of 0.1μm.

The syntheses were carried out in the static mode. The individual nutrient pools were not stirred nor replenished during the synthesis process. The membrane tubes were sealed, with Teflon plugs at both ends, with one of the source solutions, silica or alumina, on the inside. A tube was placed in a machined Teflon reactor, of which the residual volume was the same as the volume inside the capped alumina tube, as shown in Figure 4.5.

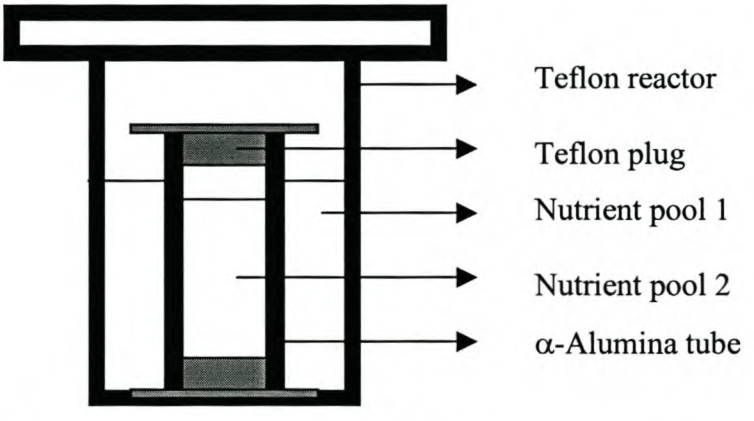

Figure 4.5: Schematic representation of the Teflon reactor and the position of the alumina tube inserted in it, as used for the static synthesis of zeolite A membranes.

A summary of the experimental parameters studied is given below. The effects of these parameters on the (i) crystal growth, (ii) crystal layer integrity (iii) continuity of the crystal layer on the internal and external surfaces of the alumina tubes were studied. In addition to this the (iv) crystal population in the matrix of the alumina tubes and (v) adhesion of the crystal layer to the respective surfaces were determined, with SEM. Different synthesis times were studied, i.e., 2-, 4-, 6-, 8- and 10 days. A parent solution, with a molar composition as shown below, was used as the basis for the concentration study. During these experiments four dilutions of the parent solution were made, namely, 2-, 4-, 8- and 16 times. The synthesis temperature study was conducted at five different temperatures between 60°C and 140°C. The above-mentioned experiments were repeated with the source solutions reversed (nutrient pools 1 and 2 in Figure 4.5 reversed).

Synthesis time:	2, 4, 6, 8, 10 days
Temperature:	60, 80, 100, 120, 140 °C
Dilution factor:	0*, 1/2, 1/4, 1/8, 1/16

* Composition of the parent solution was: 3.17 Na_2O : Al_2O_3 : 1.93 SiO_2 : 128 H_2O, sodium metasilicate and sodium aluminate were used as the sources for the experiments. (i) Si_{in} and Al_{out} and (ii) Si_{out} and Al_{in}

The influence of concentration ratios of nutrients on the crystal population in the pores of the alumina tubes was also studied. For this, an alumina solution was applied to the external surface of the tube and a silica solution was placed internally. The Si/Al ratio of these solutions varied from 1 to <<1. The number of crystals grown in the pores of the tube as a function of the position, in the pore system was determined.

The effect of individual nutrients on the dissolution of the α-alumina support was studied. For this purpose two experiments were carried out. A silica solution was enclosed in an alumina tube, while in a second experiment the alumina tube was left open for maximum contact with the silica solution.

Three experiments were conducted to investigate the influence of the filling sequence on the crystal growth of zeolite A on the surfaces of the tube. In this series silica was placed inside the tube and alumina outside. In the first experiment silica was added first, followed by the alumina. In the second experiment, the sequence was reversed, while in the third experiment both nutrients were added simultaneously.

4.2.2 Characterization

The zeolite membranes that were prepared by this static transverse synthesis (STS) method were characterised by scanning electron microscopy (SEM), X-ray diffraction (XRD) and infrared spectroscopy (IR).

4.3 Results and Discussion

The results of experiments carried out to prepare a zeolite A membrane under various conditions and the effects of changes in various parameters on crystal growth are given and discussed under the following headings: time, temperature, concentration, reversal of nutrient location, concentration gradient, blank experiments, and effects of filling sequence. Figure 4.6 gives a schematic analysis of the crystal yield as a function of temperature and time. The data depicted here were collected from experiments with the parent solution.

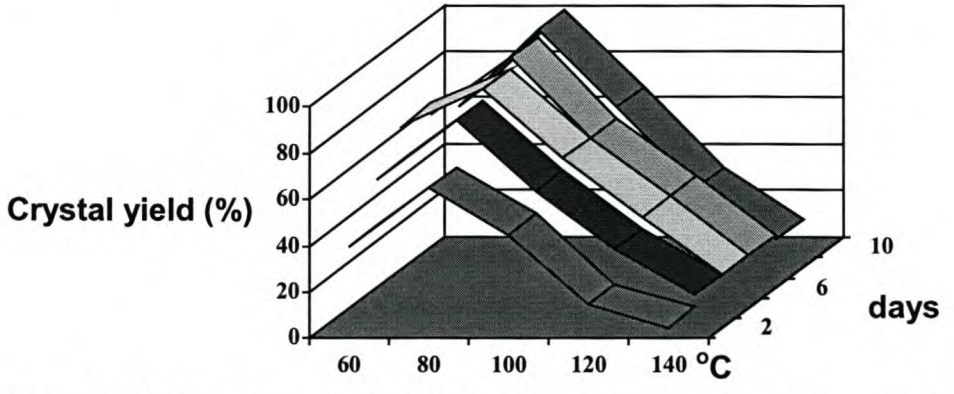

Figure 4.6: Schematic analysis, based on SEM photographs, of the crystal yield as a function of temperature and time.

4.3.1 Effect of time on zeolite crystal growth

Crystal growth on/in the pores of the tubes improved as the synthesis time was increased from 2 to 6 days. This is substantially longer, than crystallization from a mixture; normal synthesis time is ~ 2-4 h. However, the separate nutrient phases have

to diffuse through the pores, as well as into each other, and have to build up a particular ratio and concentration in the mixed areas to meet the zeolite A nucleation and crystallization conditions. Figure 4.7 shows SEM photographs of the (a) external and (b) internal surfaces of the tube after 6 days.

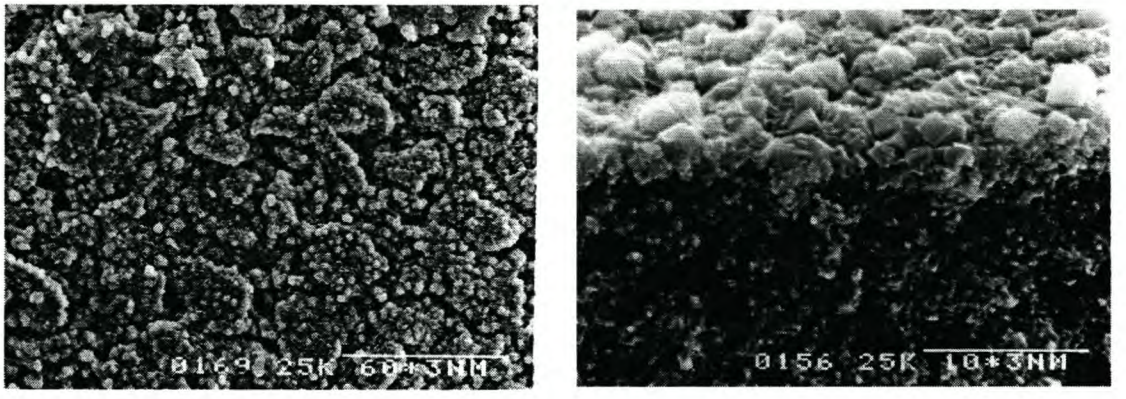

(a) **(b)**

Figure 4.7: SEM micrographs of the surface of the tube after 6 days of crystallization, resulting in zeolite phases, (a) externally - Losod crystals and (b) internally - zeolite A.

4.3.2 Effect of temperature on zeolite crystal growth

The temperature study was conducted over a relatively wide temperature range, 60°C – 140°C. Using the parent concentration, the temperature found to be optimal was 80°C, for zeolite A crystal layers.

4.3.3 Effect of nutrient concentration on zeolite crystal growth

A decrease in the concentration of (highest concentration used) the parent-solution resulted in a decrease in crystal yield on both the internal and external surfaces. This can be understood in terms of a drop in the SiO_2 and Al_2O_3 concentrations rather than a drop in the Na_2O concentration, which affects the pH. Based on this result the parent solution concentration was preferred.

4.3.4 Effect of reversal of nutrient location on zeolite crystal growth

It was found that the position of the individual nutrient pools played a major role in the crystal growth on both surfaces of the tube. With the silica solution contacting the internal surface of the tube, a film of zeolite A was achieved. See Figure 4.8. The zeolite A crystal layer on the internal surface of the tube was analysed with the aid of

XRD. See Figure 4.9. The XRD pattern of Na-A correlates well with that of the pattern given in the Atlas of zeolite structures.

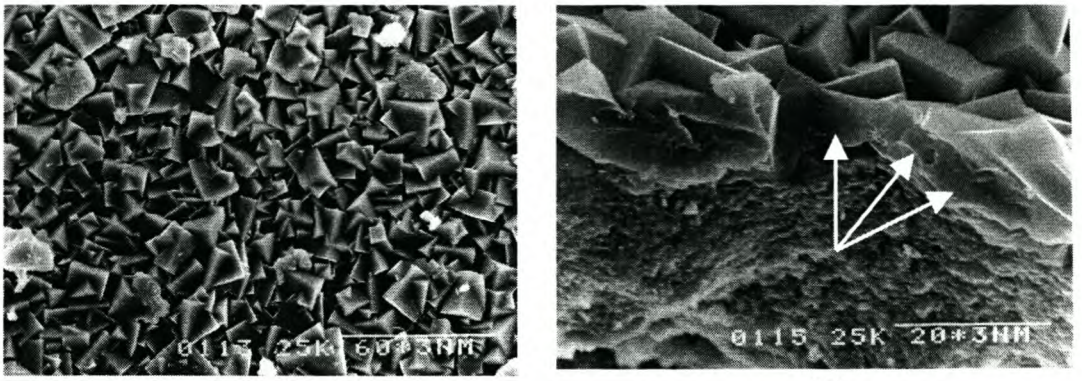

(a) (b)

Figure 4.8: SEM micrographs of a continuous 6 μm thick zeolite A layer on the internal surface of the tube, (a) top view and (b) cross section.

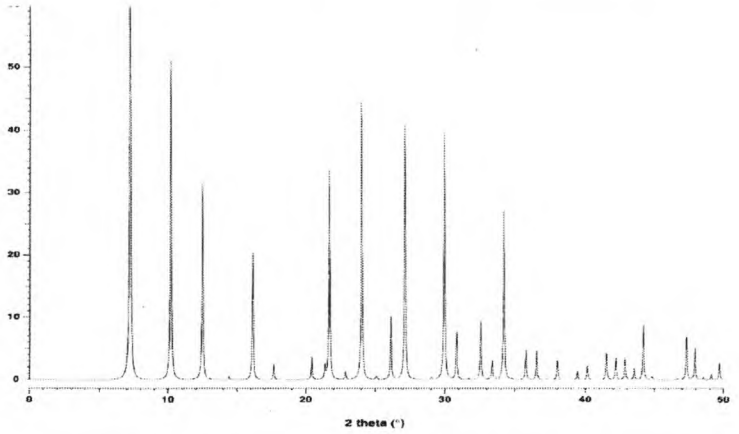

Figure 4.9: XRD spectrum of zeolite A crystals on the internal surface of the alumina tube, when the Si source was placed on the inside of the tube.

The zeolite A crystal layer was also characterised by IR spectroscopy. In the frequency range 300 - 1300 cm^{-1}, there is a very good correlation between the bands present in the spectrum and those in a typical IR spectrum of Y-zeolites[18]. The former spectrum has sharp bands at ± 950, 667 and 552 cm^{-1}. The first two spectra lines correlate with the asymmetric and symmetric stretches of the structure-insensitive vibrations, respectively. The only band that is not very strong is the one at 950 cm^{-1}. The only structure-sensitive vibration seems to be that of the double ring vibrations at 552 cm^{-1}. A broad band can be seen at a frequency of ± 3450 cm^{-1}, which is in correlation with the OH stretch. See Figure 4.10.

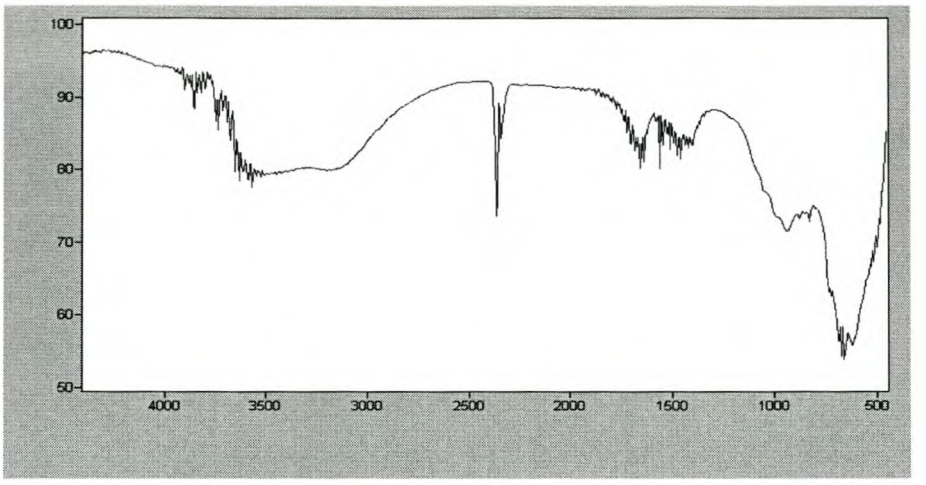

Figure 4.10: IR spectrum of zeolite A crystals on the internal surface of the α-alumina tube, prepared by the STS method.

In addition to the zeolite A crystals on the internal surface, Losod crystals were observed on the external surface of the alumina tube.

The crystal growth achieved with the Si source on the internal surface of the alumina tube proved to be very uniform after carefully studying the internal surface of the tube. SEM, further showed the crystal layer to be continuous and solid, showing no deviations in the integrity of the continous zeolite A layer. The crystal population in the matrix of the alumina tube was also determined with the aid of SEM and it was found that the population could be controlled by varying the nutrient solution concentration. Furthermore, the crystallisation front could also be studied with the help of SEM. The adhesion of the continuous zeolite A crystal layer to the internal surface of the alumina support tube was very good. This was proved with the application of nitrogen pressure on the shell-side of the tube. The pressure tests were done on pre-calcinated membranes, which showed that more than 200 kPa was necessary to destroy the crystal layer.

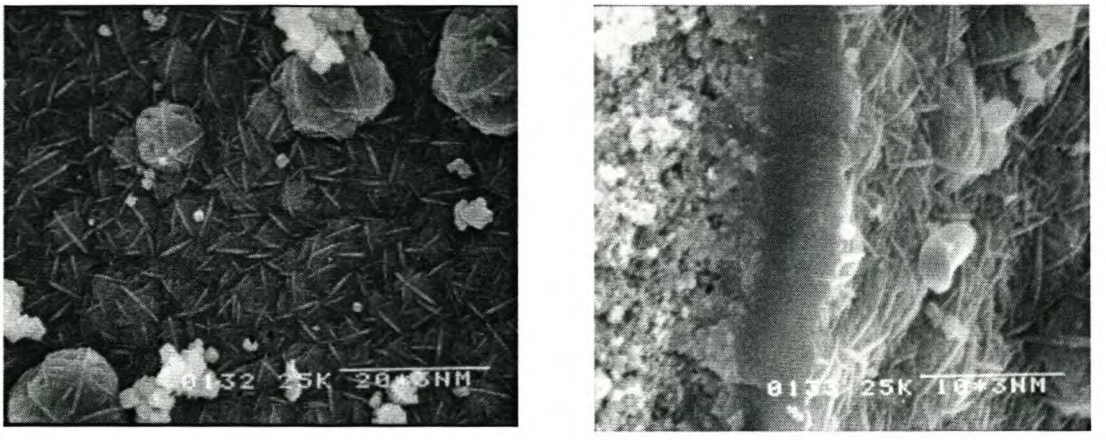

(a) **(b)**

Figure 4.11: SEM micrographs of a continuous layer of Losod crystals on the internal surface of the tube, (a) top view and (b) cross sectional view.

When the internal surface (α-alumina) was exposed to the alumina solution, Losod crystals were found on the internal surface, see Figure 4.11. Losod however is build up by 6-rings only, as shown in Figure 4.12. The maximum pore diameter is less than 2.5 Å and therefore this material is not suitable for separation purposes.

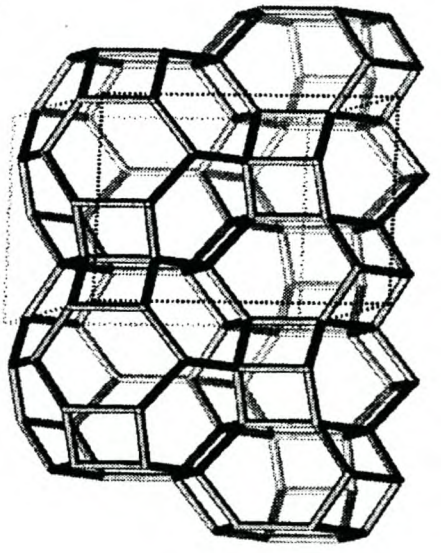

Figure 4.12: A depiction of the three-dimensional framework of Losod viewed, normal to [001].

In contrast to the outer surface (α-alumina), a *continuous* phase of zeolite A or Losod was found on the internal surface of the tube. This indicated that the crystal size and pore size of the support needed to be comparable in order to close the pores of the support and to form a continuous microporous phase. The presence of Losod was further verified by XRD analysis. See Figure 4.13. A special technique was used to analyse the internal surface of the tube. This was necessary because of the curvature of the tube. A very small x-ray beam was focused on the target area on the inner surface of the tube. Scans were made along the length of the tube, in order to try and negate the rounding of the tube. XRD spectra were recorded with a Bruker-AXS D5005 diffractometer.

Based on these results it was concluded that further static transverse syntheses should be conducted at 80°C, for 6 days, using the parent solution. In addition, the Si solution should be placed on the inside of the tube and the Al solution on the outside, in order to grow a continuous zeolite A layer on the internal surface.

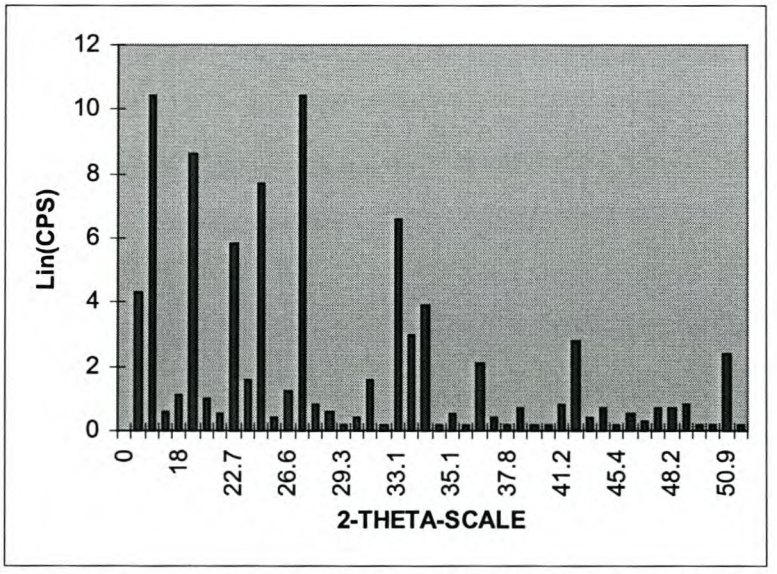

Figure 4.13: XRD spectrum of Losod crystals found on the internal surface of the alumina tube, when the Si source was placed on the outside of the tube.

4.3.5 Concentration gradient study

The influence of concentration ratios was investigated on the zeolite A crystal population *in* the pore system of the tube. Separate synthesis solutions with three theoretically different Si/Al ratios were used, namely 1, <1 and <<1.

SEM analysis of the pore systems of these tubes showed a crystal concentration gradient across the length of the large pore area. In the three experiments carried out, the highest concentration of crystals, based on the Si/Al ratios, was observed in the region of the external-, middle- and internal surfaces of the tube, respectively. In the first experiment the concentration decreased in the direction of the internal surface, in the second experiment there was almost no crystal concentration gradient, while in the third experiment the concentration gradient decreased towards the external surface. See Figure 4.14. This gradient in crystal population can be understood as the tube was filled with the Si solution first, saturating the tube completely up to the external surface, followed by the addition of the Al solution. After the Al solution was added, the Si/Al ratio of 1, which is needed for zeolite A crystallisation, was most frequently available at the interface of the Al- and Si solutions, which is at the external surface of the tube.

In the second experiment, with a higher Al concentration, the Si/Al ratio at the interface was lower than 1. Thus, Si/Al ratios of 1 were formed in the regions with lower Al concentrations which were closer to the internal surface.

In case of higher Al concentration in the external volume and lower Si concentrations in the internal volume, the Si/Al ratio of 1 was only formed close to the internal surface. A rather quantitative indication of the number of crystals counted at 500 nm intervals is given in the sub-table in Figure 4.14.

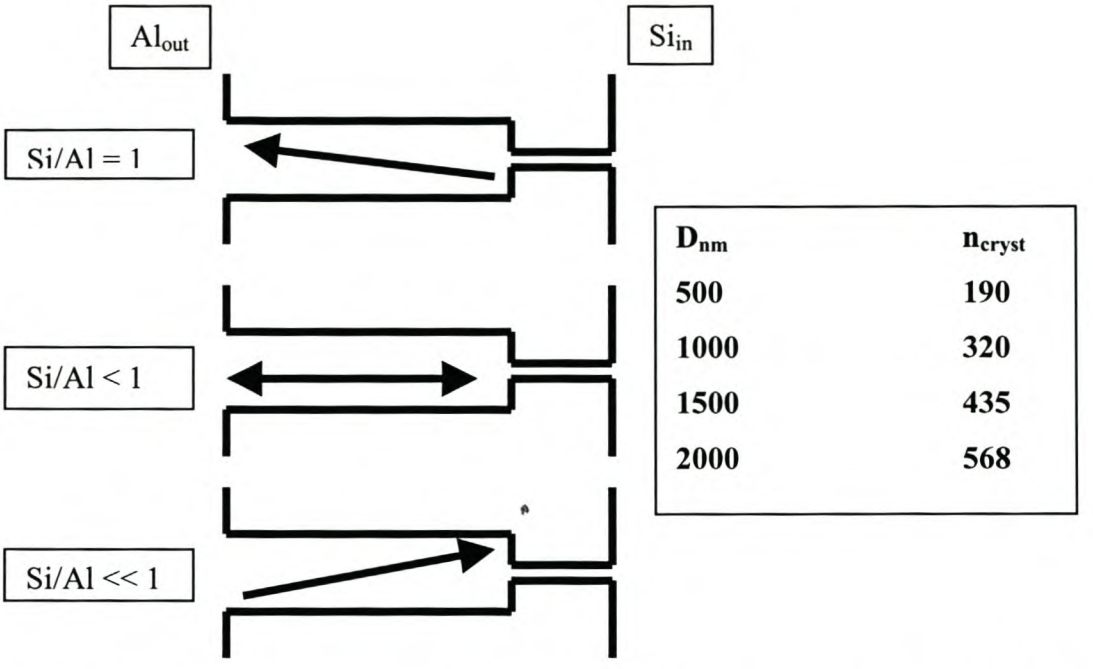

Figure 4.14: Schematic representation of the influence of the Si/Al concentration ratios on the profile of the zeolite A crystal population, indicated by arrows in the pore. D_{nm} is the distance from the external surface and n_{cryst} is the amount of zeolite A crystals at that point in the cross section of the tube.

4.3.6 Blank experiments to study dissolution of the support

In the blank experiments the main observation made was that no alumina dissolved upon exposing the entire tube to a pure silica solution. This was confirmed for the external surface comprising large particles, as well as the internal surface containing small particles.

From this it was concluded that the alumina solution added was the only source for the crystal growth of zeolite A.

4.3.7 The effect of the filling sequence of nutrients on crystal growth on the external- and internal surfaces of the α-alumina tube

The deposit on the internal and external surfaces is a function of the filling sequence. In the case of adding the silica solution first, internally, and next the alumina solution, externally, a continuous crystal layer of zeolite A is observed on the internal surface and a large amount of Losod crystals on the external surface.

In the second experiment with, again, the silica solution internally, however, supplied after the alumina solution was added externally, large amounts of Losod and zeolite A crystals were found on the internal surface and only Losod crystals on the external surface. When both nutrients are added simultaneously a NaA continuous phase is observed on the internal surface and large amounts of Losod on the external surface.

In the first scenario, when the silica is added first, the following schematic illustration applies, as given in Figure 4.15. The volume increments of the nutrient solutions are depicted as a function of time.

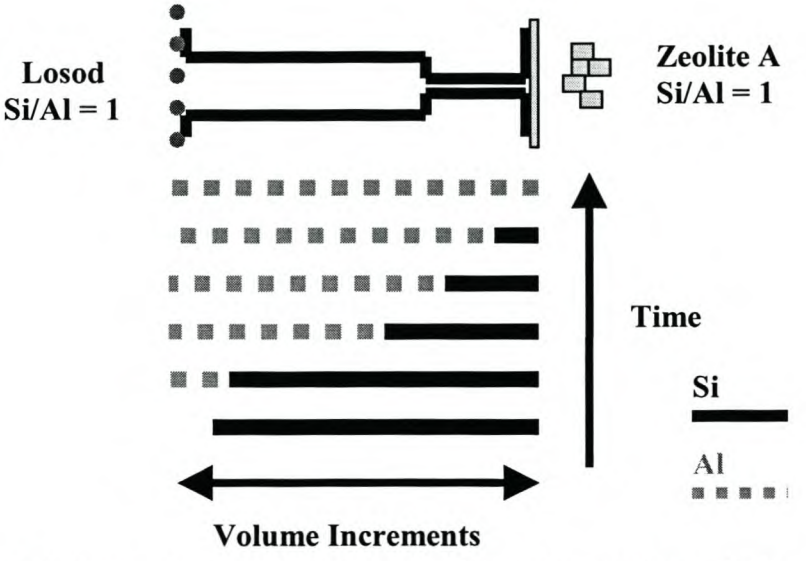

Figure 4.15: Scheme of volume increments of the nutrients (Si and Al) versus time.

Initially, after addition of the silica solution in the tube, the external wall of the tube becomes wetted. Apparently the tube wall is, due to capillary forces, saturated with the silica solution, as indicated in Figure 4.15. After addition of the alumina, externally, the silica at the external surface reacts with the alumina, resulting in the formation of an aluminosilicate gel. The silica will become relatively low in concentration upon dilution in the undiluted highly concentrated alumina solution, resulting in a Si/Al ratio $<<1$, from which the Losod crystallises. The fact that Losod can form in solutions of Si/Al with ratios $<<1$ can be explained by Figure 4.16.

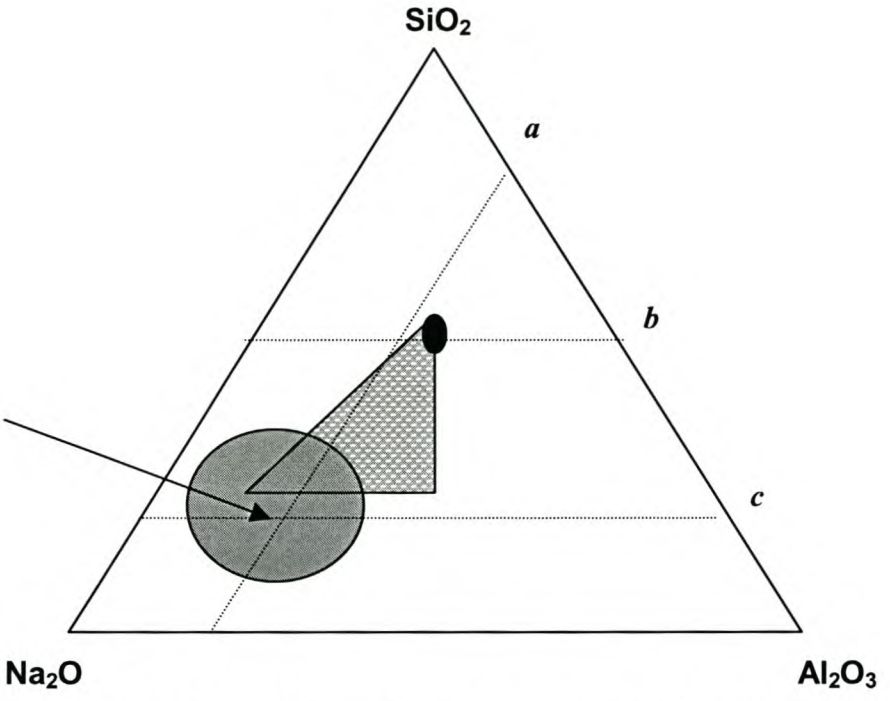

Figure 4.16: Ternary composition diagram of sodium oxide, silica and alumina.

The fields of nutrients for formation of zeolite A and Losod are indicated as well as the compositions of the zeolite products. In the case of Losod, marked by an arrow, the silica/alumina ratio of the nutrient field is calculated as follows:

A line is drawn parallel to the sodium/silica baseline through the projected position of composition. The ratio on the sodium/alumina baseline is then 1/4. A line is also drawn parallel to the sodium/alumina baseline through the projected position of composition. The ratio on the sodium/silica baseline is then 1/5. From this, the silica / alumina ratio is 1/5 divided by ¼, is 4/5. The Si/Al ratio is thus 2/5, which is <<1.

In the case of zeolite A, the ratio on the sodium/alumina baseline is then 1/4 and the ratio on the sodium/silica baseline is 1/2, resulting in a silica/alumina ratio of 2 and a Si/Al ratio of 1.

The ternary composition diagram indicates that the field of nutrient for the formation of Losod actually has a Si/Al ratio much lower than one. Due to the concentration gradients and the relatively low viscosity of the alumina nutrient, it diffuses through the large pore area of the tube. During this process most of the silica in the large pores reacts with the alumina and, sporadically, zeolite A crystals are formed. The alumina nutrient diffuses through the small pores of the tube as well and eventually contacts at the internal surface of the tube, the silica source. In contrast to

the initial supply of silica at the external surface, the supply of alumina to the internal surface is continued by a process of diffusion. Ultimately a Si/Al ratio of the nutrients, close to one, is achieved. Again, according to the ternary composition diagram, zeolite A is expected to form. Upon gel/crystal formation right at the internal surface, the further diffusion of nutrient solutions is blocked and no further progress of gel/crystal formation occurs. This results in the formation of a very thin crystal layer on the internal surface of the tube, see Figure 4.8. The zeolite A layer is approximately 6 μm thick which as concluded from a review table on zeolite A membrane thicknesses, is very thin for such a low silica/alumina ratio[19].

In the second scenario, where the alumina solution was added first, externally, the tube was immediately saturated with the Al source. After addition of the silica solution, internally, it was mainly Losod that was formed on the internal surface. The silica gradually diffused through the pores towards the external surface, resulting in Losod formation. In the third experiment the nutrients were added simultaneously, resulting in the formation of a zeolite A phase internally and a Losod phase externally. This was most probably due to the different diffusivities of the individual nutrient pools, resulting in two different phases on two different surfaces.

Regarding the zeolite A crystal layer, depicted in Figure 4.8, the cross section clearly shows a monolithic form partly identified by the crystal shape of the cubic zeolite A and partly by a form that can be described as a blanket covering the support, indicated in Figure 4.8 (b). The blanket form is actually the most preferable form to have as a membrane layer. This form is most probably created by the nanosized mixing of the alumina solution into the silica solution at the internal surface of the tube. The mixing tool here is the porous support with pores of 0.1 μm, from which the alumina solution is added to the silica solution. This 'spray' of alumina solution into the silica is quite a different process to bulk mixing. In contrast to bulk mixing, where relatively large volumes of nutrient have to mix mainly by diffusion, the spray is comprised of small volume elements that diffuse fast in the silica, on a molecular scale. With the initial high concentration of nutrient the contact of reactants in this transverse mode on a nanoscale results in fast mixing and local gel/crystallization.

4.4 Conclusions

With the approach of supplying reactants from opposite directions to the porous support layer, an extremely thin (6 μm) mono crystal layer was created on the internal surface of an alumina tube.

Depending on the position of the silica reactant, internally or externally, a continuous film of zeolite A or Losod was obtained, respectively.

Crystallization is controlled by particular Si/Al ratios of nutrients that are achieved upon diffusion of those nutrients through the porous system of the tube.

Changing the concentrations of the two nutrient pools could shift the crystallization front. The STS approach affords the use of very high nutrient concentrations, which is otherwise impossible in normal hydrothermal synthesis.

The STS method might be a useful method by which to prepare an array of highly dispersed zeolite A crystals inside a porous medium.

4.5 References

1. L. Gora, J.C. Jansen and T. Maschmeyer, *Stud. Surf. Sci. Catal.*, **125**, 1999, 173.
2. Z.A.E.P Vroon, K. Keizer, A.J. Burggraaf and H. Verweij, *J. Membr. Sci.*, **144**, 1998, 65.
3. J.C. Jansen and E.N. Coker, *Current Opinion Solid State & Mater. Sci.*, **1**, 1996, 65.
4. W.J.W. Bakker, F. Kapteijn, J. Poppe and J.A. Moulijn, *J. Membr. Sci.*, **117**, 1996, 57 and 107.
5. K. Kusakabe, S. Yoneshige, A. Murata and S. Morooka, *J. Membr. Sci.*, **116**, 1996, 39.
6. Z.A.E.P. Vroon, K. Keizer, M.J. Gilde, H. Verweij and A.J. Burggraaf, *J. Membr. Sci.*, **113**, 1996, 293.
7. E.R. Geus, M.J. den Exter and H. van Bekkum, *J Chem. Soc., Faraday Trans.*, **88**, 1992, 3101.
8. M. Matsukata, N. Nishiyama and K. Ueyama, *J. Chem. Soc., Chem. Comm.*, 1994, 339.
9. N. Nishiyama, K. Ueyama and M. Matsukata, *J. Chem. Soc., Chem. Comm.*, 1995, 1967.

10. J.C. Jansen, D. Kashchiev and A. Erdem-Senatalar, *Stud. Surf. Sci and Catal.*, **85**, 1994, 240.

11. V. Valtchev, S. Mintova and L. Konstantinov, *Zeolites*, **15**, 1995, 679.

12. J.C. Jansen, J.M. vd Graaff, N. vd Puil, S.B.G. Seijger and S.P.J. Smith, *Materials Research Society, Proceedings of the 12th International Zeolite Conference*, (Editors: M.M.J. Treacy, B.K. Marcus, M.E. Bisher and J.B. Higgins), Baltimore, U.S.A., July 1998, 603.

13. J.C. Jansen, J-H. Koegler, H. van Bekkum, H.P.A. Calis, C.M. vd Bleek, F. Kapteijn, J.A. Moulijn, E.R. Geus and N. vd Puil, *Mic. Mes. Mater.*, **21**, 1998, 227.

14. J.-H. Koegler, Ph.D. Thesis, Delft University, The Netherlands, 1999.

15. M.J. den Exter, Ph.D. Thesis, Delft University, The Netherlands, 1996.

16. A. Muller, G. Hakvoort and J.C. Jansen, *J. Thermal Analysis*, **53**, 1998, 449.

17. J.-H. Koegler, H.van Bekkum and J.C. Jansen, *Zeolites*, **19**, 1997, 262.

18. H. van Bekkum, E.M. Flanigen and J.C. Jansen (Editors), *Studies in Surface Science and Catalysis*, Vol. **58**, Introduction to zeolite science and practise, Elsevier, Amsterdam, 1991.

19. N.Nishiyama, Ph.D. Thesis, Osaka, Japan, 1997.

CHAPTER 5

The synthesis of a zeolite membrane from a continuous flow of separate reactants, in transverse mode. An explorative study

5.1 Introduction

Various synthesis techniques for the preparation of zeolite membranes have been studied and employed over the last decade. They included (i) embedding of zeolite crystals in a polymer matrix[1-6], (ii) normal hydrothermal synthesis, either self-supporting[7-15] or supported[16-33]. Several lesser known techniques were also used, such as, (iii) solid gel conversion[34-42], (iv) zeolite in metal membranes[43-46], (v) single crystal membranes[47-49], (vi) zeolite nanocrystals-colloidal suspension[50], (vii) the seed film method[51] and (viii) the static transverse mode described in the previous chapter[52].

The objective of this study was to synthesise zeolite membranes by supplying fresh nutrient to the internal and external surfaces of α-alumina tubes on a continuous basis. It was important that due to the continuous flow, the concentrations of the nutrients flowing along the tube remained more or less constant. An advantage of this continuous flow system will afford the ability to upscale. Longer tube lengths could be coated this way with zeolite crystals for separation or catalysis purposes.

The technique described here for the preparation of a zeolite A membrane is based on the static transverse synthesis, during which the separate nutrients, silica and alumina, are placed on either sides of a tube. In contrast to the previously used static synthesis method, here the separated reactants are circulated internally as well as externally along the length of the tube. For this operation the tube has to be connected and sealed to the individual nutrient-containing circuits. The heat for the crystallisation process is supplied by the heated reactant sources. In order to achieve the right temperature in the reactor it is necessary that the separate reactant sources be heated to a higher temperature than the zeolite A synthesis temperature, to

compensate for heat loss during the recirculating process. When relative short tubes (10 cm) are used, a local temperature gradient, that is over the length of the tube, is not expected. The volume of the nutrients exceeds the static volume of the reactor by orders of magnitude.

The feasibility of using continuous nutrient flow on the internal and external sides of the tube, to grow zeolite crystals *on* or *in* the support tube is described. Two different tube configurations were used in these experiments. Both were asymmetric α-alumina tubes, one had the α-alumina layer on the external side and one had the α-alumina on the internal side of the tube. See Figure 5.1. The tubes with the α-alumina on the external surface were supplied by ECN, The Netherlands, while the other tubes with the α-alumina layer on the internal side, were purchased from Atech, Germany.

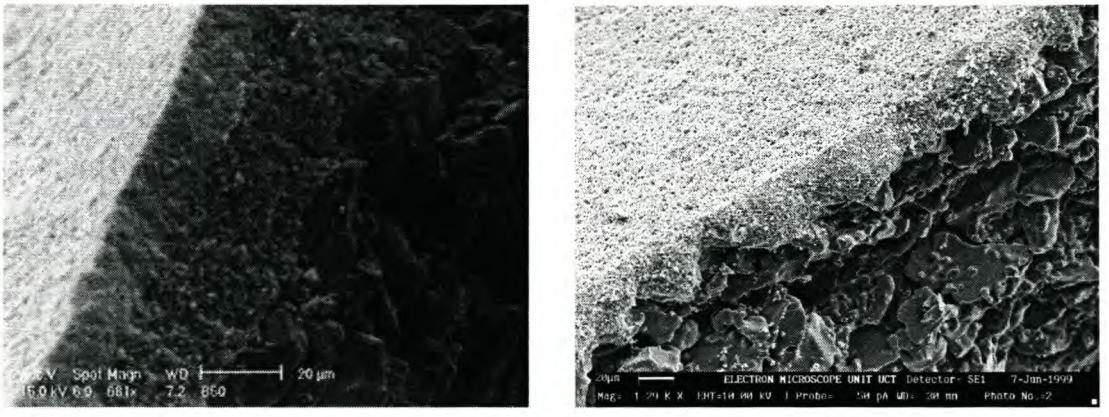

(a) (b)

Figure 5.1: A cross section of the tubes used in the continuous transverse synthesis of zeolite A membranes (a) ECN tube and (b) Atech tube.

5.2 Experimental

5.2.1 Building of the synthesis reactor

Experiments were carried out to build a synthesis reactor in which attempts will be made to coat α-alumina tubes with zeolite A in a continuous, semi plug-flow manner. A schematic drawing of the set up used for the continuous transverse flow synthesis of a zeolite A membrane is given in Figure 5.2. Peristaltic pumps were used to pump both the solutions through the reactor. The reactor was insulated by wrapping heating tape around the reactor. The residual solutions were collected in a waste container. Silicon rubber tubing was used to connect the reactor with the nutrient containers. The Si source was pumped through the inside of the tube (large pore area),

while the Al source was pumped over the external surface of the alumina tube (small pore area).

The first experiments, referred to as I, II and III, were conducted on an ECN tube and the second experiments, I, II, III, and IV, on an Atech tube.

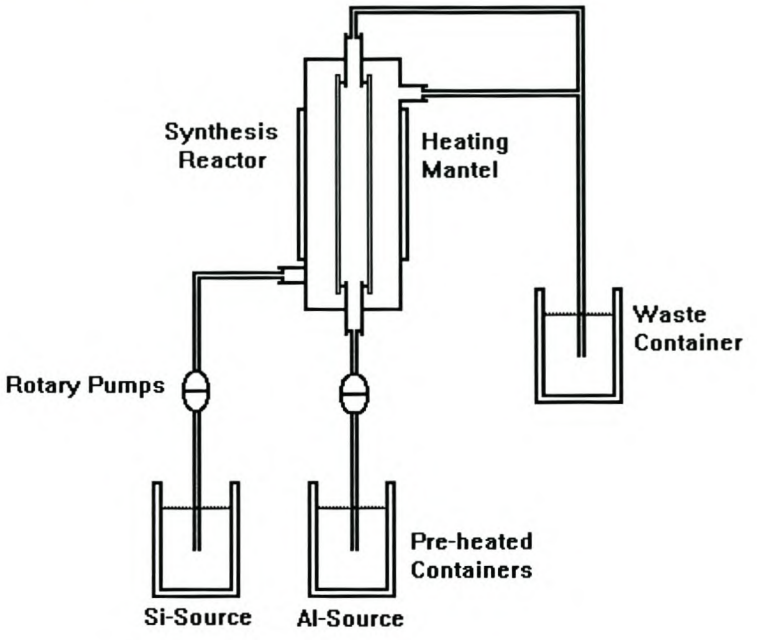

Figure 5.2: Schematic diagram of the synthesis reactor used for the synthesis of a zeolite A membrane.

5.2.2 Experiments on ECN tubes

5.2.2.1 Synthesis of a zeolite A membrane with separate reactant sources

Two solutions were prepared, one solution containing the alumina source and the second containing the silica source. The solutions were prepared as follows: 50% of the NaOH was dissolved in 50% of the H_2O. After complete dissolution, the alumina and silica were added to the respective caustic solutions, while stirring. The two source solutions were stirred until clear solutions were achieved. The amounts of reagents used are given in Table 5.1 below.

Table 5.1: Summary of composition of the synthesis solutions used in experiments with ECN and Atech tubes

	ECN			Atech			
Reagent (g)	Expt.I	Expt.II	Expt.III	Expt.IV	Expt.V	Expt.VI	Expt.VII
NaOH	150.5	17.51	17.43	13.2	13.4	12.9	13.3
H_2O	3615	3847	3846	1440	1440	1440	1440
$NaAlO_2$	8.1	198.2	198.2	148.7	223.1	234.4	148.5
Na_2SiO_3	47.4	371.6	371.5	278.6	278.7	278.4	278.6
Conditions							
Time (h)	8	8	9.5	48	48	48	96
Temp. (^oC)	55	55	75	80	80	80	80
Flow rate Ψ (ml/min)	16.7	4.17	4.2	3.5	3.7	3.4	3.5

Method: stirred transverse mode

5.2.2.2 Synthesis conditions

In an attempt to improve the crystal growth, the synthesis conditions (temperature and time) were varied.

Experiment I

The synthesis conditions are given in Table 5.1. The separate source solutions Si and Al were placed in a heat-controlled waterbath at 84°C. It was very difficult to maintain low levels of nutrient flow, partially due to the temperature of the liquids (Si and Al) and the gravitational forces that needed to be overcome in order to allow positive flow up the α-alumina tube. It was our understanding that it was important to keep the liquid flow as low as possible in order to achieve complete wetting of the alumina surface and prevent removal of the aluminosilicate gels on the surfaces. The length of the tube in the reactor was 250mm. The lowest liquid flow that could be achieved was ± 16.7 ml/min, which is about 1l/h.

Experiment II

The synthesis conditions that prevailed in the second experiment are given in Table 5.1.

In experiment II the compositions of the nutrient solutions were changed from those used in experiment I. The Si and Al contents were increased, while the NaOH concentration was decreased. The flow rate of the nutrients was decreased substantially, by selecting and using connecting tubes with a smaller diameter. The Si solution was pumped through the inside of the tube, while the Al solution was pumped over the external surface of the alumina tube.

Experiment III

As in experiments I and II no real crystal growth was detected on the external surface of the tube, therefore, it was decided to carry out a temperature profile study on the reactor. This involved the same setup and preparation steps as for the synthesis, but water was used instead of the synthesis mixtures. The water was allowed to reach the temperature of the waterbath, which was about 84°C. After thermal equilibration the water was pumped through the system and the temperature inside the reactor measured with a thermocouple. The temperature inside the reactor was found to be only 55°C, while that of the waterbath was 84°C. The former temperature was much too low for nucleation and crystallisation to take place in the reactor. Flanigen *et al.*[53] reported that it takes about 3 hours for the nucleation of a zeolite to start at a temperature of 60°C. This means that most of the actual synthesis times in experiments I and II were "used" just to start nucleation, and a possible reason why they did not yield any sort of zeolite growth on the tube surface.

The following experiments were therefore aimed at increasing the temperature in the reactor. This could not be done by increasing the temperature of the waterbath alone. The configuration of the synthesis set up was changed slightly from that used in experiments I and II in order to improve the heat transfer from the reservoir to the reactor. This was done by placing the peristaltic pumps on the outlet side of the reactor, therefore shortening the length of tubing needed to connect the reactor to the reservoir, so improving the heat transfer. Polypropylene bottles replaced the polyethylene bottles, meaning that the temperature of the waterbath could be increased. For this purpose the water in the bath was replaced with ethylene glycol, which has a boiling point of > 250°C.

The positions of the two nutrient solutions (Si and Al) were swapped, meaning that the Si solution was now pumped over the external surface of the tube (small pores) and the Al solution was pumped through the inside of the tube.

A late addition to the synthesis reactor was overhead stirrers. This afforded the ability to continuously keep the reaction mixtures homogeneous, and also mix the fresh solutions of the nutrients with the older solutions during the course of the synthesis. This also afforded a more homogeneous temperature distribution in the source-solution containers. The temperature of the waterbaths in which the two source solutions were heated was kept constant at 94-95°C. A schematic diagram of the improved synthesis reactor is given in Figure 5.3. The synthesis conditions of this experiment are summarised in Table 5.1.

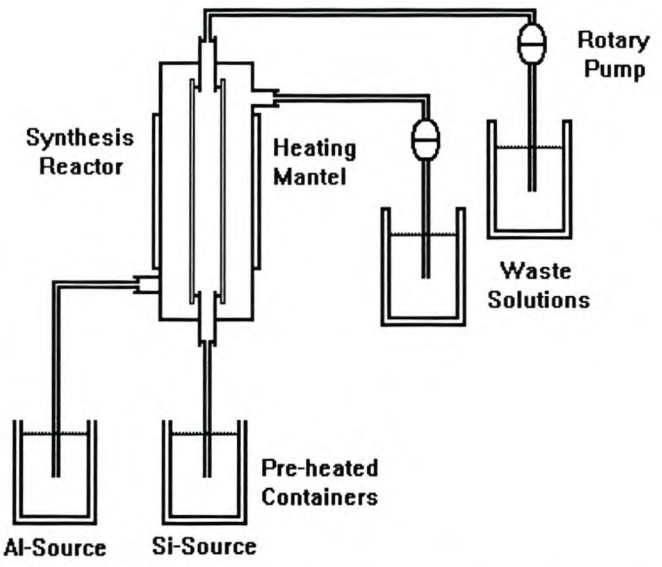

Figure 5.3: Schematic diagram of the improved synthesis reactor.

It is known that the rate at which the nutrient solutions are pumped through the reactor have an influence on the heat transfer in the reactor. The pump rate was kept at a minimum, to prevent the removal of any formed aluminosilicate gels from either of the two surfaces.

On completion of the syntheses, pure water was pumped through the reactor system for 2 hours to wash the caustic solution from the tube with water. The tubes were then dried in a hot-air oven overnight.

5.2.2.3 Synthesis results

The first attempts at running these continuous-flow syntheses were aimed at maintaining an adequately high synthesis temperature in the reactor and running the syntheses for as long as possible. During the first few attempts the synthesis time was rather short (± 10 h), compared to the synthesis time of the static transverse synthesis (6 days). The results of the first 3 experiments are given below.

Experiment I: SEM analysis of the tube prepared showed no sign of zeolite crystal growth on the external surface of the ECN tube. See Figure 5.4(a). The reason why the external surface of the tube was inspected, and not the internal surface, was because the small pores (α-alumina layer) were on the external surface. As mentioned in the previous chapter, in order to grow zeolite crystals on a porous support the support pore-size needs to be comparable with the zeolite crystal size, and this is only true for the pores of the external surface.

Experiment II: SEM analysis showed that there was almost nothing resembling zeolite crystals on this external surface, Figure 5.4(b).

Experiment III: The SEM micrograph recorded of the external surface showed some zeolitic material on the external surface of this tube. The increased temperature led to improved growth of zeolite A crystals on this tube. See Figure 5.4(c).

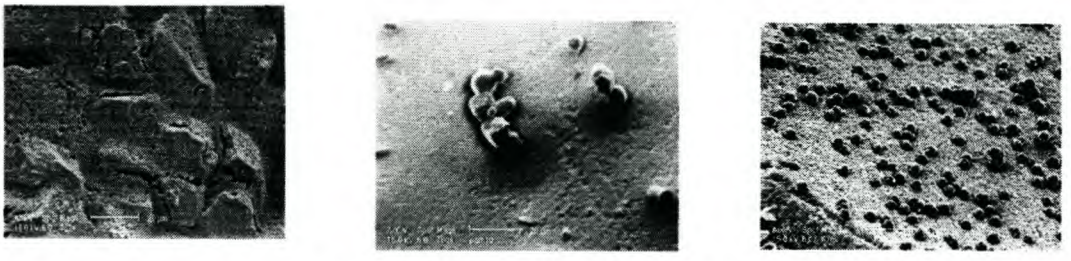

Figure 5.4: External surfaces of the ECN α-alumina tubes, (a) Experiment I, (b) Experiment II and (c) Experiment III.

5.2.3 Experiments on Atech tubes

The next series of experiments was conducted on α-alumina tubes purchased from Atech, Germany. Here the α-alumina layer is on the internal surface of the tube. The dimensions of the tubes used in these syntheses were as follows: OD – 10 mm, ID – 6 mm, Length – 95 mm, Outer pore diameter – 15 μm and Inner pore diameter – 0.1 μm.

5.2.3.1 Synthesis of a zeolite A membrane with separate reactant sources

Two solutions were prepared: one containing the alumina source and the second the silica source. The solutions were prepared as follows: 50% of the NaOH was dissolved in 50% of the H_2O and, after complete dissolution, the alumina and silica were added to the respective caustic solutions, while stirring. Due to the high concentration of the alumina some of the iron present in the sodium aluminate, precipitated and this was removed by filtering. The two source solutions were stirred until clear solutions were achieved. The amounts of the reagents used have been given in Table 5.1.

5.2.3.2 Synthesis conditions

Three synthesis variables still needed to be addressed: the synthesis time, position of the nutrients and the possible recycling of the nutrients. Four experiments are discussed here.

Experiment IV:

The synthesis conditions have been given in Table 5.1. The set up of the synthesis reactor is shown in Figure 5.5.

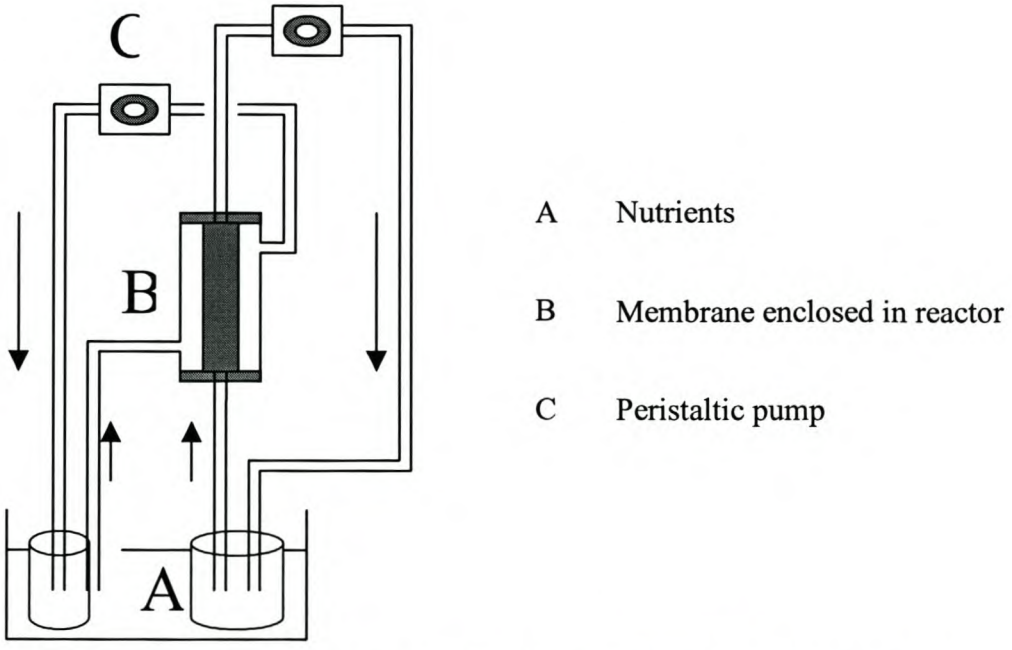

Figure 5.5: The synthesis reactor set up for the recycling of the nutrients on a continuous basis during the synthesis of a zeolite A membrane.

The ethylene glycol bath, which was used as the heat source, was pre-heated to 96°C. Two polypropylene bottles, containing the two separate nutrients (Si and Al), were placed in the bath and allowed to reach the equilibrium temperature, before the flow through the synthesis reactor was started.

Hexa-fluoro propylene (HFP) tubing, due to its durability in high pH and high-temperature systems was used.

The silica source was allowed to flow through the inside of the α-alumina tube and the Al source over the external surface of the tube. The set up for the synthesis was also slightly changed in order to avoid the continuous replacement of the nutrient, which had to be done in the first experiments (I-III), because the nutrient was not recycled. The modification of the reactor set up meant that it was now possible to recycle the nutrient continuously. This meant that less chemicals were needed for a long synthesis, resulting in a more cost-effective and less labor-intensive system.

Using different peristaltic pumps it was possible to keep the nutrient flow down to very low levels, just high enough to overcome the gravitational forces required to achieve positive flow up the α-alumina tube. Several attempts were made to run the synthesis for as long as possible (4-6 days), but this was often complicated by the formation of aluminosilicate gels in the tubes connecting the reactor with the bottles containing the nutrients. These gels formed due to a leakage in the stainless steel reactor and resulted in the termination of the flow of the nutrients through the reactor. As soon as the flow of nutrient is stopped then the heat supply is terminated, which means that there is no further zeolite nucleation and crystal growth possible. A schematic representation of the stainless steel reactor is given in Figure 5.6.

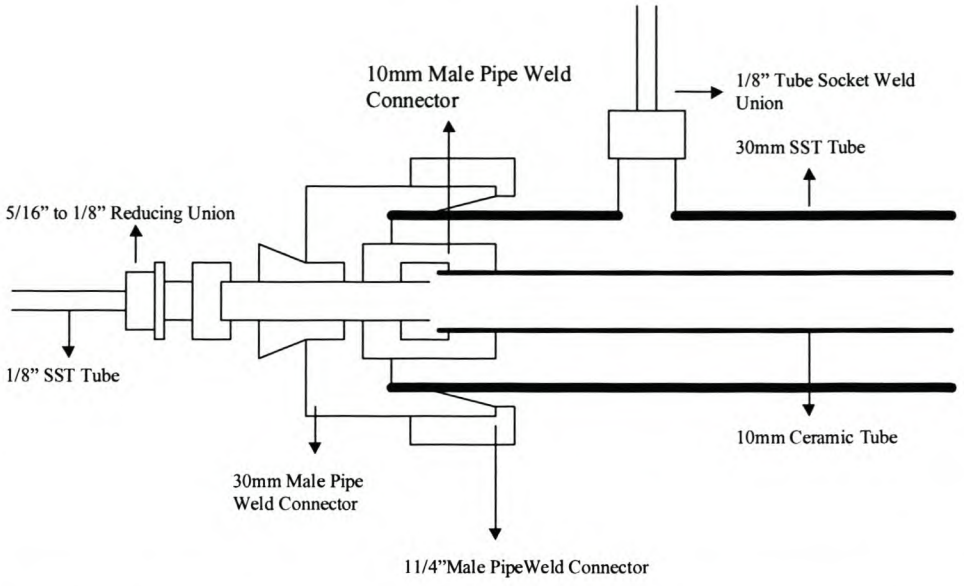

Figure 5.6: A schematic representation of the continuous flow synthesis reactor.

After two days the continuous-flow synthesis stopped due to a blockage of hardened aluminosilicate gel in the tubes. Water was pumped through the reactor system to remove the caustic solution from the tube. This was followed by treatment with three different concentrations of ethanol (50, 75 and 100%), which resulted in the replacement of the water with ethanol in the micropores of the zeolite crystals. This allowed for the effective removal of moisture from the micropores without breaking the crystals in the process. The tube was then dried in a hot-air oven overnight.

Experiment V:

The synthesis conditions have been given in Table 5.1.

In this synthesis the alumina content was increased by 50% and the synthesis was carried out for 48 h, before blocking of the tubes occurred. The nutrients were recycled continuously. The silica solution was passed through the inside of the tube.

Experiment VI:

The alumina content in this experiment was also increased by 50% and the tube first saturated with Al before the Si source was pumped through the reactor system. The nutrients were recycled continuously. The silica solution was again passed

through the inside of the tube. Unfortunately, this synthesis only ran for 48 h, due to blocking of the HFP tubes by aluminosilicate gels.

Experiment VII:

The normal IZA prescribed zeolite A synthesis mixture was used in this synthesis. The pumps were started simultaneously, meaning that both nutrients contacted the alumina tube at the same time. The nutrients were recycled continuously. The silica solution was again passed through the inside of the tube. This time the synthesis was carried out for 4 days. On completion of the synthesis the nutrients were replaced with water, to wash the caustic solution from the tube and crystals. This was followed by treatment with three different concentrations of ethanol (50, 75 and 100%), and resulted in the replacement of the water with ethanol in the micropores of the zeolite crystals. This allowed effective removal of moisture from the micropores without breaking the crystals in the process. The tube was afterwards dried in a hot-air oven overnight.

5.2.3.3 Synthesis results

The first three syntheses were conducted for only 48 h, due to the blocking of the tubing. In the final experiment (VII) we were able to run the synthesis for 96 h and although this was still shorter than the synthesis time of the static synthesis, the crystal growth improved considerably compared to experiments (I-VI).

Experiment IV: SEM analysis of the internal surface of the prepared tube showed some zeolite crystal growth. See Figure 5.7(a). There were also some crystals in the cross section of the tube, Figure 5.7(b). These results indicated that if it was possible to run the synthesis for longer periods of time, the technique should be viable.

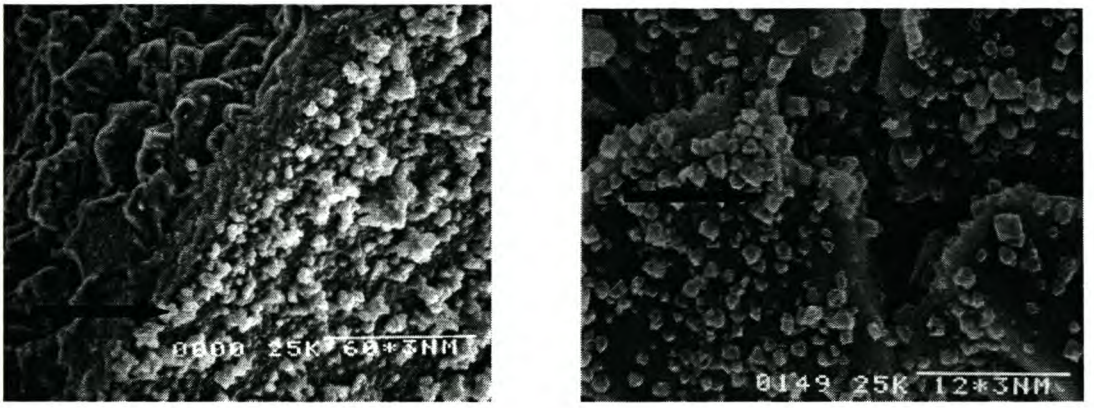

(a) (b)

Figure 5.7: SEM micrographs of zeolite A crystals on the alumina particles of (a) the internal surface and (b) cross section of the tube (as indicated with arrows).

Experiment V: Results of SEM analysis of the tube prepared in this experiment showed that there was no improvement in the crystal growth, either on the internal surface or in the cross section of the alumina tube, compared to the synthesis conducted in the previous experiment. The wetting/saturation of the tube with the Al source did not improve the crystal growth; in actual fact it probably decreased the actual synthesis time, due to aluminosilicate gel formation in the tubing.

Experiment VI: SEM analysis of this tube again showed no real improvement in the crystal growth inside the tube (cross section) compared to tube prepared in experiment IV.

Experiment VII: The tube prepared in this experiment was analysed with the aid of SEM and XRD. The SEM micrographs, depicted in Figure 5.8, show positive results as far as crystal growth is concerned. This synthesis was conducted for 96 h, the longest continuous synthesis yet. The temperature inside the synthesis reactor was high enough for zeolite A crystal growth in the transverse flow mode. This results in very good zeolite A crystal growth on the internal surface of the alumina tube. See Figure 5.8(a). Although there is probably not a continuous zeolite crystal layer, there is a large amount of zeolite A crystals present, which makes this dynamic transverse synthesis technique viable for zeolite A membrane preparation on a larger scale. There are also a large amount of crystals present in the cross section of the tube, with a crystal concentration gradient, decreasing from the external surface towards the internal surface, Figure 5.8(b-d).

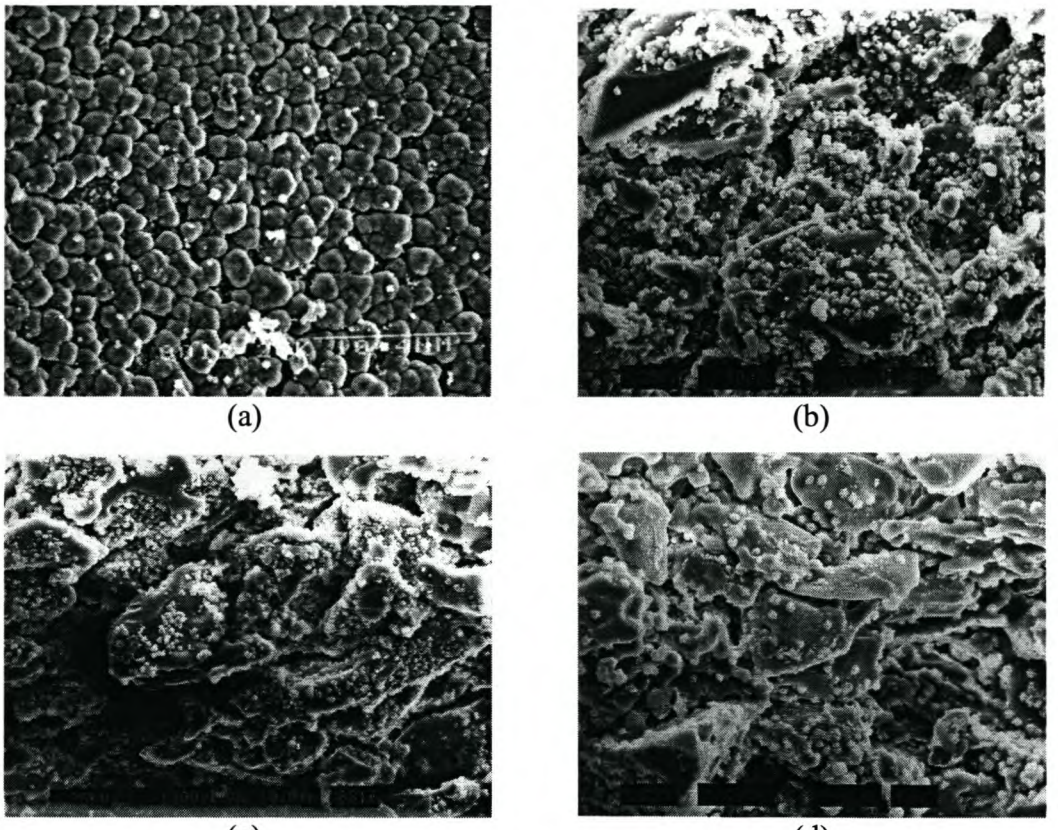

Figure 5.8: SEM pictures of zeolite A crystals present (a) on the internal surface of the alumina tube, (b) in the cross section near the external surface, (c) nearer the internal surface and (d) almost at the internal surface.

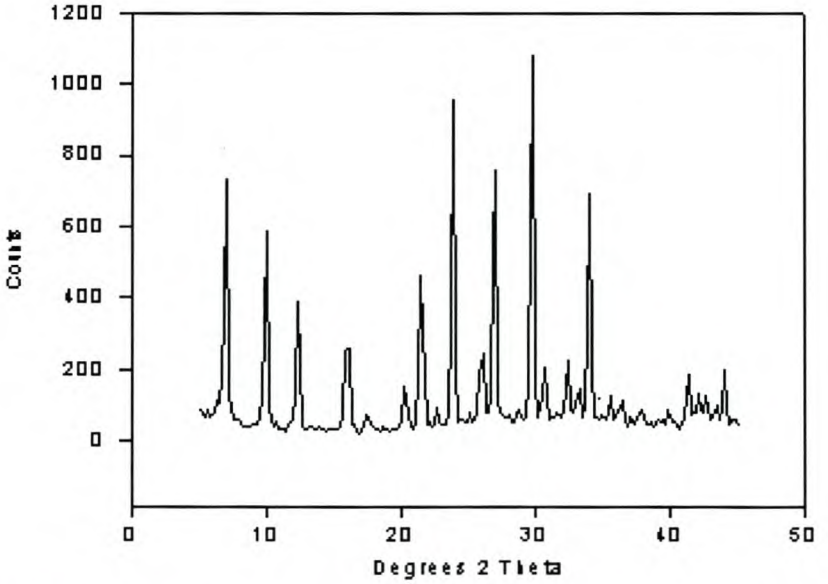

Figure 5.9: XRD spectrum of zeolite A crystals on the internal surface of the Atech α-alumina tube prepared in experiment VII.

XRD analysis of the zeolite crystals present on this tube shows that zeolite A is formed. See Figure 5.9.

5.2.4 Mass transfer from liquid to solid phase, a general analysis

The mass transfer of the nutrients, applied for the zeolite coating, from the liquid phase to the alumina tube surface will be controlled by several factors, i.e. the type of flow pattern, the diffusion coefficient(s) of monomers of aluminate and silicate, as well as oligomers and larger entities of silicate, the viscosity (at the operation temperature) of the liquid, the smoothness or roughness of the alumina tube surface, the density of functional groups on the surface and the wetting properties of the surface.

5.2.4.1 Liquid flow pattern in/around an alumina support tube

In general the following configuration of flow patterns in and around the tube is applied in the dynamic set up, see Figure 5.10.

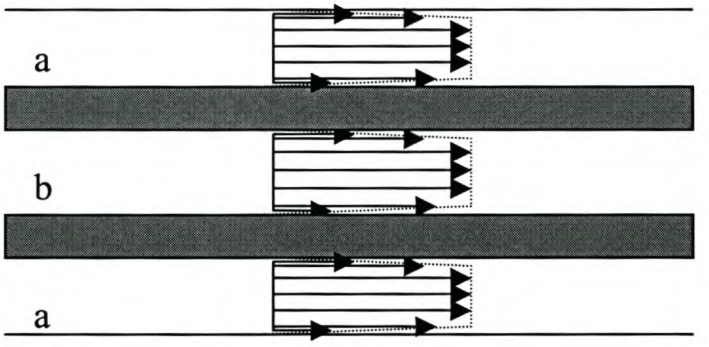

Figure 5.10: Cross-section of the membrane support, indicating the flow pattern of the individual synthesis solutions for zeolite A crystallisation on this support. (a) and (b) are the respective nutrient solutions.

$a = b = D_i$

$D_i \approx 6 \times 10^{-3} m$

$\phi_v \approx 3.5 \times 10^{-6} m^3/s$

$v_x \approx \phi_v / 0.25.\pi.D_i^2 = 0.124$ m/s

In order to calculate the Reynolds number the viscosity of the solutions were determined. The viscosity of the reactant solution was measured in a dynamic viscosity mode at the relevant crystallization temperature, which was between 60°C and 90°C. The viscosity of the reactant solution was 7.5 cp, while that of water at the same temperature was 1 cp.

$$Re \approx (\rho.v_x.D_I)/\eta = 96$$

With Re < 2000, the flow in/around the tube is laminar under the prevailing synthesis conditions.

However, 5 cases of laminar flow profiles can be distinguished, as shown in Figure 5.11.

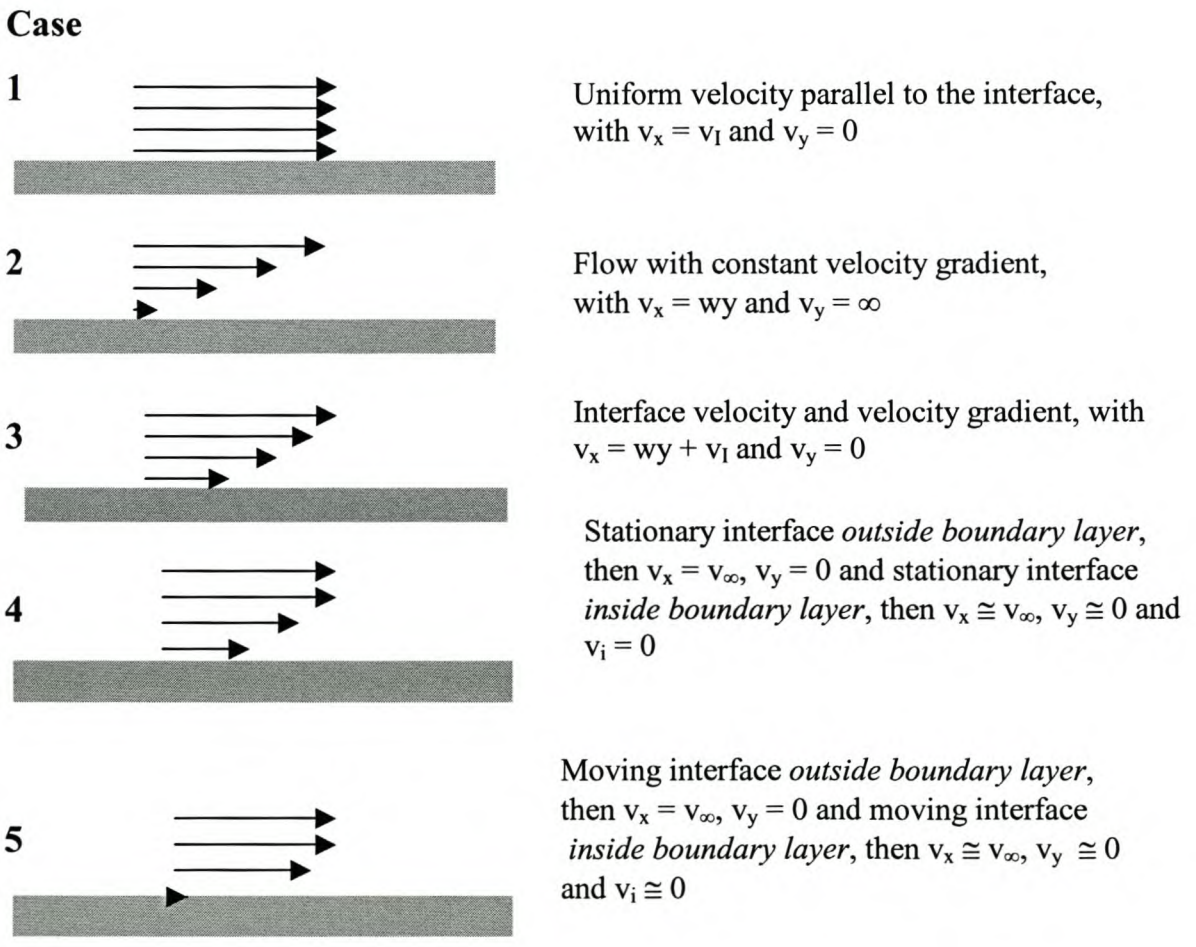

Figure 5.11: A depiction of the 5 laminar flow patterns. The coordinate system is such that x is parallel to the flow direction and y is perpendicular to the flow direction.

It is frequently assumed that the velocity of a liquid flow at a solid wall is zero[54]. This is called the non-slip condition. Furthermore, viscous fluids create a boundary layer. For the laminar flow of the reactant solution through the alumina tube, as discussed above, the best simulation is represented in case 5. This boundary layer can be described by the following equation:

$$u_x = u_o + ay + by^2 + cy^3$$

This equation could be solved further, however, for the purpose of this thesis, the data to solve the equation was not determined.

5.2.4.2 The wetting properties of the wall of the tube

The roughness of the tube wall is different for the external and internal surfaces as the pores through the wall are asymmetric. The pore diameter is 10 – 15 μm and 0.1 um at the external and internal surface, respectively.

The roughness of, for example, the external surface wall of the tube is relatively small but existing as is shown in Figure 5.12. The latter is a cross section of the tube, indicating that the largest difference between a 'hill' and a 'valley' is not more than 0.01 mm.

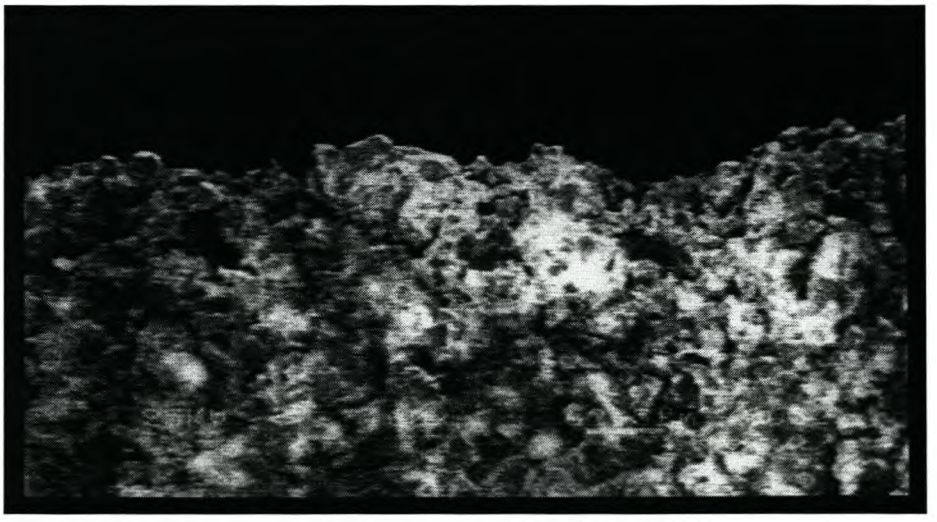

Figure 5.12: SEM micrograph of a cross section of the wall of the alumina tube used for contact angle measurements. The roughness of the surface wall is defined here as the distance between the lowest and highest points in the wall.

The chemical composition and topology of the alumina provides a typical population of ~ 4 OH/nm^2, which is a high density of functional groups, in order to effect chemical bonding between the support surface and the developing zeolite coating. This high concentration also increases the hydrophilicity of the alumina wall.

Based on the above considerations the wetting angle of the α-alumina was determined. The measurement was carried out in a so-called dynamic contact angle experiment. Figure 5.13 shows the curve generated by the contact angle measurement. The $\cos\theta = 1$ for water on this Al_2O_3 tube, indicating perfect wetting. This might be due to capillary forces, the mediocre value of the simultaneously measured internal and external surface and the surface roughness of the alumina material. This measurement ($\cos\theta = 1$) strongly indicates that the alumina material is hydrophilic. The above data show that crystallization of the zeolite on the alumina surface is indeed possible.

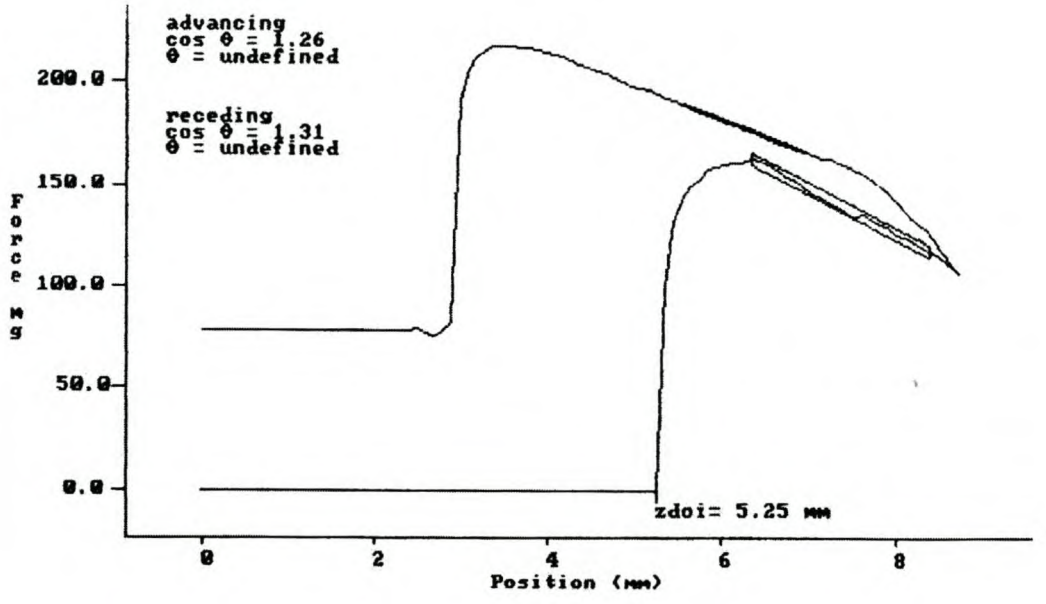

Figure 5.13: Determination of the contact angle between water and an alumina tube.

It was further noted that under the static as well as under the dynamic synthesis conditions, for zeolite coating on the alumina support surface, the velocity of the liquid close to the wall was zero. In both cases the mass transfer from the liquid to the

solid phase was due to diffusion, driven by the concentration gradients from the liquid to solid phase.

5.2.5 Principals of crystal formation on the alumina tube

First, molecular-sized species of pure silica and alumina and small oligomer species diffuse, upon concentration gradients, through the pores in the wall of the tube. Gradually elements of aluminosilicate form which settle, according to SEM observations, mainly on the internal and external tube surfaces and to a lesser extent in the pores of the wall. The aluminosilicate gel, when the stoichiometric ratio is achieved, provides building units via ion-transportation for the zeolite formation. The building units for the synthesis of the zeolite can be numerous, as depicted in Figure 5.14.

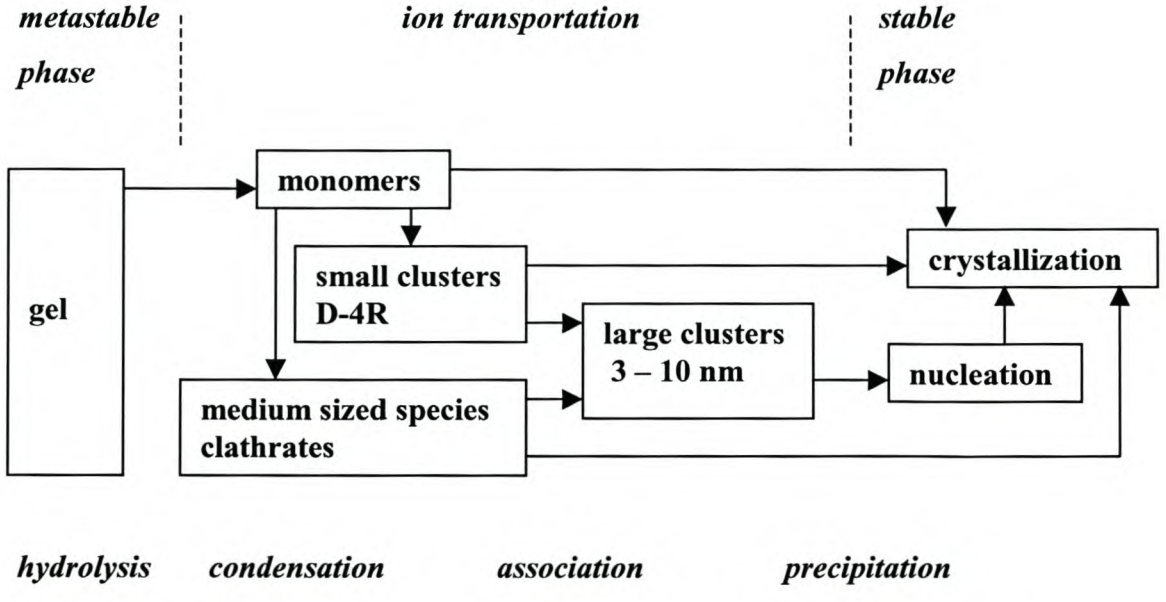

Figure 5.14: Scheme of the possible species dissolved from gel, developed in solution and upon ion transportation, used for nucleation and crystallisation of zeolites.

Most zeolite crystal building units are partly negatively charged and externally terminated with hydroxyl groups. Several types of building units contribute to the nucleation and crystallization. Interactions of the building units with the wall of the tube take place as the zeta potential of the wall is more positive (iso-electric point of

AlOH is at pH 9, while the pH of the solution is 12) than the building units of the objected zeolite (iso-electric point of SiOH is at pH 2). In addition, the wall contains hydroxyl groups that can condense, at high temperature, with the zeolite building units. The population of hydroxyl groups on the building units is 4 OH/nm^2, while the population of hydroxyl groups on the alumina support surface is 1 – 2 OH/nm^2. Hence, *in situ* crystallization on the wall of the tube can be achieved, as indicated by the zeolite A crystal that is grown from the wall. See Figure 5.15.

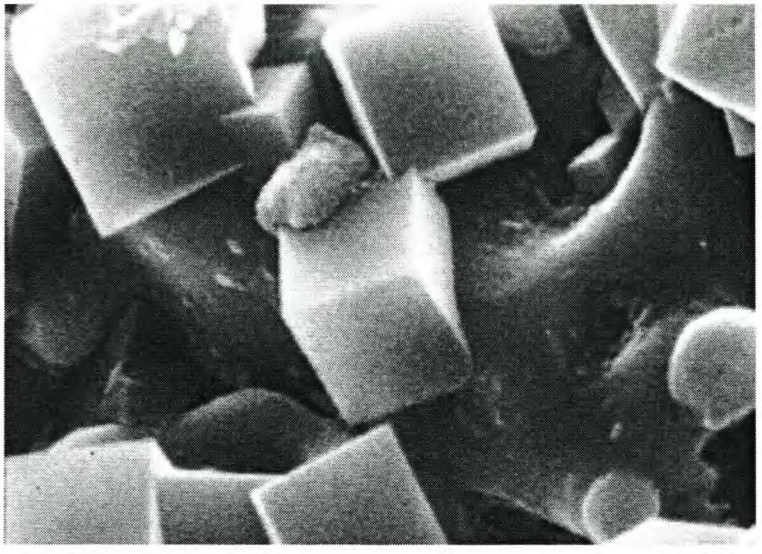

Figure 5.15: SEM micrograph showing a partly completed zeolite A crystal (cubic shape) that was most probably nucleated on the tube wall and grown from the wall.

5.3 Discussion

The two main factors that had to be addressed in the experiments described in this chapter were the synthesis temperature and synthesis time. In the first couple of experiments the synthesis temperature was too low, resulting in poor nucleation and zeolite crystal growth. As the design of the reactor set up was improved, the synthesis temperature could be increased and the synthesis time became the dominant factor to be considered. This proved to be a major problem in the latter experiments. The connecting tubing (HFP) was blocked by aluminosilicate gels, which then hardened due to the high temperatures of the circulating nutrients, resulting in a complete cut-off of the nutrient flow, therefore terminating the synthesis. As soon as this was overcome, in Experiment VII, the crystal nucleation and crystal growth could proceed as in the static transverse synthesis. The results of the dynamic transverse synthesis

experiments in terms of zeolite crystal growth were comparable to those achieved in the static syntheses. The best crystal growth was obtained when the Si source was placed on the internal side of the Atech tubes, meaning the small pore side of the alumina tube. This is because the support pore size must be comparable to the zeolite crystal size in order to obtain a continuous zeolite coating.

Due to the hydrodynamics of the continuous flow system, various factors play a role in the outcome of these experiments, for example, the roughness factor. This factor was however not included in the study, but should have been, because although the system has a constant replenishment of nutrient, there is almost no flow. Hence, it actually corresponds with the static system that was studied in Chapter 4. The viscosity of the nutrient solution is greater than that of water, meaning that the stability parameter (χ) is actually decreased during the synthesis. This in turn means greater stability and less turbulence near the boundary (surface of the tube). Therefore, mixing of nutrients is not caused by turbulence near the surface of the tube.

5.4 Conclusions and Recommendations

The viability of the continuous transverse flow synthesis was shown, but more research has to be done in order to improve the system in terms of operatability and zeolite crystal growth. Longer tubes can be used in such a reactor; this opens up opportunities for up scaling in pilot plant design. The continuous recycling of nutrients prevents the total depletion of one or both of the nutrients during the actual synthesis. The design of the reactor set up is very simple and relatively inexpensive, making it easy to reconstruct.

In order to further improve the continuous flow system, a more comprehensive hydrodynamic analysis should be carried out. The influence of certain parameters on the growth of zeolite crystals, such as: liquid flow velocity, membrane surface roughness and viscosity of the nutrient solutions, should be investigated more thoroughly.

5.5 References

1. M. Demertzis and N.P. Evmiridis, *J. Chem. Soc., Faraday Trans.* 1, **82**, 1986, 3647.
2. H.J.C. te Hennepe, W.B.H. Boswerger, M.H.V. Mulder and C.A. Smolders, *J. Membr. Sci.*, **89**, 987, 39.
3. H.J.C. te Hennepe, C.A. Smolders, D. Bargeman and M.H.V. Mulder, *Sep. Sci. Technol.*, **26**, 1991, 585.
4. M.-D. Jia, K.-V. Peinemann and R.-D. Behling, *J. Membr. Sci.*, **57**, 1991, 289.
5. I.R. Bellobono, F. Muffato, C. Ermondi, E. Selli, L. Righetto and M. Zeni, *J. Membr. Sci.*, **55**, 1991, 263.
6. S.P.J. Smith, E.P. Jacobs and R.D. Sanderson, *Proc. IMSTEC`96*, Australia, November`96.
7. T. Sano, Y. Kiyozumi, M. Kawamura, F. Mizukami, H. Takaya, T. Mouri, W. Inaoka, Y. Toida, M. Watanabe and K. Toyoda, *Zeolites*, **11**, 1991, 842.
8. J.G. Tsikoyiannis and W.O. Haag, *Zeolites*, **12**, 1992, 126.
9. T. Sano, Y. Kiyozumi, F. Mizukami, H. Takaya, T. Mouri and M. Watanabe, *Zeolites*, **12**, 1992, 131.
10. T. Sano, F. Mizukami, H. Takaya, T. Mouri and M. Watanabe, *Bull. Chem. Soc. Jpn.*, **65**, 1992, 146.
11. T. Sano, Y. Kiyozumi, K. Maeda, M. Toba, S. Niwa and F. Mizukami, *J. Mater. Chem.*, **2**, 1992, 141.
12. G.J. Myatt, M. Budd, C. Price and S.W. Carr, *J. Mater. Chem.*, **2**, 1992, 1103.
13. M.W. Anderson, K.S. Pachis, J. Shi and W. Carr, *J. Mater. Chem.*, **2**, 1992, 255.
14. S. Yamazaki and K. Tsutsumi, *Microporous Mater.*, **5**, 1995, 245.
15. Y. Kiyozumi, F. Mizukami, K. Maeda, T. Kozasa, M. Toda and S. Niwa, *Stud. Surf. Sci. Catal.*, **105**, 1997, 2225.
16. E.R. Geus, M.J. den Exter and H. van Bekkum, *J. Chem. Soc., Faraday Trans.*, **88**, 1992, 3101.
17. E.R. Geus, H. van Bekkum, W.J.W. Bakker and J.A. Moulijn, *Microporous Mat.*, **1**, 1993, 131.
18. Y. Yan, M.E. Davis and G.R. Gavalas, *Ind. Eng. Chem. Res.*, **34**, 1995, 1652.
19. M.-D. Jia, K.-V. Peinemann and R.-D. Behling, *J. Membr. Sci.*, **82**, 1993, 15.

20. M.-D. Jia, B. Chen, R. D. Noble and J.L. Falconer, *J. Membr. Sci.*, **90**, 1994, 1.

21. T. Masuda, A. Sato, H. Hara, M. Kouno and K. Hashimoto, *Applied Catalysis A: General* **111**, 1994, 143.

22. T. Sano, M. Hasegawa, Y. Kawakami Y. Kiyozumi, H. Yanagishita, D. Kitamoto and F. Mizukami, *Stud. Surf. Sci. Catal.*, **84**, 1994, 1175.

23. T. Sano, H. Yanagishita, Y. Kiyozumi, F. Mizukami and K. Haraya, *J. Membr. Sci.*, **95**, 1994, 221.

24. Y. Yan, M. Tsapatsis, G.R. Gavalas and M.E. Davis, *J. Chem Soc., Chem. Commun.*, 1995, 227.

25. P. Meriaudeau, A. Thangaraj and C. Naccache, *Microporous Mat.*, **4**, 1995, 213.

26. Bai, M.-D. Jia, J.L. Falconer and R.D. Noble, *J. Membr. Sci.*, **105**, 1995, 79.

27. Y.H. Chiou, T.G. Tsai, S.L. Sung, H.C. Shih, C.N. Wu and K.J. Chao, *J. Chem. Soc., Faraday Trans.*, **92**, 1996, 1061.

28. Z.A.E.P. Vroon, K. Keizer, M.J. Gilde, H. Verweij and A.J. Burggraaf, *J. Membr. Sci.*, **113**, 1996, 293.

29. H. Kita, K. Horii, Y. Ohtoshi, K. Tanaka and K. Okamoto, *J. Mater. Sci. Lett.*, **14**, 1995, 206.

30. T. Masuda, H. Hara, M. Kouno, H. Kinoshita and K. Hashimoto, *Microporous Mater.*, **3**, 1995, 565.

31. S. Yamazaki and K. Tsutsumi, *Microporous Mater.*, **4**, 1995, 205.

32. K. Suzuki, Y. Kiyozumi, T. Sekine, K. Obata, Y. Sindo and S. Sin, *Chem. Express*, **5**, 1990, 793.

33. H. Mimura, T. Tezuka and K. Akiba, *J. Nucl. Sci. Technol.*, **32**, 1995, 1250.

34. D.M. Bibby and M.P. Dale, *Nature*, **317**, 1985, 157.

35. Q. Huo, S. Feng and R. Xu, *J. Chem. Soc., Chem. Commun.*, 1988, 1486.

36. W. Xu, J. Li, W. Li, H. Zhang and B. Liang, *Zeolites*, **9**, 1989, 468.

37. W. Xu, J. Dong, J. Li, J. Li, and F. Wu, *J. Chem. Soc., Chem. Commun.*, 1990, 755.

38. M.H. Kim, H.X. Li and M.E. Davis, *Microporous Mater.*, **1**, 1993, 191.

39. N. Nishiyama, PhD Thesis, Osaka University, 1997.

40. J. Dong, T. Dou, X. Zhao and L. Gao, *J. Chem. Soc., Chem. Commun.*, 1992, 1056.

41. F. Crea, R. Aiello, A. Nastro and J.B. Nagy, *Zeolites*, **11**, 1991, 521.

42. R. Althoff, K. Unger and F. Schuth, *Microporous Mater.*, **2**, 1994, 557.

43. P. Kolsch, D. Venzke, M. Noack, P. Toussaint and J. Caro, *J. Chem. Soc., Chem. Commun.*, 1994, 2491.

44. P. Kolsch, D. Venzke, M. Noack, E. Lieske, P. Toussaint and J. Caro, *Stud. Surf. Sci. Catal.*, 1994, 1075.

45. J. Girnus, M.M. Pohl, J. Richter-Mendau, M. Schneider, M. Noack, D. Venzke and J. Caro, *Adv. Mater.*, **7**, 1995, 711.

46. J. Caro, F. Marlow, K. Hoffmann, J. Kornatowski, I. Girous, M. Noack and P. Kolsch, *Stud. Surf. Sci. Catal.*, **105**, 1997, 2171.

47. D.B. Shah, S. Chokchal-acha and D.T. Hayhurst, *J. Chem. Soc., Faraday Trans.*, **89**, 1993, 3161.

48. D.B. Shah and H.Y. Liou, *Zeolites*, **14**, 1994, 541.

49. D.B. Shah and H.Y. Liou, *Stud. Surf. Sci. Catal.*, **84**, 1994, 1347.

50. M. Tsapatsis, T. Okubo, M. Lovallo and M.E. Davis, *Mat. Res. Soc. Symp.Proc.*, **371**, 1995, 21.

51. J. Hedlund, B.J. Schoeman and J. Sterte, *Stud. Surf. Sci. Catal.*, **105**, 1997, 2203.

52. S.P.J. Smith, R.D. Sanderson and J.C. Jansen, *Microporous and Mesoporous Materials*, Submitted, 2002.

53. H. van Bekkum, E.M. Flanigen and J.C. Jansen (Eds.), *Stud. Surf. Sci. Catal.*, **58**, Introduction to Zeolite Science and Practice, Elsevier, Amsterdam, 1991.

54. W.J. Beek and K.M.K. Muttzall, Transport Phenomena, John Wiley & Sons, New York, 1975.

CHAPTER 6

Preliminary results of permeation and pervaporation measurements through the alumina-supported zeolite A membranes

6.1 Introduction

Molecular sieving with the aid of zeolite membranes has become a very important separation process. The separation of hydrocarbon isomers is based on the molecular sieving characteristic of certain zeolite membranes. Conventional distillation techniques are energy intensive and therefore, cost intensive. Microporous membranes offer the advantage of low-energy demand and continuous operation, which makes them most suitable for application in hydrocarbon separation processes. The use of zeolite membranes in the separation of hydrocarbon isomers has gained interest as the best alternative since the restrictions were placed on the use of tetraethyl lead, benzene, and MTBE as booster for the octane number of gasoline[1].

Numerous zeolite membranes have been prepared and tested in various separation processes. These include: MFI[2-26], zeolite A[27,28], zeolite Y[29] mordenite[30] ferrierite[30-32] and faujasite-type[33].

Zeolite membranes belong to a group of microporous materials with pores of molecular size, smaller than 2 nm. As a consequence, they are able to separate organic compounds that have very similar boiling points[19]. Separations comparable to, and even greater than, those obtained with traditional distillation have been achieved. Zeolite membranes can also separate molecules with the same molecular weights, something difficult to achieve with mesoporous membranes where transport is governed by types of diffusion other than configurational diffusion.

The gas phase separations achieved with MFI membranes can be explained on the basis of one or more of the following factors:

(a) When there is a significant difference in the kinetic diameters of the gases or vapors that permeate, molecular shape or size sieving can take place. This is

the case, for instance, in the separations of n-butane/i-butane[12,34] and n-hexane/2,2-dimethylbutane[2,20,35].

(b) When one of the components in a mixture can preferentially adsorb on the wall of the zeolite pores it can be selectively transported, blocking the membrane for permeation by the other species in the mixture. Thus, for example, when the following mixtures were separated with zeolite membranes, at sufficiently low temperatures, CH_3OH/H_2[36], $n\text{-}C_4H_{10}/H_2$[34,35], CO_2/H_2[16], the C-containing, more strongly adsorbed molecule that was preferentially separated, reduced the H_2 flux through the membrane.

(c) Sometimes the degree of separation is determined by the relationship between the organophilic or hydrophilic character of the zeolite and the polarity of the permeating molecules. Silicalite-1, the MFI-type zeolite without aluminum, is organophilic. On the other hand, the hydrophilic character in the ZSM-5 form increases as the aluminum content increases. Pure silicalite membranes can be obtained on stainless steel supports. When alumina supports are used, some alumina is incorporated into the MFI composition, due to leaching of the support during the synthesis, leading to ZSM-5 instead of silicalite-1. A low-Al/Si, ZSM-5 membrane would however still be rather organophilic, as described by Piera *et al.*[22]. The organophilic character of silicalite-1 has been used for the separation of ethanol/water[5], acetic acid/water[18,37] and acetone/water[18]. On the other hand, high water/ethanol separation factors (i.e. preferential permeation of water takes place) have been obtained with NaA[27,38] and NaY[39], both hydrophilic zeolites.

Factors (a) and (b) act simultaneously in, for example, separations of branched and linear paraffins, where linear paraffins, that have smaller kinetic diameters and also adsorb more strongly, are selectively transported through silicalite-1 membranes. Also, it is necessary to consider simultaneously the factors (a) and (c) (molecular size and polarity) to justify for instance why the solubility of several alcohols in ZSM-5-filled silicone rubber membranes or in ZSM-5 crystals increases in the sequence: methanol < 1-propanol < ethanol. In this case, adsorption is influenced by both molecular size and hydrophobicity[40].

6.2 Theoretical background

A model for the transport of gases through a zeolite membrane was proposed by Barrer in 1990[41]. A schematic illustration of the five steps involved is given below, see Figure 6.1.

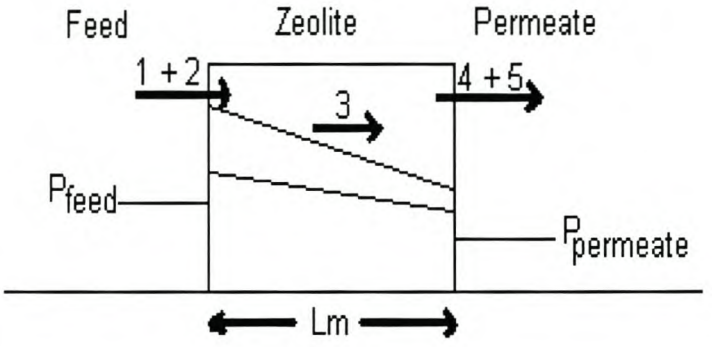

Figure 6.1: Transport model through a zeolite layer. The two lines refer to species with different adsorption strengths.

The five steps are:

(1) Adsorption from the gas phase onto the external surface

(2) Transport to the microporous phase from the external surface

(3) Intracrystalline diffusion

(4) Transport from the microporous phase to the external surface

(5) Desorption from the external surface to the gas phase.

Each step or combination of steps can be rate limiting. The conditions on either side of the membrane will determine the rate of steps 1 and 5. The properties of the gases can also determine the rate of steps 1 and 5. High temperatures and weakly adsorbing species will result in hardly any adsorption on the external surface. The steps 1 and 2 and also 4 and 5 respectively, can be regarded as combined processes. In pores with sizes matching the kinetic diameter of the gas molecule, step 3 (diffusion in pores) is assumed to be rate determining. The thicker the membrane, the greater is the validity of this assumption.

Two types of gas permeation measurements have generally been performed; these are depicted in Figure 6.2.

(a) Pressure gradient method (PG), where the flux is measured under a known pressure gradient.

(b) Concentration gradient method (CG), where the measurement is performed under constant pressure, while the driving force is a concentration difference between faces.

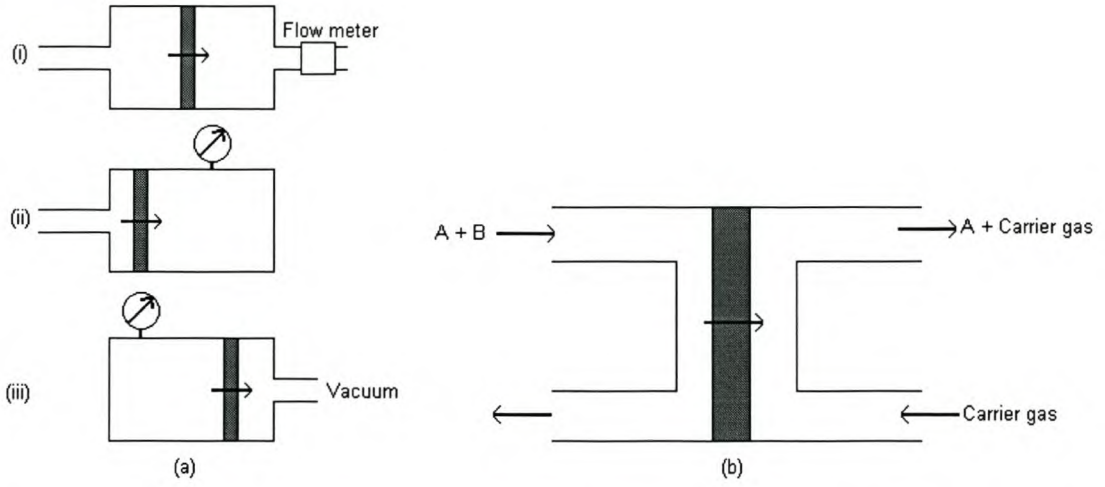

Figure 6.2: Gas permeation measurements: (a) pressure gradient (PG) method and (b) concentration gradient (CG) method.

Either of these methods can be applied under steady-state or transient conditions. In the steady-state PG methods, the flux is measured under quasi-steady state conditions, such that a constant pressure is maintained on one side of the membrane while the pressure on the other side of the membrane is maintained constant (i). In the other PG methods, the downstream pressure is monitored in a closed system of a limited volume while the upstream pressure is maintained (ii), or the upstream pressure is monitored while the downstream pressure is maintained (iii).

Although these measurements provide a simple and convenient way to measure flux, these are restricted to one-component systems, where the required sample amounts for the analysis affect the pressure at the permeate side. In methods (ii) and (iii), a time dependent model should be used because conditions are continuously changing at one side.

The second measurement method (CG) is performed by the Wicke-Kallenbach cell, which was first introduced by Wicke and Kallenbach[42]. In this method a stream

of carrier gas containing a small concentration of the test gas passes over one side of the membrane, while pure carrier gas (sweep gas) passes over the other side of the membrane. See Figure 6.2(b). The permeate is analysed by mass spectrometry or gas chromatography. Although this method is applicable for multicomponent permeation measurements, it must be kept in mind that counter diffusion of sweep gas occurs and effects the permeation behavior of the objective component.

6.3 Gas permeation tests

Gas permeation tests were carried out at ECN in The Netherlands to determine the integrity of the prepared zeolite membranes. An alumina tube (20 cm in length), coated with zeolite NaA on the internal surface was connected to an existing gas rig via conical, gas tight, carbon rings.

The membrane was tested on total zeolite coverage with helium as permeate gas. No helium was detected at the permeate side This meant that the zeolite membrane was leak-proof prior to the calcination step.

In the next experiment the membrane was carefully calcined in a hot-air oven by slowly increasing the temperature to 350°C and keeping it there for several hours.

The different samples tested gave different helium flows on the permeate side, which indicated that there were probably pinholes present in the membrane layer. Based on these observations it was decided to continue with pervaporation experiments, rather than concentrate on gas permeation experiments. Furthermore, it is well known that zeolite A membranes are used solely in pervaporation processes.

6.4 Pervaporation

Pervaporation is a well-known application of zeolite membranes to dehydrate solvents. However, this separation technique is still a subject of studies in order to improve the membrane performance in flux and separation [38, 43-49]. It is known that, increasing the temperature of pervaporation increases mainly the water flux, it has hardly any influence on the selectivity, in the case of zeolite A membranes. See Table 6.1.

Table 6.1: Flux and selectivity data at various temperatures of water/ethanol mixtures (95 wt % ethanol)

Zeolite type	**Temperature (°C)**	**Flux (kg/m²/h)**	**Selectivity**
NaA	45 – 50	0.5 – 0.8	1 500 – 46 000
NaA	75 – 80	1.1 – 2.3	6 000 – 42 000
NaA	85 – 100	2.3	6 000
NaA	120	4.3 – 8.2	6 000 – 47 000

In case of water contents higher than 5 % in the water/ethanol mixtures, a higher water flux is usually observed.

Results reported by Kita *et al.*[50-53] showed enormous potential for the application of zeolite A membranes in pervaporation. It was shown that the zeolite A (LTA) membranes synthesised on alumina supports exhibited fluxes and separation factors of water/ethanol mixtures that were superior to results obtained with polymeric membranes. The separation factors (water/ethanol) and the total flux were greater than 10000 and 2.15kg/m²h, respectively showing that the performance of LTA membranes were the most favorable for pervaporation applications. A summary of some of the results obtained are given in Table 6.2.

Table 6.2: Flux and separation factors of LTA (NaA) membranes in the pervaporation of water/organic mixtures[45]

Liquid	Feed Comp. (H_2O wt %)	Temp. (°C)	Separation Factor	Flux (kg/m²h)
Ethanol	10	75	10000	2.15
	5	75	16000	1.10
Methanol	10	50	2100	0.57
	5	50	2500	0.23
Acetone	10	50	5600	0.91
	5	50	6800	0.83
Dioxane	10	60	9300	1.87
DMF	10	60	8700	0.95

Zeolite membranes produced by microwave treatment of the precursor gels (SiO_2/Al_2O_3 = 2, Na_2O/SiO_2 = 1, H_2O/Na_2O = 120), showed good selectivity and flux through these zeolitic membranes[53]. A summary of the results are shown in Table 6.3, below.

Table 6.3: Pervaporation flux (Q) and separation factor through NaA zeolite membranes synthesised by microwave heating[53].

Mode of Heating		System	Temp	Sep. Factor	Flux (Q)
Temp (°C)	Time (min)	10wt%H_2O	(°C)	(α)	(kg/m^2h)
95	10	H_2O/EtOH	75	2600	1.3
100	15	H_2O/EtOH	75	5300	2.2
		H_2O/i-PrOH	75	5600	1.5
		H_2O/MeOH	50	640	0.4
100	20	H_2O/EtOH	75	2500	1.3
105	20	H_2O/EtOH	75	2600	1.1

In addition to zeolite A membranes, much attention has been given to high silica zeolites as attractive materials (instead of silicone rubber membranes) for organic-selective separation due to their strong hydrophobic nature. MFI (Al-free) membranes have been prepared on α-alumina and stainless steel supports[5,7]. The MFI membrane exhibited a high selectivity for ethanol with a separation factor (α) ($EtOH/H_2O$) of more than 60 for a 5 vol % aqueous solution. Adsorption experiments for alcohol and water suggested that the high alcohol selectivity was attributed to the sorption of alcohol into the MFI membrane. In their conclusion, the separation of ethanol/water mixture took place mainly through the 1nm pinholes with the high hydrophobic property. Furthermore, lower separation factors were observed in the case of the α-alumina supported MFI membrane, compared to the higher performances of the stainless steel supported MFI membranes. The suggested reason for this phenomenon was that the aluminium was incorporated into the MFI framework, in the vicinity of the alumina support. Liu *et al.* also reported lower separation factors for the alumina supported MFI membranes compared to the stainless steel supported membranes[18]. In their study methanol, ethanol and acetone were separated from their aqueous solutions by pervaporation through the MFI (Al-free) membranes. For methanol/water

separation, a relatively constant separation factor between 11 and 14 was obtained over a wide feed range of methanol feed concentration. Separation factors as high as 255 were obtained at an acetone concentration of 0.8 wt %. Generally, the overall selectivity of a pervaporation process is determined by (i) sorption properties of the organic molecule from the liquid phase into a membrane and (ii) mobility of the organic molecule in the membrane. The mobility of acetone might be less than the mobility of water in the MFI membrane, because acetone is a larger molecule than water and it has a stronger affinity to MFI than water. Therefore, they concluded that the overall separation is determined by the sorption step.

6.5 Experimental

A NaA membrane, in a tube configuration, prepared by the static method as discussed in chapter 4, was tested for its pervaporation performance in a classic set up. A mixture of water/ethanol, typically 5 wt % water was used as feed. It`s composition was kept constant by supplying the feed to the relatively large membrane (10 – 12 cm) from a large tank with the mixture. The system comprising the tank as well as the piping and zeolite A membrane tube was placed in a hot air oven at a temperature of 45°C. Analysis of the permeate that was collected in a cold trap was carried out with a GC.

6.6 Results and Discussion

The results, as presented in Table 6.4, are comparable with the results published in literature and would indicate that this synthesis method is most certainly viable for zeolite A membrane preparation. The separations could, in theory, be further optimised, most probably by improving the zeolite A coatings that formed on the internal surface of the tube. A possible drawback of the initial supersaturation and consequently explosive nucleation and grain gowth to obtain thin continuous zeolite crystal layers, can be seen here. In the persuit of thin crystal layers, unwanted grain boundaries are created, which definitely decreases (inhibits) molecular diffusion from one crystal to the next.

The water flux might also be improved by minimising the zeolite A crystals inside the alumina pores.

Table 6.4: Summary of pervaporation results, using a 5 wt% water/ethanol mixture

Feed Composition (H_2O = 5 wt %)	Temperature (°C)	Separation Factor (α)	Flux (kg/m^2h)
Water/Ethanol	45	5000	0.3
Water/Ethanol	45	7000	0.3
Water/Ethanol	45	8500	0.2
Water/Ethanol	45	9000	0.3
Water/Ethanol	45	11000	0.4
Water/Ethanol	45	13000	0.3
Water/Ethanol	45	16000	0.4

The selectivities and fluxes compare well with the values given in literature, for flat-sheet small membrane samples, at these low temperatures.

6.7 Conclusions

The helium permeation data obtained showed that the membranes are not yet fully optimised with respect to the synthesis procedure. It might also be advisable to use shorter tubes for the zeolite A membrane preparation, because this will strengthen the opportunities for zeolite growth.

The pervaporation data were better and although further optimisation is needed, it was shown in principle that the static transverse synthesis technique could be employed to produce zeolite A membranes.

The grain growth mechanism has the advantage of yielding thin crystal layers, however, it compromises the intracrystalline diffusion of molecules.

6.8 References

1. J.M. van de Graaf, F. Kapteijn and J.A. Moulijn, *J. Membr. Sci.*, **144**, 1998, 87.
2. J.G. Tsikoyiannis and W.O. Haag, *Zeolites*, **12**, 1992, 126.
3. E.R. Geus, M.J. den Exter and H. van Bekkum, *J. Chem. Soc. Faraday Trans.*, **88**, 1992, 3101.
4. M.-D. Jia, K.-V. Peinemann and R.-D. Behling, *J. Membr. Sci.*, **82**, 1993, 15.

5. T. Sano, H. Yanagishita, Y. Kiyozumi, F. Mizukami and K. Haraya, *J. Membr. Sci.*, **95**, 1994, 221.

6. P. Kolsch, D. Venzke, M. Noack, P. Toussaint and J. Caro, *J. Chem. Soc., Chem. Commun.*, **21**, 1994, 2491.

7. T. Sano, M. Hasegawa, Y. Kawakami, Y. Kiyozumi, H. Yanagishita, D. Kitamoto and F. Mizukami, *Stud. Surf. Sci. Catal.*, **84**, 1994, 1175.

8. Y. Yan, M.E. Davis and G.R. Gavalas, *Ind. Eng. Chem. Res.*, **34**, 1995, 1652.

9. Y. Yan, M.E. Davis and G.R. Gavalas, *J. Membr. Sci.*, **123**, 1997, 95.

10. C. Bai, M.-D. Jia, J.L. Falconer and R.D. Noble, *J. Membr. Sci.*, **105**, 1995, 79.

11. F. Kapteijn, W.J.W. Bakker, J. van de Graaf, G. Zheng, J. Poppe and J.A. Moulijn, *Catal. Today*, **25**, 1995, 213.

12. Z.A.E.P. Vroon, K. Keizer, M.J. Gilde, H. Verweij and A.J. Burggraaf, *J. Membr. Sci.*, **113**, 1996, 293.

13. R.D. Noble and J.L. Falconer, *Catal. Today*, **25**, 1995, 209.

14. H.H. Funke, M.G. Kovalchick, J.L. Falconer and R.D. Noble, *Ind. Eng. Chem. Res.*, **35**, 1996, 1575.

15. K. Kusakabe, S. Yoneshige, A. Murata and S. Morooka, *J. Membr. Sci.*, **116**, 1996, 39.

16. W.J.W. Bakker, F. Kapteijn, J. Poppe and J.A. Moulijn, *J. Membr. Sci.*, **117**, 1996, 57.

17. J.F. Smetana, J.L. Falconer and R.D. Noble, *J. Membr. Sci.*, **114**, 1996, 127.

18. Q. Lui, R.D. Noble, J.L. Falconer and H.H. Funke, *J. Membr. Sci.*, **117**, 1996, 163.

19. H.H. Funke, A.M. Argo, C.D. Baertsch, J.L. Falconer and R.D. Noble, *J. Chem. Soc., Faraday Trans.*, **92**, 1996, 2499.

20. H.H. Funke, A.M. Argo, J.L. Falconer, R.D. Noble, *Ind. Eng. Chem. Res.*, **36**, 1997, 137.

21. T. Sano, S.Ejiri, K. Yamada, Y. Kawakami and H. Yanagishita, *J. Membr. Sci.*, **123**, 1997, 225.

22. E. Piera, A.Giroir-Fendler, J.-A. Dalmon, H. Moueddeb, J. Coronas, M. Menendez and J. Santamaria, *J. Membr. Sci.*, **142**, 1998, 97.

23. Z.A.E.P. Vroon, K. Keizer, A.J. Burggraaf and H. Verweij, *J. Membr. Sci.*, **144**, 1998, 65.

24. A.J. Burggraaf, Z.A.E.P. Vroon, K. Keizer and H. Verweij, *J. Membr. Sci.*, **144**, 1998, 77.
25. K.Keizer, A.J. Burggraaf, Z.A.E.P. Vroon and H. Verweij, *J. Membr. Sci.*, **147**, 1998, 159.
26. F.Kapteijn, J.M. van de Graaf and J.A. Moulijn, *J. Molec. Catal. A: Chem.*, **134**, 1998, 201.
27. H. Kita, K. Horii, Y. Ohtoshi, K. Tanaka and K.-I. Okamoto, *J. Mat. Sci. Lett.*, **14**, 1995, 206.
28. K. Aoki, K. Kusakabe and S. Morooka, *J. Membr. Sci.*, **141**, 1998, 197.
29. K. Kusakabe, T. Kuroda, A. Murata and S. Morooka, *Ind. Eng. Chem. Res.*, **36**, 1997, 649.
30. N. Nishiyama, K. Ueyama and M. Matsukata, *Microporous Mater.*, **7**, 1996, 299.
31. J.E. Lewis Jr., G.R. Gavalas and M.E. Davis, *AIChE J.*, **43**, 1997, 83.
32. M. Matsukata, N. Nishiyama and K. Ueyama, *Stud. Surf. Sci. Catal.*, **84**, 1994, 1183.
33. K. Kusakabe, T. Kuroda and S. Morooka, *J. Membr. Sci.*, **148**, 1998, 13.
34. J. Coronas, J.L. Falconer and R.D. Noble, *AIChE J.*, **43**, 1997, 1797.
35. A. Giroir-Fendler, J. Pereux, H. Mozzanega and J.-A. Dalmon, *Stud. Surf. Sci. Catal.*, **111**, 1996, 127.
36. M.D. Jia, B. Chen, R.D. Noble and J.L. Falconer, *J. Membr. Sci.*, **90**, 1994, 1.
37. T. Sano, S. Ejiri, M. Hasegawa, Y. Kawakami, N. Enomoto, Y. Tamai and H. Yanagishita, *Chem. Lett.*, 1995, 153.
38. A. Ishikawa, T.H. Chiang and F. Toda, *J. Chem. Soc., Chem. Commun.*, **12**, 1989, 764.
39. H. Kita, T. Inoue, H. Asamura, K. Tanaka and K. Okamoto, *Chem. Commun.*, 1997, 45.
40. C. Bartels-Caspers, E. Tusel-langer and R.N. Lichtenthaler, *J. Membr. Sci.*, **70**, 1992, 75.
41. R.M. Barrer, *J. Chem. Soc. Faraday Trans.*, **86**, 1990, 1123.
42. E. Wicke and R. Kallenbach, *Kolloid Z.*, **97**, 1941, 135.
43. Kondo, M. Komori, H. Kita and K. Okamoto, *J. Membr. Sci.*, **133**, 1997, 133.
44. K. Okamoto, H. Kita, K. Tanaka and M. Kondo, *Ind. Eng. Chem. Res.*, **40**, 2000, 163.

45. H. Kita, K. Horii, Y. Ohtoshi, K. Tanaka and K. Okamoto, *J. Mater. Sci. Lett.*, **14**, 1995, 206; H. Kita, K. Horii, K. Tanaka, K. Okamoto, N. Miyake and M. Kondo, *Proceedings of 7th International Conference on Pervaporation Processes in the Chemical Industry*, R. Bakish Ed., Bakish Materials, Englewood, USA, 1995, p.364.

46. S.M. Holmes, et al., *Trans Ichem. E,* **78**, 2000, 1084.

47. D. Shah, K. Kissick, A. Ghorpade, R. Hannah and D. Bahattacharya, *J. Membr. Sci.* **179**, 2000, 185.

48. W. Guiru, G. Hongchen and L. Yushan, *12th IZC*, 1998, 1795.

49. I. Kamakiri, T. Yamaguchi and S. Nakao, *Ind. Eng. Chem. Res.* **38,** 1999, 4682.

50. H. Kita, *Maku (Membrane)*, **20**, 1995, 169.

51. H. Kita, K. Tanaka and K. Okamoto, *Proceedings ICOM`96*, 1996, 1102; H. Kita, T. Inoue, H. Asamura, K. Tanaka and K. Okamoto, *J. Chem. Soc., Chem. Commun.*, **47**, 1997.

52. H. Kita, K. Tanaka, K. Okamoto and M. Kondo, *Proceedings Am. Chem. Soc., PMSE*, **77**, 1997, 327.

53. H. Kita, T. Harada, H. Asamura, T. Tanaka and K. Okamoto, *Proceedings of the Fith International Conference on Inorganic Membranes*, Nagoya, Japan, June 1998.

CHAPTER 7

Catalytic membrane reactors: State of the art and future scenarios

7.1 Introduction

Membrane catalysis has become increasingly important over the last 20 years, as indicated by numerous review papers on this subject[1-12]. These include papers on the incorporation of inorganic membranes into reactors. Current research is aimed at expanding the technology of catalytic membrane reactors (CMR) to the potential commercial application. Some of the key issues in this process are (i) the membrane, (ii) the membrane module and (iii) the applicable chemical process to be studied. In order for CMRs to be successful in industrial applications, these above-mentioned issues must be addressed.

Membranes are expensive and their use is therefore only favorable when there is (a) a high-pressure feed, (b) a high concentration of permeable components in the feed, (c) a minimal amount of contaminants present, which could influence the performance of the membrane, (d) a need for a high purity product and (e) the permeate is acceptable at lower pressures[13]. Both polymeric and inorganic membranes are used for separation purposes. In catalytic membranes, however, the low temperature-resistance of polymer membranes is an inhibiting factor, hence only inorganic membranes will be discussed here. An understanding of the opportunities and limitations of membranes is required prior to integrating membranes and catalytic reactors.

7.1.1 Catalytic inorganic membranes

A typical catalytic inorganic membrane is comprised of a mesoporous catalytic film that is supported on an inert, macroporous layer. The intra-membrane species transport may occur by several different mechanisms, including: Knudsen diffusion,

bulk diffusion, surface diffusion, viscous flow and activated transport. Membranes of the Knudsen-type have some intrinsic permselectivity due to large differences in species molecular weights. Additional permselectivity is possible because of differences in surface transport of the various species. Catalysis occurs in the active layer only.

7.1.2 Catalytic membrane reactors

The material exchange between the two chambers of a catalytic membrane reactor depends on the stoichiometries and extents of the catalytic reactions, the fluxes of the various species through the membrane, and the species flow rates to and from each chamber[14]. See the generic catalytic membrane reactor design in Figure 7.1. An important design feature is the nature of the gas flow through both chambers, with plug flow and the two limiting situations ideally mixed. For the former the transport flux (and local reaction rates) varies along the length of the membranes. For the latter, the intra-membrane flux is independent of the position in the coordinate plane parallel to the membrane surface. In either case the effluent stream compositions and flow rates determine the conversions of the main reactants as well as the product selectivities or yields.

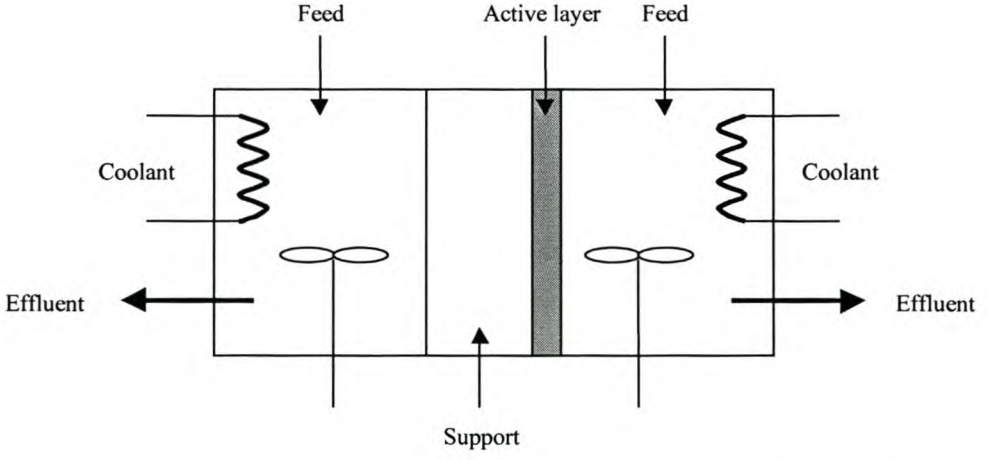

Figure 7.1: A schematic representation of a model catalytic membrane reactor[14].

The main feature of a catalytic membrane reactor that distinguishes it from other catalytic reactor types is the existence of two feed streams and two product streams. That is, one has the flexibility of prescribing the compositions and flow rates of two feed streams. The intention is that this added flexibility will lead to improved

performance over that obtained with the same catalyst in a more conventional arrangement consisting of a single feed and single effluent stream.

7.1.3 Membranes for separation and catalysis

Membranes have been used commercially for many years. The aim of using a membrane to separate a particular reactant or product from a stream, is to increase the turnover of the reaction by shifting the concentration of a reactant or product as it moves through the membrane. A membrane also offers a barrier to prevent two incompatible reactants, such as H_2 and O_2, from being on the same side of the reactor. In addition, the concept of producing a purified product (by using the membrane to perform a selective separation) further enhances the value of the product. Since separation and purification are key steps in the production of most chemicals, there is keen interest in incorporating a membrane into a reactor in order to reduce the number of operating units and the cost of production.

The current approach taken by most researchers in the field of CMRs is to use coated mesoporous supports as membranes. The most widely used support of this type is commercially available α-alumina tubes. A catalytically active layer is then deposited on the support. The aim is to create a thin layer, while still ensuring that it is continuous. In some cases permselective, dense oxide- (ion transport membranes) and metal alloy membranes have been employed. The permselective membranes ensure that a pure stream of one component in a multi component feed diffuses through the membrane. This is advantageous in some CMR applications.

The driving force behind the integration of catalytic reactors and membranes is the reduction in the number of unit operations, which lowers operating costs. One can unfortunately not substitute the membrane with a very exotic separating device, as this would increase the cost of the reactor once again. There are certain criteria for membrane operation which need to be fulfilled in order to have a cost-effective CMR system:

(a) Separation factors of >5 or approaching infinity are required.

(b) High membrane fluxes (rate of flow of permeating species per unit area of membrane surface) are required.

(c) High quality membrane materials are required. The membrane must be chemically and physically stable over a period of months, and the active layer must be defect-free.

(d) Regeneration

Numerous membrane reactors use a sweep gas or vacuum to promote the permeation of a species, but this is unacceptable in commercial applications. Ultimately, the separation has to be driven by a method which does not lead to the dilution of the permeating species nor demand high energy input to perform additional separation[11].

7.2 Types of catalytic membrane reactors

Two types of CMRs can be envisaged:

(i) A microporous (< 20Å) membrane layer, in which the active catalyst can be contained in the pores, or the catalyst is deposited on the external surface of the membrane layer;

(ii) A permselective membrane, which allows only one component through. This means that no further separation of the permeated gas(es) is necessary. The permselective layer could either be the catalyst or a support containing the catalyst.

Reviewing CMRs, it is simpler to consider at the membrane and catalytic reactor separately.

7.2.1 Membranes for possible application in CMRs

The membranes useful for CMR applications can be either organic in nature, i.e. polymeric, or inorganic. The latter can withstand substantially higher temperatures and harsher chemical environments than their polymeric counterparts[15]. Due to their superiority, only inorganic membranes will be discussed here. There are at least 5 types of inorganic membranes: precipitated oxides, carbon, dense oxides, dense metals and zeolites. Advances in catalytic membrane reactor technology have been limited by the absence of commercially acceptable inorganic membranes, capable of molecular size or permselective separations.

Some of the early research into CMRs was done on the precipitation of fine oxide particles onto mesoporous supports. By packing these particles closely together one

could produce a microporous membrane with a pore size of < 20Å. This dense packing of particles presented new problems; de-alumination occurred and there were occasional defects in the surface, which could only be prevented by increasing the layer thickness, at the expense of permeability. Furthermore, because these composites were produced when the oxides were in a metastable form, heating these materials above and below their preparation temperatures often causes collapse or pore size changes. These limitations have prevented the precipitation approach from being used in commercial processes.

Carbon-based membranes are now emerging[16-18]. These membranes are usually made by the decomposition of an organic material, which produces a dense layer with a microporous sieving network. Granular activated carbon materials have been used commercially for molecular size separation by adsorption[19]. Carbon-coated supports, prepared by vapor deposition techniques, were used to recover H_2 from targeted refinery streams[20,21]. The use of tubular carbon molecular sieve membranes has been reported for the separation of gaseous mixtures[16,22]. These membranes are difficult to prepare because of micro-crack formation and the lack of physical stability.

Dense oxide membranes are being used for oxygen transport. The membranes are non-porous and transport oxygen atoms through the membrane layer via oxygen atom vacancies[23,24]. The driving force for the oxygen transport is a differential O_2 partial pressure across the membrane. The kinetics of O_2 incorporation at the oxide surface limit the transport of O_2 when the membrane layer becomes too thin (< 25μm). The O_2 transport can be enhanced by application of a catalyst to the surface of the oxide layer[25,26]. Most of the current interest in applicable membranes evolves around mixed cation conductors, where divalent cations are replaced by trivalent cations. Charge compensation takes place via the creation of oxygen vacancies and electronic holes. Unfortunately these membranes are limited in supply and although they have been made into large tubular membranes there is doubt about the long-term stability of these membranes[27]. An added disadvantage of these materials is the high temperatures (> 700°C) at which reasonable O_2 transport is achieved.

Dense metal membranes have been employed for a number of years, mostly due to the fact that they are commercially available and can be made into large devices. The drawback of these membranes is that only a limited number of permselective separations can be achieved with them. Pd-based alloys are used for H_2 permselectivity and Ag-based alloys for O_2 permselectivity. Pd membranes can undergo phase changes which can cause catastrophic failure of the membrane due to expansion of the lattice, resulting in micro-cracks in the bulk metal[28]. These phase changes are temperature and pressure dependent. In order to overcome some of these difficulties, research has been focused on the deposition of Pd alloys on mesoporous supports. Thick Pd layers are still required to produce a defect-free membrane, and this in turn lowers the flux through the membrane.

In recent years there has been an explosion in the field of zeolite membranes, these are prepared either by hydrothermal growth or precipitation[29-36] on a mesoporous support. The zeolite layers are still thick (10 μm) and permselectivity is difficult to achieve. The thickness of the layers is due to the fact that it is difficult to grow a sheet of a single crystal layer. Pinholes are present in these thin crystal layers and multiple syntheses have to be carried out in order to reduce the chances of pinholes. Current synthesis efforts are aimed at producing thin continuous zeolite crystal layers. One of the first attempts in this regard is reported in Chapter 4 in this document, where an alternative synthesis approach, static transverse synthesis, is presented. Jansen and Coker have recently pointed out that it is a major challenge to crystallise a pinhole-free zeolite film while maintaining a very thin microporous phase for optimal flux[36]. In addition to the preparation problems associated with zeolite membranes there are the operational problems. The separation of bulky organic molecules is complicated by the fact that these materials also adsorb on the surface of the pore and can actually block smaller molecules from permeating while being able to slip through themselves. Adsorption of components on the surface can be very temperature dependent, thus changing the characteristics of the membrane as one changes the temperature. Jansen`s group at the University of Delft in The Netherlands[33] published some preliminary examples of zeolite membrane catalysis.

7.2.2 The catalytic reactor

As soon as one has an acceptable membrane layer to use in a catalytic membrane process, one realises that there are device-related problems. A very simple schematic representation of a catalytic membrane reactor is illustrated in Figure 7.2. The most common problem is that of the seal between the membrane and the extension (for instance quartz glass).

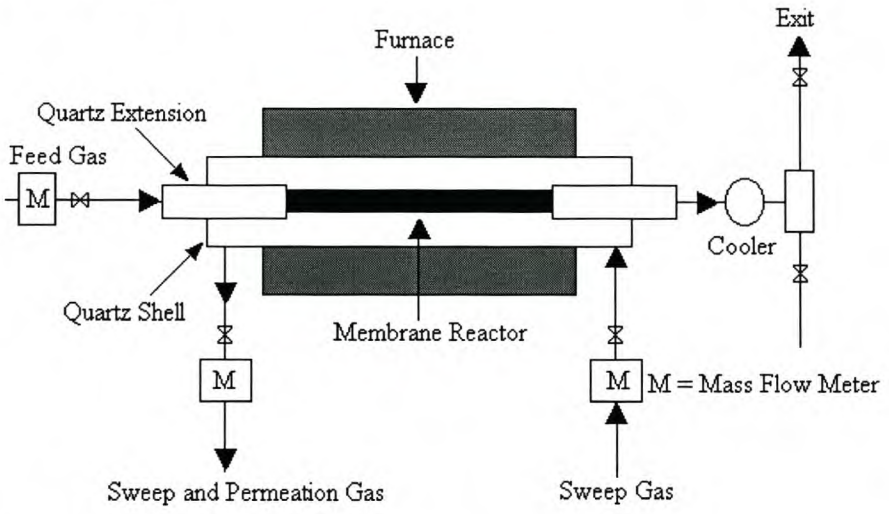

Figure 7.2: Simple schematic representation of a bench catalytic membrane reactor.

The catalyst is contained in the tubular membrane, inside the furnace. Any membrane layer which is part of the catalytic reactor will have to be encapsulated into a device to capture the permeating gas and handle the retentate stream. The seal between the membrane layer and the device often becomes the process limitation, as a result of the materials incompatibility or a difference in thermal expansion coefficients. For instance, it is difficult to connect Pd alloys with stainless steel or ceramic walls and take the entire device through temperature changes from ambient to > 900°C. In any production unit, as one starts and restarts the reactor unit, the seals between the membrane and the rest of the unit can eventually fail. With Pd, Pd-coated or dense oxide membranes, coefficients of thermal expansion are different enough that on repeated temperature cycling the seals can weaken and fail, thus destroying the purpose of a membrane layer. Another limitation of the reactor system is the inherent low surface area of the most popular membrane materials.

Unlike a catalyst particle, the current popular membrane materials have no real microporosity, except for zeolite membranes. Building elaborate cross-flow channel-like designs, which maximise the gas-to-surface contact areas, can fortunately

circumvent this physical limitation. This is however very costly and difficult to achieve on a commercial scale.

A more severe process limitation that has yet to be resolved with these membrane reactors is the issue of mass transport. It is relatively easy to pack a tubular membrane with catalyst, heat the catalyst, and get the reaction to take place. However, the products of this reaction must now find their way to the walls of the membrane and permeate the membrane without being swept away in the retentate stream. Looking at this problem on a molecular level – the reactants must first get to the surface of the catalyst particle, then some adsorption and dissociation must occur on the surface of the catalyst particle. Reaction on the catalyst can proceed to produce a permeating product such as H_2. The H_2 must desorb from the catalyst particle surface, flow along other catalyst particles and arrive at the membrane surface. If the membrane is, for instance, a Pd layer then the molecular H_2 must dissociate on the surface and permeate the membrane layer, then re-associate on the permeate side as H_2 where it is then collected as a pure product. It can therefore be seen that the operation of a membrane reactor can become mass-transfer limited if one does not have a membrane with sufficient flux to meet the productivity of the catalyst.

Various reactor flow models for optimal dehydrogenation have recently been described[37]. Two configurations of CMRs have been studied and applied. For example, the catalyst can be packed inside a tubular membrane or, alternatively, the membrane separating unit can be separate from the catalysis unit[38]. From an industrial point of view, the application of this development in the field of catalytic membrane reactors is limited. This is due to the lack of suitable membrane materials, and the inability to fabricate membranes from those materials within a device, resulting in productivities acceptable to the chemical industry.

7.3 Opportunities for catalytic membrane reactors

The multitude of reactions in a petroleum refinery are efficiently operated by way of heat and mass transfer balance, with regard to optimal productivities[11]. There may however be an opportunity for the use of catalytic membrane reactors if these can be matched with membrane features. Whereas refineries used to produce H_2 a decade

ago[39], they now consume large quantities of H_2 for desulfurising fuels and, as environmental demands become tougher, more and more H_2 is needed.

7.3.1 Dehydrogenation reactions

The dehydrogenation of alkanes became very popular after the initial groundbreaking work was done in the early 80s[40,41]. Itoh achieved >99% conversion for the dehydrogenation of cyclohexane to benzene with his Pd/Ag membrane tube containing a 0.5% Pt/Al_2O_3 catalyst. An argon sweep was used to carry away the H_2 permeating the Pd layer. The reaction was run at 200°C and 1 atm pressure, using an argon stream saturated with cyclohexane. Furthermore, the feed rate was kept very low in order to achieve reasonable conversions.

More recently, membranes have been made of Pd alloys coated on a mesoporous support[42]. When isobutane was passed over a Pt/Al_2O_3 catalyst, contained in the membrane, the yield of isobutylene rose from an equilibrium value of 6% to 23% at 400°C. The membrane did, however, show some signs of deactivation after 350h.

Gokhale *et al.* simulated a dehydrogenation reaction, of the form A <=> B + H_2, in a cocurrent, isothermal, membrane-enclosed catalytic reactor, to study the effects of reactant permeation rate, hydrogen permselectivity, feed composition and reactant space times on reaction conversion[43]. They used two dimensionless numbers, the Damkohler number and the permeation number, to quantify the effects of reactant space time and reactant loss on conversion, respectively. They concluded that in a dehydrogenation reaction of this type, high(er) trans-membrane pressure drops give high(er) conversions, but the highest pressure drop that could be maintained across the membrane decreased as the maximum reactant permeation rate increased. For H_2 permeation selectivities between 3 and 1000 and reactant space times (at STP) between 0.3 and 30 s, conversion decreased as the maximum reactant permeation rate exceeded the inlet reactant flow rate, because reactant loss controls the conversion. For H_2 permeation selectivities between 30 and 40, maximum conversions were obtained when the maximum reactant permeation rate equaled the inlet reactant flow rate. For H_2 permeation selectivities greater than 40, the lower reactant permeation rate gave higher conversions at low space times because the amount of H_2 available for permeation limited the equilibrium shift. At high space times, however, higher

conversions were obtained when the maximum reactant permeation rate equaled the inlet reactant flow rate.

Collins *et al.* studied the dehydrogenation of propane to propylene, using a Pd-coated alumina membrane[44]. A propylene yield of 39.6% was reported at 823 K for the Pd thin film membrane, compared to the 29.6% yield for the conventional reactor (without the membrane). Unfortunately, the membrane deactivated after a few hours of operation and consequently failed. Weyten *et al.* also reported on the direct dehydrogenation of propane to propylene[45]. A chromia/alumina catalyst was used and the propylene yield remained constant for almost 10h. Using the Cr_2O_3/Al_2O_3 catalyst the yield improved from the equilibrium value of 18% to 36%. Deactivation of the membrane occurred again, due to coke formation on the catalyst.

A tubular fixed bed catalytic membrane reactor was used by Gobina *et al.*[46] to effect the equilibrium shift during the catalytic dehydrogenation of ethane to ethylene. A membrane consisting of a 6 μm thick film of Pd/Ag alloy on the external surface of a Vycor glass tube was used. The catalyst, 0.5% Pd on γ-alumina, was packed in the bore of the membrane tube. Conversions of 6-7 times the equilibrium value were reported at 660K. They also reported on the high temperature dehydrogenation of n-butane[47]. The same catalytic membrane as described above was used. Increases in the conversion at 670K of 4 and 6 fold above the equilibrium value was reported when CO and O_2 were used as sweep gases, respectively. They also studied the influence of three different sweep gases, N_2, N_2/CO and N_2/O_2, on the conversion of n-butane in the catalytic dehydrogenation reaction[48]. The membranes used again comprised a 6μm thick Pd/Ag layer on an alumina support. Conversions well above the equilibrium value of 5% were achieved, varying from 13.5% in N_2 to 26% in N_2/CO and approximately 40% in N_2/O_2. The effect of film thickness on the conversion of n-butane was also shown. Indications were that for these enhanced conversions a very thin film (< 6μm) was needed. See Figure 7.3.

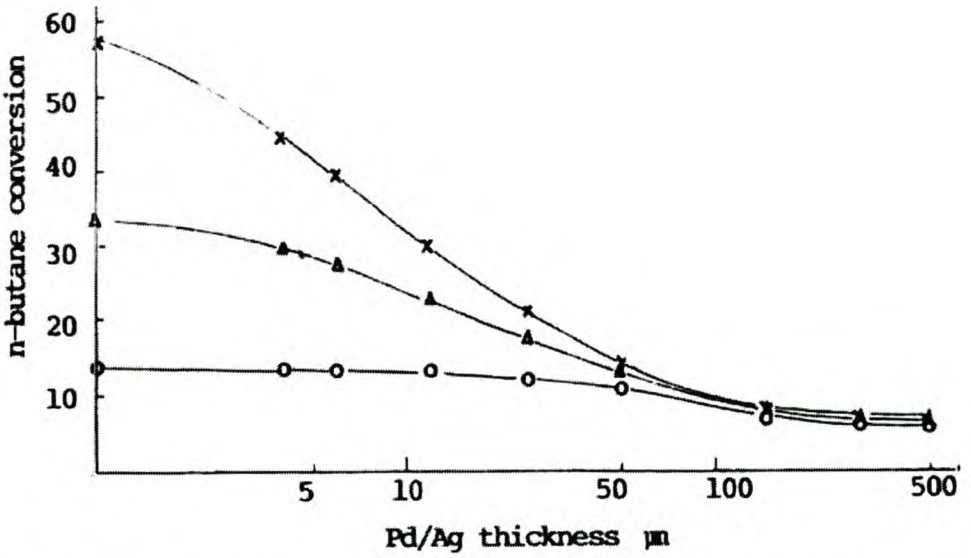

Figure 7.3: Effect of Pd film thickness on n-butane conversion with different sweep gases[48].

Another important dehydrogenation reaction, especially for the petrochemical industry, is the dehydrogenation of ethylbenzene to styrene. Gallaher *et al.* studied a two stage, packed bed reactor, followed by a membrane reactor vs a reactor without a membrane unit[49]. A tubular 40Å alumina membrane was packed with a commercial potassium (K) promoted iron oxide catalyst used for styrene production. Using the membrane, a 4% increase in styrene yield was observed. Unfortunately, carbon deposits rapidly reduced H_2 permeability, even when a co-feed of steam was added to the reaction feed.

Abdalla *et al.* also studied the dehydrogenation of ethylbenzene to styrene, using fluidised bed reactors with and without selective membranes for hydrogen removal[50,51]. A 0.5μm thick Pd membrane on an alumina support was used for this purpose. The application of the selective membranes to a series of fluidised bed reactors considerably increased the ethylbenzene conversion (96.5%) and the styrene yield (92.4%), compared to normal fixed bed units. The H_2 removal also increased the selectivity to styrene.

The dehydrogenation of methylcyclohexane (MCH) to toluene was studied by Ali *et al.*[52]. They compared the performance of a mono- and bimetallic noble-metal catalyst in the dehydrogenation reaction. The monometallic catalyst (Pt/Al_2O_3)

performed considerably better than the bimetallic (Pt-Re/Al_2O_3) catalyst at the same temperatures. This was due to deactivation of this catalyst. In addition, they also studied the effects of relative rates of MCH dehydrogenation to toluene and the H_2 permeation through Pd-Ag membranes on the performance of the catalytic membrane reactor[53]. Use of a catalyst for MCH dehydrogenation with no toluene inhibition, in conjunction with a membrane < 50μm thick, performed exceptionally well in a CMR, giving conversions considerably above equilibrium values at favorable operating conditions and economically viable space velocities.

The two main process issues that come to the fore are the carbon deposition and the catalyst activity. Raich and Foley studied the dehydrogenation of alkanes in a membrane reactor and concluded that the use of these devices was very limited by the availability of dehydrogenation catalysts with high reactivity[54]. Most available catalysts are limited by excessive carbon formation, which accumulates on the catalyst. Another fact that has to be considered here is that the dehydrogenation reactions are endothermic and that their high demand for heat means that the products of the reaction can get trapped inside the pores of the catalyst. Due to the fact that the reaction rates are slow, it is even possible that the olefinic products can polymerise before they permeate away from the catalyst particles. Even the removal of H_2, which is done as it formed in a CMR, can be a disadvantage, because H_2 formation actually serves to reduce the carbon formation tendency. The carbon that is formed during dehydrogenation reactions can be disadvantageous to the CMR in three ways: (i) it blocks the surface of the catalyst, (ii) it fouls the reactor and plugs the unit and (iii) it coats the membrane layer and thus block further H_2 permeation through it. Raich and Foley[54] further concluded that much improved dehydrogenation catalysts are needed to be developed. After that one can try and solve the problems of thermodynamics and the tendency for carbon formation in these reactions. The successful application of membranes to assist catalytic dehydrogenation cannot occur without these catalyst and process improvements.

7.3.2 Catalytic decomposition of volatiles

Increasing environmental awareness in the last two decades has prompted the emergence of stricter regulations covering industrial activities. Among these, the reduction of volatile organic compounds (VOC`s) was mandated in the USA and

Europe. VOCs are produced in a variety of industries. They are common pollutants in the chemical industry, they are also present in the manufacture of plastics, in food processing and in many small- and medium-size industries, (e.g., paints, cleaning agents, adhesives, coatings and solvents). Catalytic combustion is perhaps the most suitable alternative to thermal combustion for the removal of VOC's from air streams, due to lower costs of energy and materials[55]. It is more flexible than other means of VOC elimination, such as retention on specific adsorbents which must be regenerated, or condensation which requires sufficiently high concentrations. The catalytic systems used must, however, operate under very demanding conditions: VOCs are usually present in diluted streams, and the rate at which they are produced may vary with time and location in a given industrial facility. Also, a large portion (> 95%) of the organic compounds in the feed must be eliminated. Therefore, the removal of VOCs requires a highly efficient technology which, simultaneously, provides sufficient flexibility to accommodate significant changes in the operating conditions. Finally, the catalytic system chosen should be able to handle large feed rates with a relatively low pressure drop and avoid or minimise catalyst deactivation (by sulphur compounds, chlorides, silicon polymerising materials, sintering processes, etc.)[56].

Collins *et al.* reported on the catalytic decomposition of ammonia in a membrane reactor[57]. The catalytic decomposition of ammonia in the gas feed to the turbine is a potential method for reducing NO_x emissions in coal gasification power plants. A packed bed palladium-ceramic (11.4μm thick Pd layer) membrane reactor was used for this study. See Figure 7.4. The experimental conditions were similar to those that would be used in an industrial application since no inlet sweep gas was used and the membrane was operated at a high trans-membrane pressure difference. The results indicated that the membrane reactor could significantly improve on the ammonia conversion of a conventional reactor when dilute concentrations of ammonia and high concentrations of H_2 and N_2 were in the feed gas. An ammonia conversion of over 94% was achieved in the membrane reactor at 873K. Since the equilibrium conversion of the feed was only 58%, a significant equilibrium shift was obtained with the membrane reactor. The equilibrium was even higher at lower temperatures. At 823K the conversion was 79%, compared to the equilibrium conversion of 33% for the feed gas, and a conversion of only 17% in a conventional packed bed reactor operated under the same conditions as the membrane reactor.

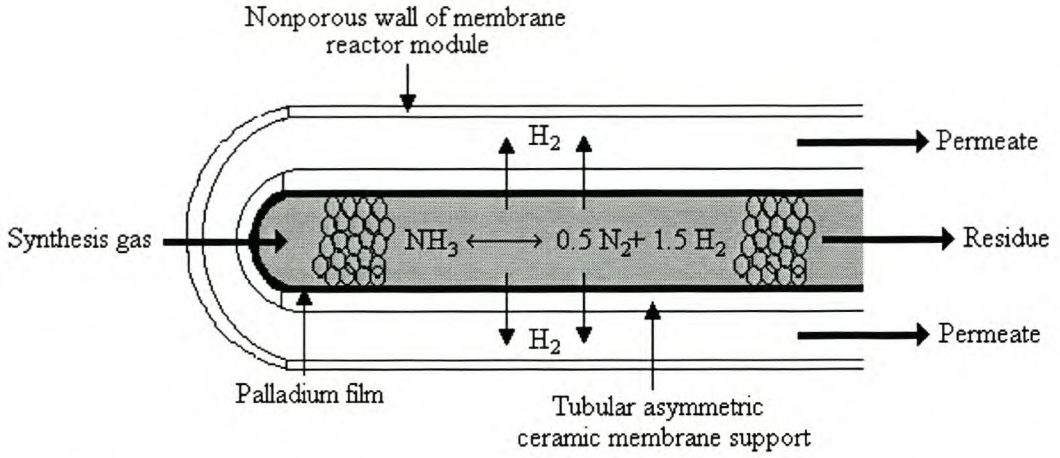

Figure 7.4: Cross section of a packed bed membrane reactor for the decomposition of high-temperature, high-pressure synthetic gas.

The membrane reactor is based on a composite palladium-ceramic membrane. Gobina *et al.* also reported on the elimination of ammonia from coal gasification streams using a catalytic membrane reactor[58]. A 6 μm thick Pd-Ag layer was deposited on the external surface of a porous Vycor tube. The ammonia was decomposed over a bed of Ni/Al_2O_3 catalyst. They showed that NH_3 decomposition rates much higher than those attainable in conventional fixed-bed operations and other gas clean-up systems were feasible under gasifier conditions. The countercurrent mode of operation was shown to be superior to the cocurrent mode, at relatively lower temperature (< 723K), but there was very little difference between these modes when no sweepgas was used. The sensitivity of the NH_3 decomposition rate on the composition of the feed gas mixture was found to be an important factor in the operation of such a system. Furthermore, since hydrogen was the only permeable species, such a membrane system was versatile and complete destruction of the NH_3 could be achieved even at a low upstream pressure of 5 atm.

Pina *et al.* used a Knudsen-diffusion catalytic membrane reactor as an efficient contactor for the combustion of volatile organic compounds[56]. The membrane was prepared by coating an α-alumina membrane with a γ-alumina phase. The catalytic material (Pt) was introduced by wet impregnation with chloroplatanic acid, followed by drying and calcination. The Pt loading was reported to be 0.13 wt%, which is very low. It was shown that complete combustion of toluene could be achieved at lower

temperatures (170°C), at a feed rate of 400 ppm toluene, than reported by Pina *et al.* in the literature (240°C)[56]. Unfortunately, in spite of the good results for the combustion of toluene at low temperatures, the Knudsen-diffusion contactor used in this study presented the problem of a considerable pressure drop across the membrane. Pressure drops measured ranged from 0.18 – 0.35 bar. This would obviously represent a significant increase in operating cost in an industrial reactor operating at high feed rates.

7.3.3 Steam reforming of methane.

There have been some recent studies on the use of Pd-based membranes for application to steam reforming (SMR). SMR technology is the major route to industry`s production of merchant H_2 on a worldwide scale. Reaction 7.1 is a very endothermic reaction that operates at ~800°C and at ~20 atm pressure in order to achieve near equilibrium conversions and to meet the customers need for high pressure H_2.

$$CH_4 + H_2O \rightarrow CO + 3H_2 \qquad \text{Reaction 7.1}$$

By using a Pd alloy membrane which is packed with traditional SMR catalyst, the intent was to shift the reaction to produce more H_2 at lower operating temperatures. The Pd based membrane also would produce pure H_2, thus simplifying the current operation which included extensive H_2 purification steps[59]. In the early 1990s, Uemiya *et al.* showed that SMR could be enhanced by using an alumina-supported Ni catalyst contained within an 80 μm thick Pd on Pd/23% Ag alloy membrane coated onto a porous glass tube[60]. At a steam to CH_4 ratio of 3, they achieved enhanced conversion of CH_4; it approached 80% at 1 atm and 500°C vs an equilibrium value of 42%. Their productivity rates were low and diluted H_2 was produced. Increasing the sweep rate enhanced the H_2 productivity but the rate was limited by the permeability of the membrane. Interestingly, increasing the CH_4 pressure to 8 atm increased the CH_4 conversion.

Ziaka *et al.* reported on the use of a polyimide membrane in the production and recovery of H_2 and CO_2 from the catalytic methane-steam reforming reaction[61]. The

unique feature of this permselective polyimide separator was the simultaneous removal of H_2 and CO_2 versus CH_4 and CO from the reformed steams. They used the 6FDA-3,3`5,5`-TMB aromatic polyimide, which exhibited superior permselective properties compared to other polyimides of the same or different dianhydride sequence. They showed that the simulated reactor permeator cascade system for methane steam reforming gave competitive CH_4 conversions and CO_2 and H_2 yields under a range of reforming pressures and temperatures. According to the author, in terms of conversions and yields, this system "outperforms" the conventional reaction separation system that operates at equilibrium reforming conditions, by providing 90% H_2 yield through the intermediate separation unit.

Barbieri *et al.* carried out simulation studies of reactors with parallel-flow and counterflow configurations in a packed-bed inert membrane reactor[62]. The effects of different parameters such as temperature, reactor pressure, feed and sweep flow rate, feed molar ratio, membrane thickness and space velocity on the degree of conversion were determined. A 20 μm thick, stainless steel supported Pd layer was used as the membrane. Their results were in good agreement with those of Shu *et al.*[63]. They found that, at high temperatures, results from the counterflow configuration were marginally better than those from the parallel-flow reactor. They concluded that space velocity, as such, could not be considered as a design variable for membrane reactors, owing to the complex interaction between the relative permeation rate and residence time, both depending on flow conditions.

Jorgensen *et al.* showed that a commercial Ni/MgO SMR catalyst, contained within a 100 μm Pd/Ag tubular alloy membrane could be used on a laboratory scale[64]. At 6 atm and 500°C they obtained CH_4 conversions of 51%, compared to equilibrium values of 21%. They found that they had to operate at higher than normal steam/methane ratios (which are undesirable from a process point of view) in order to avoid carbon formation. Members of the same group carried out a process economic analysis of a SMR membrane reactor, assuming ideal conditions, with a 2 μm Pd alloy coated ceramic tube[65]. In their model they incorporated tubular Pd membranes directly into a traditional SMR catalyst bed. They found that they had to operate at >650°C to maintain sufficient CH_4 conversion and that membrane assisted SMR was only attractive if the cost of electricity was very low and the membranes were 100%

selective to H_2. This was because they found it necessary to run at a lower permeate product pressure, which then required costly compression to typical H_2 pressure levels in commercial SMR units. Their conclusion, based on current information, was that a membrane-integrated process was currently not competitive with traditional SMR.

Another group also conducted a process economic study on a membrane assisted SMR reactor[66]. They concluded that the use of size selective mesoporous silica membranes was not cost effective, but that Pd/Al_2O_3 membranes offered ~18% lower investment costs vs conventional SMR.

In summary, there seems to be scope for the use of membrane reactors in SMR, but there are still some significant challenges regarding the H_2 permeation through these membranes. This will need to be addressed and improved before membrane reactors can compete with current SMR technology. A further issue that will have to be addressed is the long-term stability of the membranes (carbon formation). The current membranes seem to have problems as far as stability is concerned, since the current catalyst life is approximately 5 years[67].

7.3.4 Methane to synthesis gas

The availability of natural gas has prompted intense interest in the conversion of CH_4 to mixtures of CO/H_2 (reaction 7.2) by selective oxidation. This reaction is, however, difficult to control because of over-oxidation of the CH_4 to CO_2 at the high temperatures needed to initiate the reaction.

$$CH_4 + \tfrac{1}{2}O_2 \rightarrow CO + 2H_2 \qquad \text{Reaction 7.2}$$

There are presently a number of groups studying the use of O_2-selective, dense ceramic membranes for assisting this reaction. Such a membrane would allow one to separate the methane from the O_2, offering an extra margin of safety in avoiding explosive mixtures of these two reactants. Since the membrane material is permselective to O_2, one can use air as a feed. The diffusion of O_2 through the membrane wall further allows one to add small amounts of O_2 to the CH_4 on the

permeate side. A catalyst layer is often incorporated where the permeating O_2 and CH_4 react.

A variety of membrane types have been studied for incorporation into catalytic reactors for the oxidative coupling of methane (OCM). Chanaud *et al.* reported the preparation of a LaOCl inorganic membrane on commercial alumina tubular supports which were catalytically active for the oxidative coupling of methane[68]. The potential of this type of membrane was explored by Borges *et al.* and several factors were shown to play significant roles in the catalytic performances of LaOCl membrane reactors for the OCM reaction[69]. These factors were (i) a solid/solid reaction between the selective LaOCl and the non-selective Al_2O_3 phase of the support should be avoided at all cost, (ii) these membranes need to have a low surface area and a high permeability, at least in the present macroporous domain where transport effects are not dominant, (iii) for optimised performances the membrane reactor must run under separate feeding modes, in order to obtain the advantage of concentration profiles. Unfortunately, the harsh operating conditions required for this reaction (from 650 - 800°C, in the presence of water vapor) caused textural instability, which led to a partial sintering of the LaOCl phase and restricted any transport effects to the macroporous domain. In spite of moderate Knudsen separation effects between methane and oxygen, beneficial effects of the membrane reactor, subject to surface composition and structural and feeding configuration requirements, have been observed.

Santos *et al.* investigated the partial oxidation of methane to synthesis gas in a two-zone fixed bed of a Ni/Al_2O_3 catalyst inside a modified ceramic membrane[70]. The first zone of the reactor was surrounded by an impervious wall and therefore behaved as a conventional fixed bed reactor. In the second zone, some of the reaction products could preferentially diffuse out of the reactor, which yielded higher than equilibrium methane conversions. Studies were carried out at both 1 and 2 atm pressure, with the latter yielding good conversions and selectivities. It was shown that hydrogen permeates preferentially and, as a consequence, higher than equilibrium conversions could be achieved. At the higher pressures (2 atm), a decrease in the methane conversion took place, due to the unfavorable equilibrium shift. However, the use of the membrane reactor resulted in an increase in conversion, which compensated for

the lower equilibrium values. The same group studied the effect of membrane activity on the performance of CMR in the OCM[71]. In these experiments they used silica membranes impregnated with Li and/or Na. Such a membrane acted as an oxygen distributor to a bed of catalyst, while the methane was fed axially. These changes led to an improvement in the yield of the desired products, with respect to the conventional reactor, with co-feeding of both reactants.

The application of perovskite-type ceramic membranes in the OCM was studied by Zeng *et al.*[72]. The co-precipitation method proved to be the most suitable for the preparation of the $La_{1-x}Sr_xCo_{1-y}O_{3-\delta}$ (LSCF) powders, in terms of processibility into dense ceramic membranes. The steady-state oxygen permeation fluxes through a 1.85 mm thick LSCF membrane exposed to O_2/N_2 and He were 1.6×10^{-9} and 9.5×10^{-8}, respectively, at 650°C and 950°C, respectively. The OCM was performed in the LSCF membrane reactor, with one membrane surface exposed to the O_2/N_2 mixture stream and the other to the CH_4/He mixture stream. At temperatures higher than 850°C, high C_2 selectivity (70-90%) and yield (10-18%) were achieved with a feed ratio (He/CH_4) of 40-90. The C_2 selectivity dropped dramatically to less than 40% as the He/CH_4 ratio decreased to 20. The surface catalytic properties for the OCM of LSCF membranes strongly depended on the oxygen activity of the membrane surface exposed to the methane stream.

A group at Amoco and Argonne has worked with non-perovskite-type oxides for permselective O_2 transport[27,73,74]. Hollow-tube membranes of SrFeCo oxides have been fabricated in lengths of up to 30 cm, with a 6.5 mm diameter. A Rh-based reforming catalyst was contained inside the tubular membrane. A mixture of 80% CH_4 and 20% Ar was passed through the inside of the tube, while air was passed over the outside of the tube. The optimal operating temperature was 850°C, during which > 98% CH_4 conversion with 90% CO selectivity was achieved for ~ 70 h. It was necessary to employ a gold mesh to physically separate the Rh reforming catalyst from direct contact with the membrane wall in order to avoid loss of lattice oxygen. Unfortunately, results of long term tests indicated that there was a 43% decrease in O_2 flux over a period of 1000 h. In a similar effort, another group at BP Chemicals[75] has fabricated a tubular membrane reactor from the mixed conductor,

$La_{0.2}Sr_{0.8}Fe_{0.8}Cr_{0.2}O_x$ and have used this reactor for the partial oxidation of methane for > 1000 h at 1100°C.

The selected substitution of metal ions into the brownmillerite lattice, having a large population of oxide ion vacancies, has led to new materials with high ionic conductivities[76]. The combined partial oxidation of methane with steam and CO_2 reforming reactions, using a membrane reactor, have recently been demonstrated. One side of the reactor was exposed to an air flow, while the permeate side was exposed to 80% CH_4 in He. The 8.6 mm long tubular membrane was coated with a Ni-perovskite catalyst for the reforming reaction on the outside of the tube. Initial operation for > 3500 h has been demonstrated with a H_2/CO ratio of 1.8 – 2 at 900°C.

Recently, Galuszka *et al.* studied the conversion of CH_4 gas to syngas and made some preliminary process engineering calculations[77,78]. They used a 10 μm Pd coating on an Al_2O_3 tubular membrane filled with 5% Pd/Al_2O_3 catalyst. A feed of 3:1:4 $CH_4/O_2/N_2$ was passed through the catalyst at 500°C with an Ar sweep on the permeate side. The Ar assisted in the transport of the H_2 away from the catalyst with a resulting increase in the H_2 yield, from 18% to 36%. Unfortunately, 30% of the H_2 produced remained in the retentate stream and after 20 h they saw extensive amounts of filamentous carbon on the membrane. This would ultimately lead to the termination of the membrane function.

Sobyanin *et al.* studied an alternate process, the electrocatalytic conversion of methane over Ag-, Pt-, Ni- and Pt + CeO_2-based electrode-catalysts in an electrochemical reactor with an yttria stabilised zirconia (YSZ) electrolyte-membrane[79]. Schematically the reactor looked like this;

$$CH_4, \text{electrode-catalyst}|0.9ZrO_2 + 0.1Y_2O_3|Pt + PrO_2, \text{air}$$

The reaction was studied at temperatures ranging from 660 – 850°C and ratios of methane and electrochemically pumped O_2 flows ranging from 0.8 – 2.0. Unlike Ag and Pt + CeO_2 electrodes, the Ni and Pt electrodes were found to be active electrode-catalysts for the partial oxidation of methane to syngas with the concentration ratio of $[H_2]/[CO] \sim 2$. The Ni electrode-catalyst showed a CH_4 conversion and CO yield of

93% and 82-88% at 800 - 850°C, respectively. An increase in the temperature led to an increase (65% – 85%) in the CO yield. This was shown to be the case for both the Pt and Ni catalysts. They further concluded that there was no change in the electrocatalytic activity of Pt and Ni electrodes, no imbalance with respect to carbon (± 5% accuracy) and current-voltage characteristics of the solid oxide fuel cells (SOFC) systems were observed during electrocatalytic oxidation of methane. This observation allowed to them to conclude that the Pt and Ni electrodes were stable under the conditions of syngas production.

7.3.5 Water gas shift

The water gas shift (WGS) reaction (Reaction 7.3) is another valuable process operation within a refinery. It is used to convert CO to H_2 and CO_2. The reaction (reaction 7.3), is an exothermic reaction and typically gives high conversion. There is therefore little incentive to apply membrane reactor technology to this reaction.

$$CO + H_2O \rightarrow CO_2 + H_2 \qquad \text{Reaction 7.3}$$

There have, however, been a few membrane reactor studies carried out in attempts to enhance water gas shift. In the mid 90s Violante *et al.* developed a model to simulate the WGS reaction[80]. They used a 1mm thick, porous ceramic support, coated on the external surface with a 25 μm thick Pd/Ag layer. The catalyst[81], suitable for the WGS reaction, was contained in the lumen of the support. Maximum conversion (> 99.8%) was obtained at 600 K; Pd/Ag CO was poisoned at lower temperatures[82]. They concluded that the permeability of the multilayer metallic/ceramic membrane was higher than that of traditional metallic membranes. The exchange area was thus reduced, minimising the amount of expensive material (Pd & Ag), since both the exchange surface and the metallic film thickness were reduced. The hydrogen flux through the multilayer membrane was 5 times larger than through a Pd/Ag membrane (0.15 mm thick). In order to obtain good conversions and avoid stability problems, the CMR should be operated under the appropriate conditions of temperature and pressure.

Members of the same group have recently reported results of studies using some very thin (0.2 μm) Pd coated, 25 cm long tubular Al_2O_3 membranes[83]. The membrane

was filled with a commercial, low temperature WGS catalyst and the reactor operated at 322°C. Because the Pd coating was so thin, some of the N_2 permeated the membrane with the H_2. With a steam/CO of 0.96, conversions were always below the expected equilibrium level of 78% H_2.

Uemiya *et al.*[84] used a 20 μm layer of Pd coated onto a porous glass tube to enhance CO conversion and H_2 production using a commercial Fe-Cr high temperature WGS catalyst at 400°C and 1 atm, with steam/CO = 2/1. Conversion of CO was ~ 88% with a feed rate of 100 cm^3/min and an Ar sweep of 400 cm^3/min vs an equilibrium value of 78%. They were able to demonstrate that the use of a membrane permitted one to reduce the amount of steam needed to achieve reasonable levels of CO conversion.

In modeling the WGS reaction, Ross and Xue reported on the use of a porous membrane unit which was separate from the catalyst bed[38]. They envisaged using recirculation of reactants and products in order to continually drive reaction 7.3 to the right. Separating the membrane from the catalyst unit eliminated some of the problems associated with membrane stability and the seals to the device, especially since the membranes no longer had to operate at the same temperature as the catalyst. This adds more complexity and potential cost to the overall process operation. In a later report[85] they concluded that while the development of the process was considered to be technologically feasible, it was clear that the technology of high selectivity, inorganic membrane manufacture and high temperature ceramic materials engineering were not sufficiently mature; they require further development.

7.3.6 Applications of zeolite membranes

There has been a great deal of enthusiasm in the literature for the potential use of zeolite membranes in CMRs. This has been based on upon the established utility of zeolites in extrudate form for the separation of hydrocarbons. If it was possible to make these materials in membrane form, it would be possible to combine these membranes with catalytic reactors and carry out both separation and catalysis in one unit, such as in the isomerisation of n-butane to i-butane, the recovery of H_2 from off-gases, membrane distillation and monomer recovery in vent gases[86]. As mentioned earlier, in Section 7.2.1, one has to temper these applications with the fact that

performance of such microporous sieves with large organic molecules will be temperature dependent, since at lower temperatures adsorption can block the zeolite pores. This has been confirmed by Morooka *et al.*[87], who deposited Y-type zeolites on an alumina support. They found that CO_2 in a feed of CO_2 and N_2 could block N_2 permeation. Nobel and coworkers have shown that permeability measurements of single components through zeolite membranes was not satisfactory[29]; one should rather measure selectivities of the individual components in the actual mixture one intends to separate.

Very few papers have been published in the literature on the subject of the application of zeolite membranes in catalytic membrane reactors. Van de Graaf *et al.* reported on the application of a silicalite-1 membrane reactor in metathesis reactions[88]. The metathesis of propene to ethene and *trans*-2-butene and *cis*-2-butene to *trans*-2-butene were studied. The reactions were carried out at 296 K, using a 16.4 wt% Re_2O_7/γ-Al_2O_3 catalyst, which was activated *ex situ* using tetraethyltin as a promoter. The performance of a membrane reactor was dependent on the permeability and selectivity of the membrane. Single component fluxes of ethene, propene and *trans*-2-butene at 303 K are given in Figure 7.5. The selectivity of the membrane in binary mixtures of the reactant (propene or *cis*-2-butene) and one of the products (ethene or *trans*-2-butene) is given in Figure 7.6. The separation of ethene from propene and *trans*-2-butene from propene is based on differences in adsorption strengths, while the separations of *trans*-2-butene and *cis*-2-butene are based on the difference in shape[89]. The selectivities of the membrane *trans*-2-butene over the reactant in both these metathesis reactions is 5 and 1.6 respectively.

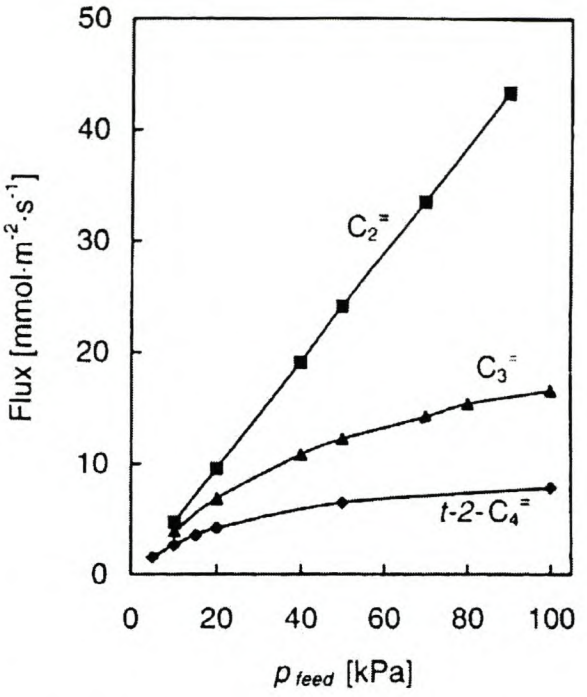

Figure 7.5: Single component permeation fluxes of propene, ethene and *trans*-2-butene through a silicalite-1 membrane as a function of their partial pressures in the feed. Propene, ethene and trans-2-butene[88].

It was shown that the conversion of propene could be increased by 13% compared to the thermodynamic equilibrium conversion. The ratio between *trans*-2-butene and *cis*-2-butene formed increased by 34% compared to the thermodynamic equilibrium. The *trans*-2-butene yield from the geometrical isomerisation of *cis*-2-butene increased by 4% from the thermodynamic equilibrium value. It was further concluded that comparison of the real time yield of the silicalite-1 membrane with the space time yield of catalytic reactors revealed that the current permeability of the membrane was not far from realistic for industrial application.

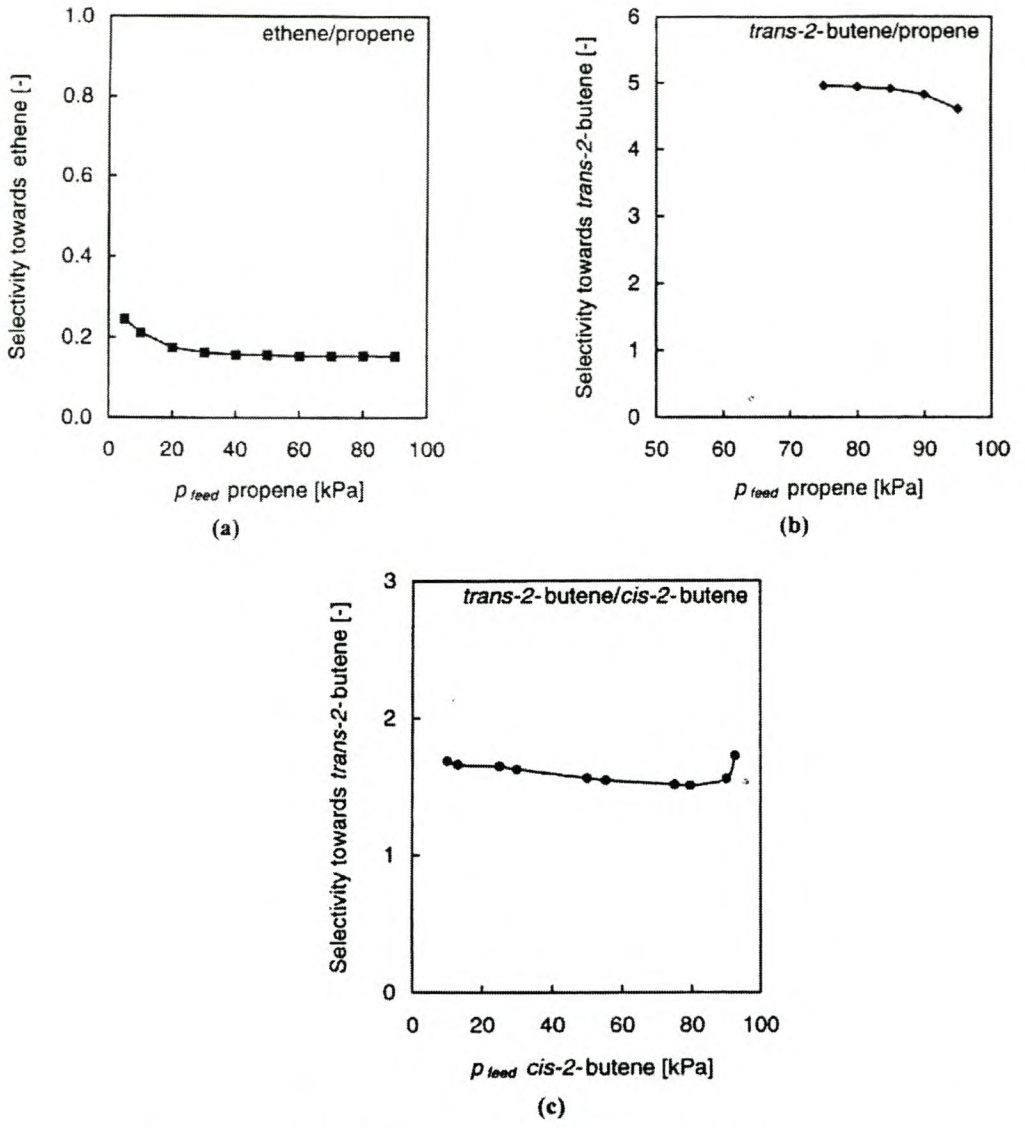

Figure 7.6: Selectivity of the silicalite-1 membrane towards the products in the metathesis reactions, for binary product/reactant mixtures, as a function of the feed concentration of the reactant. For the metathesis of propene: (a) ethene/propene; (b) trans-2-butene/propene and for the metathesis of cis-2-butene: (c) trans-2-butene/cis-2-butene[88].

Recently Casanave *et al.* reported the use of a zeolite membrane reactor, with a Pt/In catalyst, for i-butane dehydrogenation[90]. They reported enhanced dehydrogenation yields in the membrane reactor due to the separation of H_2 from the reaction medium. Two sweeping modes were studied, namely, co-current and countercurrent modes. Although the countercurrent mode yielded a higher separation factor than the co-current mode, the yield of reaction was similar. Reactor operation was described through theoretical modeling. There was good agreement between the

model and the experimental data in the co-current mode. However, the model overestimated the yield of the reaction in the countercurrent mode. This was due to the high permeation of H_2 which induced catalyst deactivation and/or made the kinetic law inadequate.

A review carried out by the research group at Delft University provided an interesting assessment of the current technology in this field, relative to the current level of materials available[86]. They concluded that unlike distillation, membrane separations do not have the economies of scale. Therefore, opportunities using zeolite membranes in catalytic processes will be limited to small and medium scale operations. Costs to compete against existing alternative technologies dictate that any early commercial examples will arise when there is a need for a new unit or a replacement.

7.3.7 Intermediate product yield enhancement with a catalytic inorganic membrane

Most previous studies of CMRs have addressed the problem of reaction equilibrium limitations in catalytic dehydrogenation reactions[1,5,7,12,91]. Harold *et al.*[14] focused on membrane reactor performance in the consecutive-parallel reaction system, given by:

$$A + \nu_B B \rightarrow \nu_{R1} R \qquad \text{Reaction 7.4}$$

$$A + \nu_{R2} R \rightarrow \nu_P P + \nu_Q Q \qquad \text{Reaction 7.5}$$

Many commercially important chemicals are the desired intermediate product (R). The best examples are partially oxygenated hydrocarbons such as ethylene oxide and acetaldehyde, both obtained from the reaction between ethylene (B) and oxygen (A), acrolein from propylene and oxygen and maleic anhydride from butane and oxygen. The main goal in the design and operation of catalytic reactors is to selectively produce the desired intermediate R at sufficiently high conversion levels of either of the main reactants (A,B). Various factors such as intraparticle diffusion limitations, catalyst overheating and safety constraints undermine this goal.

In a previous study it was shown that the point yield of the desired intermediate (R) could be increased by segregating the main reactants on opposite sides of a supported catalytic membrane[92]. More specifically, the main reactant A (B) is primarily fed from the support (active layer) side. The concept chiefly relies upon the dependence of the intrinsic selectivity of R on the concentration of the reactant common to both reactions (A). Power law rate expressions of the form

$$r_1 = k_1 p_A^{\alpha_{A1}} p_B^{\alpha_B} \qquad r_2 = k_2 p_A^{\alpha_{A2}} p_R^{\alpha_R}$$

were used. Performance improvements were shown to be highest if the following three conditions were met:

(i) $\alpha_{A1} < \alpha_{A2}$,

(ii) k_1, k_2 sufficiently large,

(iii) $\delta_a << \delta$.

Condition (i) simply suggests that a reduction in the concentration of reactant A leads to an increase in the point yield of R. The price that one pays is a reduction in the overall rate of consumption of A. The simulation results are applied only to the situation of differential conversion. Moreover, simple Fickian constitutive relations were used to model the intramembrane transport and heat effects were ignored. Obviously, if such a concept is to have practical applications it must result in the overall improvement in the yield of R.

The concept of improving intermediate yield in using a nonpermselective membrane reactor has been investigated experimentally[93-95]. It was demonstrated that the yield of acetaldehyde could be increased during ethylene oxidation by segregating the feeds of ethylene and oxygen. The acetaldehyde yield was higher when the oxygen was supplied through the membrane support (α-Al_2O_3) at a fixed overall feed flow rate of ethylene and oxygen. A higher catalyst temperature was however needed to achieve the ethylene conversion level at which this increase was observed. Coronas *et al.* studied the oxidative coupling of methane to C_2 hydrocarbons with the non-selective production of carbon oxides as the test reaction system[94]. The membrane system used consisted of a porous tube impregnated with silica for permeability reduction. It was shown that for a given methane conversion the hydrocarbon selectivity could be increased over levels achieved with a standard fixed-bed reactor approach. The investigators attributed the improved performance to the controlled

supply of oxygen to the catalyst along the length of the reactor. The controlled supply apparently reduced the extent of deeper heterogeneous or homogeneous oxidation of methane. Tonkovich *et al.* developed a non-permselective reactor for the oxidative dehydrogenation of ethane to ethylene[95]. The experiments revealed that the distributed addition of oxygen through a porous tube along the length of a catalyst bed could improve the ethylene yield over that obtained in a standard fixed-bed arrangement. The improvement was greatest at low ethane to oxygen feed ratios.

7.4 Summary

The development of catalytic membrane reactors is actually a multistep task. Currently, there is no really adequate membrane material with a large surface area available on commercial scale to meet the rigors of process operations[96]. Challenges concerning membranes, membrane reactors and reactions still remain and need to be addressed before catalytic membrane reactors can be integrated into industrial processes.

This field of research, however, remains a very attractive one for academic and industrial scientists. An important effort is still needed to develop methods of preparation and characterisation, novel membrane materials and reactor configurations and new applications to different reaction systems. Industrial applications are not foreseen in the immediate future, perhaps not due to lack of opportunities, but because of the formidable practical problems involved in moving from laboratory to industrial scale in such a new technology. However, even if only a few of the potential applications eventually materialise, their impact on our current approach to Catalytic Reaction Engineering would certainly be significant. Membrane reactors offer the prospect of higher yields and selectivities in many different processes as well as a safer and more environmentally friendly reactor operation[97].

7.5 References

1. J.N. Armor, *Appl. Catal.*, **49**, 1989, 1.
2. J.N. Armor, *Chemtech*, **22**(9), 1992, 557.
3. G. Saracco and V. Specchia, *Catal. Rev.-Sci. Eng.*, **36**, 1994, 305.
4. J. Shu, B.P.A. Grandjean, A. van Neste and S. Kaliaguine, *Can. J. Chem. Eng.*, **69**, 1991, 1036.

5. M.P. Harold, C. Lee, A.J. Burggraaf, K. Keizer, V.T. Zaspalis and R.S.A. de Lange, *MRS Bulletin*, 1994, 34.
6. N. Itoh, *Sekiyu Gakkaishi*, **33**, 1990, 136.
7. H.P. Hsieh, *Catal. Rev.-Sci Eng.*, **33**, 1991, 1.
8. J.-A. Dalmon, in: G. Ertl, H. Knozinger and J. Weitkamp (Eds.), *Handbook of Heterogeneous Catalysis*, VCH, Weinheim, Germany, 1997, 1387.
9. J. Zaman and A.Chakma, *J. Membr. Sci.*, **92**, 1994, 1.
10. G. Saracco, G. Versteeg and W. van Swaaij, *J. Membr. Sci.*, **95**, 1994, 105.
11. J.N. Amor, *J. Membr. Sci.*, **147**, 1998, 217.
12. T.T. Tsotsis, R.G. Minet, A.M. Champagnie and P.K.T. Liu, Catalytic membrane reactors in: *Computer-Aided Design of Catalysts*, C. Pereira and R. Becker (Eds.), Marcel Dekker, New York, 1993, 471.
13. R.McBride and D. McKinley, *Chem. Eng. Prog.*, **61**, 1965, 81.
14. M.P. Harrold and C. Lee, *Chem. Eng. Sci.*, **52**, 1997, 1923.
15. L.A. Bernstein, C.M. Reo and C.R.F. Lund, *J. Membr. Sci.*, **118**, 1996, 93.
16. H. Kita, M. Maeda, K. Tanaka and K. Okamoto, *Chem. Lett.*, 1997, 179.
17. F. Katsaros, T. Steriotis, A. Stubos, A. Mitropoulos, N. Kanellopoulos and S. Tennison, *Microporous Mater.*, **8**, 1997, 171.
18. V. Linkov, R.D. Sanderson and E.P. Jacobs, *J. Membr. Sci.*, **95**, 1994, 93.
19. J.N. Armor, in: *Separation Technology*, (Eds.) E.F. Vansant, Elsevier, Amsterdam, The Netherlands, 1994, 163.
20. M. Rao and S. Sircar, *J. Membr. Sci.*, **85**, 1993, 253.
21. M. Rao, S. Sircar, J. Abrardo and W. Baade, US Patent, 5 332 424, 1994.
22. A. Damle, S. Gangwal and V. Venkataraman, *Gas Sep. Purif.*, **8**, 1994, 137.
23. A. Sammells, M. Schwartz and J. White, World Organisation Patent, 97 410 60-A1, 1997.
24. J. Kilner, S. Bensen, J. Lane and D. Waller, *Chem. Ind.*, **22**, 1997, 907.
25. M. Carolan and P. Dyer, US Patent, 5 534 471, 1996.
26. M. Carolan and P. Dyer, US Patent, 5 569 633, 1996.
27. U. Balachandran, J. Dusek, P. Maiya, B. Ma, R. Mieville, M. Kleefisch and C. Udovich, *Catal. Today*, **36**, 1997, 265.
28. A. Darling, *Plat. Met. Rev.*, **2**, 1958, 16.
29. J. Coronas, J. Falconer and R. Noble, *AIChE J.*, **43**, 1997, 1797.
30. Y. Yan, M. Davis and G. Gavalas, *J. Membr. Sci.*, **126**, 1997, 53.

31. Y. Yan, M. Davis and G. Gavalas, *J. Membr. Sci.*, **126**, 1997, 95.
32. J. Fehlner and Z. Zhang, US Patent, 5 618 435, 1997.
33. M. den Exter, J.C. Jansen, J. vd Graaf, F. Kapteijn, J. Moulijn and H. van Bekkum, in: Recent Advances and New Horisons in Zeolite Science and Technology, (Eds. H. Chon, S. Woo and S.-E. Park), *Stud. Surf. Sci.*, **102**, 1996, 413.
34. S. Barri, G. Bratton, and T. Naylor, US Patent, 5 567 664, 1996.
35. T. Bein, *Chem. Mater.*, **8**, 1996, 1636.
36. K. Jansen and E. Coker, *Current Opinions in Solid State & Mater. Sci.*, **1**, 1996, 65.
37. N. Itoh, *Catal. Today*, **25**, 1995, 351.
38. J. Ross and E. Xue, *Catal. Today*, **25**, 1995, 291.
39. P. Courty and A. Chauvel, *Catal. Today*, **29**, 1996, 3.
40. N. Itoh, *AIChE J.*, **33**, 1987, 1576.
41. V.M. Gryaznov, *Plat. Met. Rev.*, **30**, 1986, 68.
42. T. Maksuda, I. Koike, N. Kubo and E. Kikuchi, *Appl. Catal. A*, **96**, 1993, 3.
43. Y.V. Gokhale, R.D. Noble and J.L. Falconer, *J. Membr. Sci.,* **105**, 1995, 63.
44. J.P. Collins, R.W. Schwartz, R. Sehgal, T.L. Ward, C.J. Brinker, G.P. Hagen, and C.A. Udovich, *Ind. Eng. Chem.* Res., **35**, 1996, 4398.
45. H. Weyten, K. Keizer, A. Kinoo, J. Luyten and R. Leysen, *AIChE J.*, **43**, 1997, 1819.
46. E. Gobina, K. Hou and R. Hughes, *Catal. Today*, **25**, 1995, 365.
47. E. Gobina and R. Hughes, *Appl. Catal. A: General*, **137**, 1996, 119.
48. E. Gobina and R. Hughes, *Chem. Eng. Sci.*, **51**, 1996, 3045.
49. G. Gallaher Jr., T. Gerdes and P. Lui, *Sep. Sci. Tech.*, **28**, 1993, 309.
50. B.K. Abdalla and S.S.E.H. Elnashaie, *J. Membr. Sci.*, **101**, 1995, 31.
51. B.K. Abdalla and S.S.E.H. Elnashaie, *AIChE J.*, **40**, 1994, 2055.
52. J.K. Ali and D.W.T. Rippin, *Ind. Eng. Chem. Res.*, **34**, 1995, 722.
53. J.K. Ali and D.W.T. Rippin, *Sep. Sci. Tech.*, **28**, 1994, 2475.
54. B.A. Raich and H. Foley, *Appl. Catal. A*, **129**, 1995, 167.
55. E. Moretti and N. Mukhopadhyay, *Chem. Eng. Prog.*, **89**, 1993, 7, 20.
56. M.P. Pina, M. Menendez and J. Santamaria, *Appl. Catal. B: Environmental*, **11**, 1996, 19.
57. J.P. Collins and J.D. Way, *J. Membr. Sci.*, **96**, 1994, 259.

58. E.N. Gobina, J.S. Oklany and R. Hughes, *Ind. Eng. Chem. Res.*, **34**, 1995, 3777.

59. H. Gunardson, Industrial Gases in Petrochemical Processing, Marcel Dekker, New York.

60. S. Uemiya, N. Sato, H. Ando, T. Matsuda and E. Kikuchi, *Appl. Catal.*, **67**, 1991, 223.

61. Z.D. Ziaka and S.P. Vasileiadis, *Chem. Eng. Comm.*, **156**, 1996, 161.

62. G. Barbieri and F.P. di Maio, *Ind. Eng. Chem. Res.*, **36**, 1997, 2121.

63. J. Shu, B.P.A. Grandjean and S. Kaliaguine, *Appl. Catal. A*, **119**, 1994, 305.

64. S. L. Jorgensen, P.H. Nielsen and P. Lehrmann, *Catal. Today*, **25**, 1995, 303.

65. K. Aasberg-Petersen, C. Nielsen and S.L. Jorgensen, Proceedings of the Fourth European Workshop on Methane Activation, June 1997, Limerick Ireland.

66. J. Sogge and T. Strom, *Stud. Surf. Sci.*, **107**, 1997, 561.

67. D. Ridler, M.V. Twigg, in: *Catalyst Handbook*, (Ed. V. Twigg), 2nd Ed., Wolfe, Frome, UK, 1989, 225.

68. P. Chanaud, A. Julbe, A. Larbot, C. Guizard, L. Cot, H. Borges, A Giroir-Fendler and C. Mirodatos, *Catal. Today*, **25**, 1995, 225.

69. H. Borges, A Giroir-Fendler C. Mirodatos, P. Chanaud and A. Julbe, *Catal. Today*, **25**, 1995, 377.

70. A. Santos, J. Coronas, M. Menendez and J. Santamaria, *Catal. Lett.*, **30**, 1995, 189.

71. J. Coronas, A. Gonzalo, D. Lafarga and M. Menendez, *AIChE J.*, **43**, 1997, 3095.

72. Y. Zeng, Y.S. Lin and S.L. Swartz, *J. Membr. Sci.*, **150**, 1998, 87.

73. U. Balachandran, R. Poeppel, R. Mieville and T. Kobylinski, *Bull. Amer. Cer. Soc.*, **74**, 1995, 71.

74. U. Balachandran, *Appl. Catal. A*, **133**, 1995, 19.

75. T. Mazenec, T. Cable, J. Frye, Jr. and R. Kliewer, US Patent, 5 306 411, 1994.

76. M. Schwartz, J. White, M. Myers, S. Deych and A. Sammells, Proceedings of the AIChE 1997 Spring National Meeting, Houston, TX, March 1997.

77. J. Galuszka, R.N. Pandey and S. Ahmed, Proceedings of Fifth European Workshop on Methane Activation, June 1997, Limerick, Ireland.

78. J. Galuszka, R.N. Pandey and S. Ahmed, *Catal. Today*, **46**, 1998, 83.

79. V.A. Sobyanin, V.D. Belyaev and V.V. Gal`vita, *Catal. Today*, **42**, 1998, 337.
80. V. Violante, A. Basile and E. Drioli, *Fusion Eng. Design*, **30**, 1995, 217.
81. M.E. Agnelli, M.C. Demicheli and E.N. Ponzi, *Ind. Eng. Chem. Res.*, **26**, 1987, 1704.
82. H. Yoshida, S. Konishi and Y. Naruse, *Nucl. Technol./Fusion*, **5**, 1984, 178.
83. A. Basile, A. Criscuoli, F. Santella and E. Drioli, *Gas Sep. Purif.*, **10**, 1996, 243.
84. S. Uemiya, N. Sato, H. Ando and E. Kikuchi, *Ind. Eng. Chem. Res.*, **30**, 1991, 585.
85. M. Bracht, P. Alderliesten, R. Kloster, R. Pruschek, G. Haupt, E. Xue, J. Ross, M. Koukou and M. Papayannoakos, *Energy Convers. Managem.*, **38**, 1997, 159.
86. F. Kapteijn, J. van de Graaf and J.A. Moulijn, Proceedings of Fourth Workshop on Catalytic Membrane Reactors, Oslo, Norway, May 1997.
87. S. Morooka, *Ind. Eng. Chem. Res.*, **36**, 1997, 649.
88. J.M. van de Graaf, M. Zwiep, F. Kapteijn and J.A. Moulijn, *Appl. Catal. A: General*, **178**, 1999, 225.
89. J.M. van de Graaf, E. van der Bijl, A. Stol, F. Kapteijn and J.A. Moulijn, *Ind. Eng. Chem. Res.*, **10**, 1998, 4071.
90. D. Casanave, P. Ciavarella, K. Fiaty and J.-A. Dalmon, *Chem. Eng. Sci.*, **54**, 1999, 2807.
91. V.T. Zaspalis, PhD Thesis, Twente University, 1990.
92. M.P. Harrold, V.T. Zaspalis, K. Keizer and A.J. Burggraaf, *Chem. Eng. Sci.*, **48**, 1993, 2705.
93. V.T. Zaspalis, R. de Lange, K. Keizer, M.P.Harrold and A.J. Burggraaf, in: *Membrane Processes in Separation and Purification*, (Eds.) J. Crespo and K. Boddeker, Kluwer Academic Publishers, Dordrecht, 1994, 415.
94. J. Coronas, M. Menendez and J. Santamaria, *Chem. Eng., Sci.*, **49**, 1994, 2015.
95. A.L.Y. Tonkovich, R.B. Secker, E.L. Reed, G.L. Roberts and J.L. Cox, *Sep. Sci. Technol.*, **30**, 1995, 1609.
96. J.N. Armor, *J. Membr. Sci.*, **147**, 1998, 217.
97. J. Coronas and J. Santamaria, *Catal. Today*, **51**, 1999, 377.

CHAPTER 8

Conclusions and Recommendations

This study was aimed at investigating the feasibility of a new synthesis approach for the preparation of improved zeolite A membranes. The concept of the static transverse synthesis (STS) method proposed here focussed on providing as much nutrient mass as possible to the liquid/solid interface, in actual fact to the surface of the porous support, during the synthesis of zeolite A crystals. This is not possible with the hydrothermal synthesis methods employed to date.

This concept comprises a synthesis process in which the highest *single* nutrient concentrations are contacted at the interface of the nutrients to form an aluminosilicate gel, which eventually leads to the formation of zeolite crystals.

It was shown that the α-alumina tubes were the best candidates for the preparation of zeolite A membranes, using this STS technique.

It was shown that the filling sequence had an important effect on the formation of different zeolite crystal phases on the internal and external surfaces. Simultaneous filling of the nutrients resulted in the most favourable crystal growth on the internal surface.

The static transverse synthesis process proved especially successful in the cases where the highest possible nutrient concentrations were used. Thin, continuous zeolite A crystal layers were formed on the small-pore surface, when the Si nutrient source was placed on the internal side of the support (small pore surface), due to the fact that the zeolite crystal sizes were comparable to the alumina support pore sizes.

It was also shown that the crystallisation front inside the pores of the alumina support could be shifted from the external surface of the tube towards the internal surface of the tube by adjusting the individual nutrient concentrations.

In an experiment with a single nutrient (pure silicate) as opposed to the two nutrients in the alumina support tube it was shown that the alumina particles could not

be dissolved in order to form an alumino-silicate gel and eventually a zeolite layer on the support surface.

The continuous tranverse flow synthesis (CFS) was shown to be a viable option for improving the STS process, especially with the laminar liquid flow at the support surface being zero, therefore simulating the static synthesis conditions. The contact angle measurements showed that the alumina support was perfectly wettable, therefore transport of nutrients from external to internal and internal to external surfaces could be easily achieved.

It was shown that continuous zeolite A membranes could be prepared successfully by using the STS technique. The reproducibility on the synthesis of the zeolite A membranes were very good.

The characterisation techniques (SEM, IR and XRD) were sufficient to show the continuity of the crystal layers as well as confirm identity of the crystal phases present.

The STS method also made it possible to chemically bind the zeolite crystals to the support surface, proving that the adhesion of the crystal layer is very stable and that is not kept on the support surface by a physical attraction.

In addition to preparing a continuous zeolite A crystal layer on the small-pore side of the tubular support surface, it was also shown for the first time that it was possible to make a continuous phase of zeolite type losod on the alumina support.

The flux and selectivity data obtained from the pervaporation experiments with water/ethanol mixtures are comparable to values reported in literature. An average water flux of 0.2 – 0.4 $kg/m^2/h$ was obtained, while the separation factors varied between 5000 – 16000. It was also seen that the formation of the grain boundaries between the individual crystals limit the intracrystalline diffusion of molecules, hence the relatively low flux values for these thin membranes.

Recommendations for future study

It is clear that crystallisation from both sides in a pore is highly diffusion-limited. Therefore, with the still attractive concept of single nutrient solutions the crystallisation must occur on the external surface, preferably on the silica side, so that the less viscous and small ion containing alumina solution can diffuse fast through the pore.

Thus it is envisaged that a silica dense gel layer in intimate contact with one surface of the support tube and the other surface exposed to the highest possible concentration of the alumina solution will provide, upon interaction, the best crystal layer.

Further optimisation of the STS and CFS methods might improve the crystal growth results even further, in future.